NUCLEAR MEDICINE AND MOLECULAR IMAGING

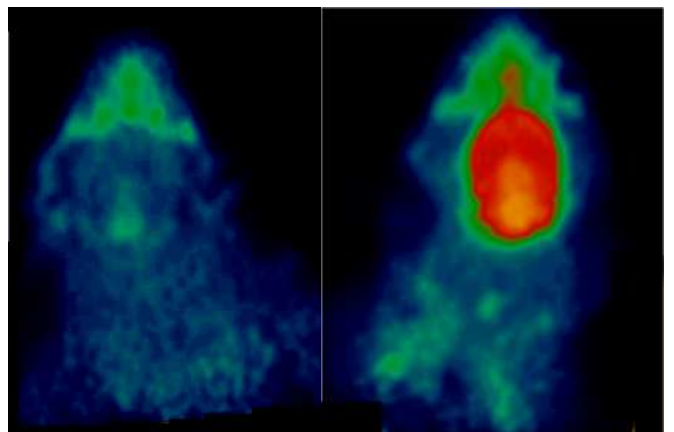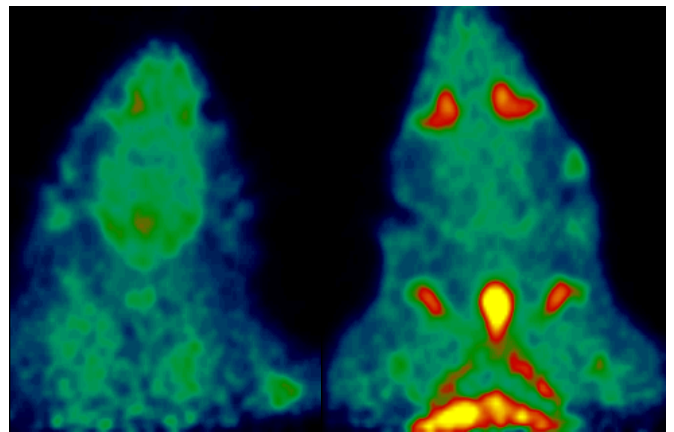Annual Report

2008

University Medical Center Groningen

umcg

Nuclear Medicine and Molecular Imaging

Annual Report 2008

Nuclear Medicine and Molecular Imaging
University Medical Center Groningen
P.O.Box 30001
9700 RB Groningen
The Netherlands

Cover illustration: By injecting either a radiolabeled inhibitor or a radiolabeled substrate for P-glycoprotein, the expression or function of this efflux pump at the blood-brain barrier can be visualized. See pages 37-39 of this Annual Report.

EDITORS: A.van Waarde
          A.M.J.Paans

CONTENTS

CLINICAL APPLICATIONS

Table 1 presents an overview of the nuclear medicine studies which were performed in 2008. The total number of single-photon and positron emission studies was increased in 2008 as compared to 2007 (from 15966 to 16484, i.e. by 3 %). The production of the Department of Nuclear Medicine and Molecular Imaging was increased by 33% between 2003 and 2008.

When the data from 2008 are compared to those of the previous year, a few trends are evident.

In the category "blood, infection, tumor", major increases occurred in sentinel node scintigraphy (176 examinations in 2007, 296 in 2008), whole body FDG-PET (1712 in 2007, 1969 in 2008) and whole body choline-PET (31 in 2007, 56 in 2008).

In the category "central nervous system", a sharp decline of the number of DAT scans (53 in 2007, 11 in 2008) was offset by increases of the number of FDOPA (34 in 2007, 83 in 2008) and FDG-PET scans of the brain (127 in 2007, 164 in 2008). This gradual shift from SPECT towards PET was already noted in the Annual Report of 2007.

In the category "digestive tract" a strong increase of oesophagus scintigraphy should be noted (62 examinations in 2007, 295 in 2008).

The total number of examinations in the field of "endocrinology" was declined by 10% (from 372 in 2007 to 334 in 2008) and the number of examinations regarding "heart and vessels" remained virtually constant (3122 in 2007, 3133 in 2008).

The gradual decline of lung perfusion scintigraphy since 2005 was continued in 2008 (646 examinations in 2007, 427 in 2008).

In the category "skeleton" the number of bone densitometry measurements was again increased (from 5491 in 2007 to 5609 in 2008). The total number of scintigraphic examinations of the skeleton increased from 7063 in 2007 to 7118 in 2008.

The number of applications of nuclear medicine techniques for therapeutic purposes was increased (from 146 in 2007 to 176 in 2008) and the number of renography scans with furosemide (138 in 2007, 193 in 2008) and renal scintigraphic examinations with ^{99m}Tc-DMSA (133 in 2007, 160 in 2008) also showed a relatively strong increase.

Statistics for the reliability of tracer production are presented in Table 2. The reliability of most production methods was (much) greater than 90%, although a second attempt at tracer production was sometimes required, which could result in 1 to 2 h delay of the scanning time. ^{11}C-5-hydroxytryptophan and ^{11}C-verapamil were the tracers with the lowest reliability (89% and 90%, respectively). The complexity of the (enzymatic) procedure for synthesis of ^{11}C-5-hydroxytryptophan explains why the reliability of tracer production did not exceed 90%. ^{11}C-Verapamil was only produced for animal studies in 2008, not for any study in patients.

Table 3 shows that the overall reliability of tracer production in 2008 was 93.9% (failure rate 6.1%, based on a single attempt at tracer synthesis). In reality, reliability of the tracer synthesis was higher since a second attempt at tracer production was often possible.

Table 4 indicates that five tracers (FDG, FDOPA, methionine, raclopride, and choline) could be produced in multidose quantities.

Table 1. Nuclear medicine examinations in 2008

Type of study	Number of studies	Radiopharmaceutical	Average dose (MBq)	Subject Age			Sex	
				0-15	16-40	>40	Male	Female
BLOOD, INFECTION, TUMOR								
Bone marrow scintigraphy	5	Tc-99m Nanocolloid	149	0	1	4	2	3
Bone marrow scintigraphy	1	In-111 Chloride	53	0	0	1	0	0
Bevacizumab scan	19	In-111 Bevacizumab (Avastin)	111	0	6	13	5	14
Choline whole body scan	56	C-11 Choline	388	0	0	56	56	0
Hydroxytryptophan scan	32	C-11 5-hydroxytryptophan	309	0	4	28	16	16
Methionine whole body scan	21	C-11 Methionine	452	0	2	19	14	7
Erythrocyte volume assessment	7	Cr-51 Na-chromate	1.3	0	2	5	5	2
FDOPA whole body scan	152	F-18 FDOPA	180	8	18	126	66	86
FDG whole body scan	1969	F-18 FDG	380	23	179	1767	1178	791
Fluoroestradiol scan	4	F-18 FES	206	0	0	4	0	4
FLT whole body scan	14	F-18 FLT	377	0	6	8	6	8
Sodium fluoride scan	3	F-18 NaF	214	0	0	3	3	0
Gallium scan	1	Ga-67 Gallium citrate	183	0	0	1	1	0
Leukocyte scan detail	27	Tc-99m Leukocytes	343	0	2	25	12	15
Leukocyte scan total body	91	Tc-99m Leukocytes	357	0	9	82	35	56
Lymph node arms	6	Tc-99m Nanocolloid	21	0	0	6	2	4
Lymph node legs	36	Tc-99m Nanocolloid	20	2	12	22	12	24
Plasma volume assessment	7	I-125 HSA serum albumin	0.26	0	2	5	5	2
Schilling test	14	Co-57 Cyanocobalamin	0.02	0	6	8	6	7
Schilling test with intrinsic factor	3	Co-57 Cyanocobalamin	0.02	0	1	2	1	2
Sentinel node	14	Tc-99m Nanocolloid	60	0	2	12	2	12
Sentinel node mamma	221	Tc-99m Nanocolloid	60	0	9	212	0	221
Sentinel node other	31	Tc-99m Nanocolloid	60	0	5	26	19	12
Sentinel node vulva	30	Tc-99m Nanocolloid	102	0	2	28	1	29
Somatostatin receptor scintigraphy	67	In-111 Octreotide	196	2	6	59	39	28
Trastuzumab scan	7	Zr-89 Trastuzumab (Herceptin)	38	0	1	6	0	7
TRM-1 scan	6	In-111 TRM1	149	0	0	6	3	1
subtotal	**2844**							

CENTRAL NERVOUS SYSTEM

Methionine scan of the brain	65	C-11 Methionine	205	0	8	57	27	38
PK11195 scan	8	C-11 PK11195	404	0	2	6	8	0
PiB scan	2	C-11 PiB	322	0	0	2	1	1
Raclopride scan	69	C-11 Raclopride	203	0	66	3	68	1
Cisternography – leakage	6	In-111 DTPA	20	0	3	3	1	5
DaT scan	11	I-123 FP-CIT	185	0	0	11	6	5
FDG scan of the brain	164	F-18 FDG	204	1	10	153	92	72
FDOPA scan of the brain	83	F-18 FDOPA	188	1	5	77	49	34
Liquor drain function	1	In-111 DTPA	20	0	0	1	0	1
subtotal	**409**							

DIGESTIVE TRACT

Abdominal scan	1	Tc-99m Tin-colloid	145	0	0	1	1	0
Gastrointestinal blood loss	1	Tc-99m Erythrocytes	75	1	0	0	1	0
Bile duct scintigraphy	15	Tc-99m Mebrofenine	42	4	2	9	12	3
Liver and spleen scintigraphy	5	Tc-99m Tin-colloid	75	0	2	3	2	3
Gastric emptying	1	Tc-99m Tin-colloid	10	0	0	1	0	1
Gastric emptying (solids)	130	Tc-99m CMC-gel	10	3	37	90	41	89
Meckel scan	13	Tc-99m Na-Pertechnetate	134	9	3	1	9	4
Oesophagus scintigraphy	259	Tc-99m Tin-colloid	10	12	68	179	54	205
Oesophagus scintigraphy nanocolloid	36	Tc-99m Nanocolloid	10	8	12	16	12	24
Salivary gland scintigraphy	1	Tc-99m Na-Pertechnetate	44	0	0	1	0	1
subtotal	**462**							

ENDOCRINOLOGY

Adrenal cortex scintigraphy	1	I-131 Norcholesterol	21	0	1	0	0	1
Adrenal medulla scintigraphy	41	I-123 MIBG	149	17	9	15	27	14
Parathyroid scintigraphy	43	Tc-99m Sestamibi	518	0	6	37	16	27
Thyroid scintigraphy I-123	105	I-123 Na-iodide (capsule)	13	1	28	76	28	77
Thyroid scintigraphy I-131	1	I-131 Na-iodide (solution)	1.1	0	0	1	1	0
Thyroid scintigraphy I-123 i.v.	6	I-123 Na-iodide, i.v.	38	4	0	2	0	5
Thyroid cancer fluid	1	I-131 Na-iodide (solution)	567	0	1	0	0	1
Thyroid cancer scintigraphy (1 mCi)	33	I-131 Na-iodide solution	38	0	8	25	10	22
Thyroid cancer scintigraphy (2 mCi)	26	I-131 Na-iodide solution	76	0	11	15	5	21
Thyroid uptake	74	I-131 Na-iodide, diluted	0.25	4	21	49	18	55
DMSA-V total body	3	Tc-99m DMSA (V)	288	0	1	2	0	3
subtotal	**334**							

HEART, VESSELS

m-Hydroxyephedrine scan	15	C-11 MHED	420	0	0	15	11	4
Myocardial metabolism (FDG)	22	F-18 FDG	193	0	2	20	15	7
Haemangioma	1	Tc-99m Erythrocytes	515	0	0	1	1	0
Heart l-r shunt	1	Tc-99m HDP	508	1	0	0	1	0
Heart r-l shunt	1	Tc-99m albumin aggregates	87	1	0	0	0	1
MUGA first pass	385	Tc-99m Na-Pertechnetate	460	34	22	329	280	82
MUGA rest	838	Tc-99m Na-Pertechnetate	505	1	79	758	500	338
Myocardial metabolism (DISA)	1	F-18 FDG	983	0	0	1	1	0
Myocardial innervation	21	I-123 MIBG	190	0	1	20	13	8
Myocardial scintigraphy (at rest)	924	Tc-99m Tetrofosmin	593	2	47	875	542	382
Myocardial scan (with adenosine)	639	Tc-99m Tetrofosmin	597	0	21	618	351	288
Myocardial scintigraphy (exercise)	275	Tc-99m Tetrofosmin	599	2	24	249	183	92
Myocardial scan thallium adenosine	4	Tl-201 Thalliumchloride	99	0	0	4	1	3
Myocardial scan thallium (exercise)	5	Tl-201 Thalliumchloride	100	0	2	3	2	3
Myocardial scan thallium (at rest)	1	Tl-201 Thalliumchloride	26	0	0	1	0	0
subtotal	**3133**							

LUNGS

Lung perfusion scintigraphy	242	Tc-99m albumin aggregates	109	18	54	170	107	135
Lung ventilation scintigraphy	185	^{81m}Kr						
subtotal	**427**							

SKELETON

Skeletal scintigraphy total body	792	Tc-99m HDP	685	37	112	643	355	437
Skeletal scintigraphy total body +flow	44	Tc-99m MDP	649	8	12	24	16	28
Skeletal scintigraphy detail	401	Tc-99m MDP	683	26	146	229	163	237
Skeletal scintigraphy detail + flow	272	Tc-99m MDP	686	7	89	176	105	167
Yttrium citrate colloid scan	1	Y-90 Yttriumcitraatcolloide	181	0	1	0	1	0
Bone dsitometry measurements	5609	----						
subtotal	**7118**							

THERAPY

Metastatic bone disease	1	Sr-89 Strontiumchloride	150	0	0	1	1	0
Polycytemia vera	8	P-32 Na-orthophosphate	174	0	0	8	6	2
Neuroendocrine tumors	7	I-131 MIBG	6053	0	4	3	3	4
Hyperthyroidism (treatment 1)	74	I-131 Na-iodide (solution)	456	2	19	53	21	52
Hyperthyroidism (treatment 2)	13	I-131 Na-iodide (capsule)	896	2	3	8	3	10

Thyroid carcinoma	73	I-131 Na-iodide (capsule)	4965	1	22	50	24	49
subtotal	**176**						

UROGENITAL SYSTEM

Renal scintigraphy	160	Tc-99m DMSA (succimer)	42	114	19	27	75	85
Priming hippuran clearance children	4	I-131 Hippuran	0.29	4	0	0	2	2
Renography	34	Tc-99m MAG-3 (Tiatide)	56	14	8	12	19	15
Renography / captopril	3	Tc-99m MAG-3 (Tiatide)	79	0	1	2	3	0
Renography / lasix	193	Tc-99m MAG-3 (Tiatide)	66	52	43	98	106	87
Renography of renal transplant	27	Tc-99m MAG-3 (Tiatide)	79	0	7	20	14	13
Iothalamate	4	I-125 Na-iothalamate	0,21	4	0	0	2	2
I131-hippuran clearance children	4	I-131 Hippuran	0,43	4	0	0	2	2
Iothalamate clearance children	4	I-125 Na-iothalamate	0,15	4	0	0	2	2
Clearance studies ERPF/GFR	1044	I-125-iothalamate or hippuran						
subtotal	**1477**							

MISCELLANEOUS

Measurement of perfusion leak Tc	7	Tc-99m Na-Pertechnetaat	7.5	0	1	6	3	4
Measurement of perfusion leak I	7	I-131 HSA, verdund	0.5	0	1	6	3	4
Amyloid scintigraphy (SAP scan)	68	I-123 SAP	186	0	6	62	35	33
Tc-99m Tin-colloid	1	Tc-99m Tin-colloid	21	0	1	0	1	0
Lacrimal / lymp scintigraphy	21	Tc-99m Na-Pertechnetate	62	1	6	14	7	14
subtotal	**104**							
TOTAL NO. EXAMINATIONS	**16484**							

* Not included in Table 1 are tracer production data for animal experiments. See Table 2 and chapter 4 for information on animal scans.

Table 2. Statistics Radiopharmacy/Radiochemistry 2008

Preparation of radiopharmaceuticals for PET

Month →	1	2	3	4	5	6	7	8	9	10	11	12	Total	Reliability * (%)
^{18}F-FDG	26	23	14	23	21	22	24	18	16	27	19	23	256	96 / 99
^{13}NH$_3$	9	13	12	6	13	5	17	5	8	10	14	8	120	94 / 100
^{18}F-Dopa	7	12	9	15	11	10	16	17	15	12	13	7	144	94 / 94
^{11}C-Methionine	6	5	3	6	4	3	6	4	8	5	2	4	56	94 / 96
^{11}C-Raclopride	3	2	9	6	8	12	4				17	14	75	91 / 95
^{11}C-PK11195	7	6	3	4	1	1				1		1	23	96 / 96
^{11}C-HTP	5	4	3	2	4	4	1	5	4	5	1		38	89 / 89
H$_2$^{15}O		1								1	9	9	20	100 / 100
^{11}C-Choline	4	4	1	3	3	2	3	3	3	2	5	5	38	87 / 92
^{18}F-FLT		2	1	3	2	1	3			2	2	1	17	94 / 94
^{11}C-mHED	1	2	2	2	3		5	5	3	1			24	92 / 92
^{11}C-Verapamil	6	1	4	10	2	1	3	3	6	8			44	90 / 90
^{18}F-NaF	2				1								3	100 / 100
^{18}F--FES											2	1	3	100 / 100
^{11}C-PIB						2		1	3				6	100 / 100
													867	

* The second figure relates to reliability after 2 attempto synthesize the tracer

Tracer delivery for animal studies (micro-PET)

	1	2	3	4	5	6	7	8	9	10	11	12	Total
^{18}F-FDG	10	13	6	6	11	12	11	3	6	2	11	4	95
^{13}NH$_3$						4	2	3		1	11	9	21
^{11}C-MPDX				4	2								6
^{11}C-Bari											5	5	10
^{11}C-Raclopride	2	1	1	4		1							9
^{11}C-PK11195	4	3	2	4	1	1							15
^{11}C-DAA1106		2	5	4		1							12
H$_2$^{15}O						1	3	3	5	1		8	21
^{11}C-Choline	2	1				1							4
^{11}C-mHED							2	4	4				10
^{11}C-Verapamil	6		4	9	2	1	3	3	6	6			40
^{18}F-Ranibizumab	3	3											6
^{89}Zr-labeled moAbs	3	18	15	8	2	4	7	9	7	18	8	6	105
													354

Table 3. Failures of radiopharmaceutical production for human PET studies

Radiopharmaceutical	Production failures in 2008
^{18}F-FDG	11
^{13}NH$_3$	7
^{18}F-Dopa	8
^{11}C-Methionine	3
^{11}C-Raclopride	7
^{11}C-PK11195	1
^{11}C-HTP	4
H$_2$^{15}O	0
^{11}C-Choline	5
^{18}F-FLT	1
^{11}C-mHED	2
^{11}C-Verapamil	4
^{18}F-NaF	0
^{18}F--FES	0
^{11}C-PIB	0
Total	**53 or 6.1 %** **(based on 100 % = 867)**

Table 4. Multi dose vial preparation of radiopharmaceuticals in 2008

Radiopharmaceutical for multi dose vial	Number of preparations for human use (n)	Number of doses (d)	d / n
^{18}F-FDG	245	2159	8.8
^{18}F-Dopa	136	235	1.7
^{11}C-Methionine	53	86	1.6
^{11}C-Raclopride	68	68	1.1
^{11}C-Choline	33	56	1.7

CLINICAL RESEARCH

2.1   Cardiology

2.1.1   Myocardial perfusion falls during uncomplicated hemodialysis

In cooperation with Dialysis Center Groningen, Dept Internal Medicine, Division of Nephrology, Dept Cardiology, Groningen, and Dept Renal Medicine, Derby City General Hospital, Derby, England.

Whereas hemodialysis (HD) is life-saving by replacement of renal function there is data to suggest that the HD procedure itself may contribute to the high cardiovascular risk in HD patients. Previous studies have shown that HD may elicit myocardial ischemia but the effect of HD on myocardial blood flow (MBF) has not been quantified. We studied the effect of HD on global and regional MBF.

Previous studies have shown that cardiac output (CO) falls during HD. We questioned whether the decrease in CO is primarily caused by hypovolemia-induced reduction of the filling volume of the left ventricle (LV) or by compromised myocardial contractility due to a diffuse or regional reduction in myocardial perfusion.

Gated ^{13}N-ammonia Positron Emission Tomography (PET) was used to quantify changes in LV volume, LV function and myocardial perfusion in 7 chronic HD patients during a single HD session of 4 h duration. A total of 3 PET scans was made: before the start of HD, and 30 and 200 minutes into the HD session (Table 5). Participating patients had an uneventful cardiovascular history and had stable HD sessions in the preceding 3 months. HD sessions were uneventful. Total ultrafiltrate volume was 2.8 ± 1.0 l.

Table 5. Changes of heart function during hemodialysis

	Before HD	30 min into HD	200 min into HD
Systolic BP (mmHg)	125 ± 10	123 ± 6	119 ± 5 #
Diastolic BP (mmHg)	74 ± 11	74 ± 9	68 ± 9
Heart rate (bpm)	69 ± 9	70 ± 9	78 ± 11#
Cardiac output (l/min)	4.1 ± 1.0	3.9 ± 0.8	3.1 ± 0.4 *#
LV end-diastolic volume (ml)	111 ± 25	105 ± 23 *	77 ± 20 *#
LV end-systolic BP (ml)	54 ± 18	51 ± 18 *	35 ± 14 *#
Myocardial perfusion (ml/min/100 g)	75 ± 17	64 ± 14 *	54 ± 10 *#

Data shown are Mean±SD; *denotes $p<0.05$ compared with baseline.
#denotes $p<0.05$ compared with 30 min into the HD session.

CO, LV end-diastolic, LV end-systolic volume and myocardial perfusion all decreased significantly during HD. Interestingly, myocardial perfusion had already significantly declined at 30 minutes into HD, i.e. without significant fluid removal.

The reduction in myocardial perfusion was diffuse in 5 patients and predominantly regional in 2 patients. These 2 patients developed regional hypokinesia/akinesia in those regions with the greatest fall in MBF. There was a significant correlation between the change in myocardial perfusion and the change in CO at 200 min into the HD session (r=0.84; p=0.03). We found no significant correlation between the change in end-diastolic or end-systolic LV volume and the change in either CO or myocardial perfusion at 200 min.

In conclusion, cardiac volumes and myocardial perfusion decrease significantly during HD in selected non-hypotension-prone HD patients with an uneventful cardiovascular history. As MBF fell already early during HD, not only hypovolemia but also acute dialysis-associated factors seem to play a role. Further studies to clarify the mechanism behind the link between the reduction in myocardial perfusion and cardiac output are necessary.

2.1.2   Myocardial perfusion reserve determined with PET: an independent prognostic factor in patients with advanced coronary artery disease

In cooperation with Dept Cardiology

Coronary artery disease is a diffuse disease not only affecting large epicardial coronaries but also smaller resistance vessels. The functionality of these smaller vessels is the main determinant of myocardial perfusion reserve (MPR). Next to left ventricular ejection fraction (LVEF), myocardial perfusion reserve (MPR) determines survival in patients with hypertrophic as well as dilated cardiomyopathies. The purpose of this study was to assess the prognostic value of myocardial perfusion reserve in patients with coronary artery disease.

Between 1995 and 2003, 480 patients with chronic CAD underwent dipyridamole stress and rest ^{13}N-ammonia PET to determine MPR. Additionally FDG PET was performed for viability (mismatching defects) and infarction (matching defects) assessment. Patients were followed for all cause mortality and major cardiovascular events

In 463 out of 480 patients valid MPR data could be acquired (368 male; mean age 66±11 years; LVEF 35±15%). One-hundred and nineteen patients underwent a PET-driven revascularization (67 percutaneous coronary intervention [PCI] and 52 coronary artery bypass graft [CABG]). The remainder of 344 patients was subject of this study. The overall MPR was 1.71 ± 0.50 (inter-tertile boundaries: 1.49 and 1.84). After adjustment for conventional risk factors and medication, MPR was associated with a multivariate relative risk for cardiac death of 1.32 (95% confidence interval [CI]: 0.69 – 0.83).The relative risk for LVEF was 0.67 (95% CI: 0.53-0.84). MPR was a stronger predictor for cardiac death than LVEF

In summary, MPR assessed with PET is an important predictor for cardiac death in patients with obstructive coronary artery disease, with a predictive value of comparable magnitude as LVEF. CAD patients not eligible for revascularisation with a low myocardial perfusion reserve are at higher risk of cardiac death. Therefore,

therapeutic strategies to improve MPR may be of value, especially in case of a low MPR.

2.1.3 Left ventricular volume assessment by planar radionuclide ventriculography validated with MRI

In cooperation with Dept.Cardiology, Thorax Center

Assessment of left ventricular (LV) ejection fraction (LVEF) and LV volume are essential for the evaluation of prognosis in cardiac disease. LVEF and LV volumes can be measured with several imaging modalities, such as magnetic resonance imaging (MRI) or computed tomography (CT), however, these are relatively expensive and time consuming. In contrast, planar radionuclide ventriculography (PRV) for LVEF assessment is a low-cost, fast and reliable technique, but PRV for LV volumes calculation is less common.

The aim of this study was the development and validation of a new hybrid geometrical count-based method (HGCBM) in comparison with two count-based methods (CBMs) and a geometrical method (GM) for the calculation of LV volumes with PRV using MRI as reference.

Thirty cardiac patients underwent routine PRV with a standard dose of 500 MBq of ^{99m}Tc-pertechnetate and additional cardiac MRI as reference method. LV volumes from PRV data were calculated by four different methods. The CBMs and GM are based on the assumption that the shape of the LV can be approximated by an ellipsoid or sphere, and the new HGCBM extracts the volume from the projected count rates themselves.

All methods underestimated the left ventricle volumes as compared to the MRI measured volumes. The correlation coefficients for EDV between PRV methods and MRI were r = 0.90 for GM and r = 0.85 for HGCBM. The CBMs showed poor correlation r = 0.64 with the MRI data and a high SD. The correlation coefficients for ESV between PRV methods and MRI were r = 0.955 for GM and r = 0.914 for HGCBM, r = 0.85 for CBM1 and CBM2.

Although GM showed the highest correlation with MRI, the difference of EDV and ESV between PRV and MRI was much higher for GM in comparison with HGCBM. Both CBMs showed poor agreement with MRI data. PRV using the new HGCMB method in comparison to previous methods is an easy and accurate approach to determine LV volumes.

2.1.4 Ischemia in idiopathic dilated cardiomyopathy: a comparison between PET perfusion and MRI dobutamine stress testing

In cooperation with Dept Cardiology

Although Idiopathic Dilated Cardiomyopathy (IDC) is characterized by the absence of significant coronary artery disease, an imbalance between myocardial oxygen

consumption and supply has been postulated. So, ongoing and subclinical myocardial ischemia may contribute to progressive deterioration of LV function in IDC. We aimed to prove that in IDC reduced regional myocardial perfusion reserve (MPR) is associated with reduced contractile performance, in the same myocardial regions.

Patients with newly diagnosed IDC, not treated yet with a beta-blocker, were eligible for inclusion in this study. Patients were examined with PET scanning, using the perfusion tracer $^{13}NH_3$ (ammonia) at baseline and after dypiridamole stress, and the viability tracer ^{18}F-fluoro-deoxyglucose. Within one week, a dobutamine stress MRI was performed. MPR (assessed by PET) as well as wall motion score (WMS, assessed by MRI) were evaluated in a 17 segment-model.

Twenty-two patients were included (age 49±11 years; 15 males). Left ventricular ejection fraction before inclusion was 33 ± 10 %. Five patients were judged to have heart failure NYHA class I, 16 class II, and 1 class III. With MRI, a total of 305 segments could be analysed. Wall motion abnormalities at rest were present in 127 (35.5%) segments and in 103 (29.9%) segments during dobutamine stress. A mean WMS per segment at rest of 1.7 ± 0.9 was found. During dobutamine stress, WMS did not increase (1.6 ± 0.9). A total of 21 segments deteriorated during dobutamine stress. We determined that MPR was reduced in the deteriorating segments compared with the segments without deterioration or improvement (see Fig.0).

Our data comparing wall motion changes during dobutamine stress MRI with PET-data on segmental myocardial perfusion show that regional ischemia in IDC is present and may be severe enough to cause contractile dysfunction.

Figure 0. Myocardial perfusion reserve in different segments of the heart
(vertical axis indicates the number of segments)
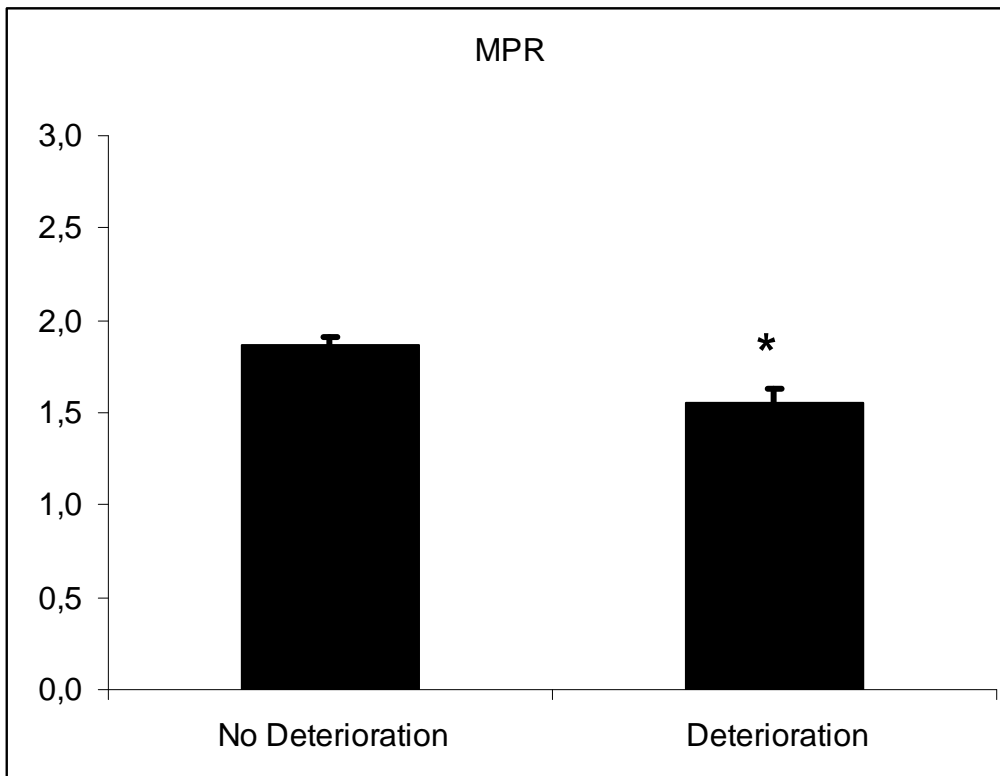
2.2 Neuroscience

2.2.1 [^{11}C]-PK11195 PET: a technique to monitor anti-inflammatory treatment in Parkinson's disease?

In cooperation with Dept. Neurology

[^{11}C]-PK11195-PET has been used for *in vivo* brain imaging of microglia activation in Parkinson's disease (PD) patients. COX-2 inhibition has been shown to reduce neuroinflammation and neurodegeneration in animal models of PD. This pilot study assessed the use of [^{11}C]-PK11195 PET to evaluate the ability of COX-2 inhibition to reduce neuroinflammation in PD patients.

Fourteen PD patients and eight healthy, age matched control subjects underwent both [^{11}C]-PK11195 PET and MRI scans. Five PD patients were scanned before and after one month of treatment with celecoxib (200 mg/day). Arterial plasma sampling and metabolite analysis were performed to generate input curves. A 2-compartment model and Logan analysis were applied and parametric DV images were compared using a t-test in SPM2. Also, a simplified reference region model (SRTM) was applied, with either the cerebellum as reference or a reference region derived from cluster analysis.

Using the cluster analysis, PD patients showed higher contralateral putamen BP and midbrain BP compared to controls, although considerable overlap was seen and differences were not statistically significant. Unexpectedly, BP and DV after celecoxib were slightly higher. Cerebellum as reference region resulted in lower BP values and k_3/k_4 gave 10-fold higher BP values. Linearization of the data did not show any differences between PD patients and controls.

In current practice, [^{11}C]-PK11195 seems unsuitable for assessment of the effect of anti-inflammatory medication. Refinement of the analysis methods for quantification of [^{11}C]-PK11195 uptake and, more importantly, the development of better tracers for activated microglia are necessary to allow accurate measurement of the effect of anti-inflammatory medication in patients.

2.2.2 Neuroinflammation in schizophrenic patients: a positron emission tomography study with [^{11}C]-*(R)*-PK11195

In cooperation with University Center of Psychiatry, Groningen. Funded by the Stanley Medical Research Institute

Schizophrenia is a chronic and disabling brain disease of which the etiology is not exactly known. It has been suggested that neuroinflammation plays a role in the pathophysiology of schizophrenia. Neuroinflammation is characterized by the activation of microglia. Following neuronal damage, microglia cells are activated and show an increase in the expression of the peripheral benzodiazepine receptor. The isoquinoline *(R)*-PK11195 [*(R)*-*N*-methyl-*N*-(1-methylpropyl)-1-(2-chlorophenyl) isoquinoline-3-carboxamide)] is a ligand for the peripheral benzodiazepine receptor

and can, after labeling with carbon-11, be used for PET imaging of neuroinflammation.

Neuroinflammation was hypothesized to be more profound during the episodes of positive symptoms in schizophrenia and therefore 7 schizophrenic patients were included that had a score of at least 5 on a positive item of the PANSS, or a score of 4 on two items. The patients were compared to 8 age-matched healthy controls. The PET scans were performed using an ECAT-EXACT HR+ scanner. A dynamic 3D scan of 60 minutes, consisting of 22 frames, was acquired after a bolus injection of 404 ± 49 MBq of $[^{11}C]$-*(R)*-PK11195. During the PET scan, radioactivity in whole blood was continuously monitored using an automated sampling system. In addition, blood samples were drawn 20, 45 and 60 minutes after tracer injection to correct for metabolites. A T1-weighted MRI scan was made of all subjects and was acquired with a Philips 3 Tesla scanner. The T1-weighted MRI image was co-registered with the PET image of the same subject and both the MRI and PET images were normalized to a T1-template in SPM2. Regions of interest were defined using an automated procedure. Time-activity curves were fitted to a two-tissue compartment model to calculate the binding potential for each region of interest.

The whole brain binding potential appeared to be higher in schizophrenic patients (2.0 ± 0.6) than in healthy controls (1.6 ± 0.4), although the difference was not statistically significant. A significantly higher binding potential of $[^{11}C]$-*(R)*-PK11195 was observed in the basal ganglia $(1.7 \pm 0.5$ vs. 1.3 ± 0.2; p=0.037), the right parahippocampal cortex $(1.9 \pm 0.4$ vs. 1.3 ± 0.3; p=0.009) and in the right hippocampus $(2.3 \pm 0.7$ vs. 1.6 ± 0.5; p=0.033). No abnormalities were found on the MRI images. These increased binding potentials are consistent with decreases in the volumes of these brain areas in schizophrenic patients that have been reported in the literature.

In a small group of patients, the present study indicates that neuroinflammation may play an important role in schizophrenia, especially during the episodes of positive symptoms. This neuroinflammation may precede brain atrophy.

2.2.3 Locally increased P-glycoprotein function in major depression. A PET study with $[^{11}C]$-verapamil

In cooperation with Dept.Psychiatry

The etiology of depressive disorder remains unknown, although a genetic susceptibility and exposure to neurotoxins are currently being discussed as possible contributors to this disorder. In normal circumstances, the brain is protected against blood-borne toxic substances by the blood-brain barrier, which includes the molecular efflux pump P-glycoprotein (P-gp) in the wall of brain capillaries. We hypothesised that P-gp function in the blood-brain barrier is changed in patients with major depression.

Positron-emission tomography was used to measure the brain uptake of $[^{11}C]$-verapamil, which is normally expelled from the brain by P-gp. The cerebral volume of distribution (V_T) of $[^{11}C]$-verapamil was used as a measure of P-gp function. Both

region of interest (ROI) analysis and voxel analysis using statistical parametric mapping (SPM2) were performed to assess the function of P-gp.

We found that patients with a major depressive episode which were using antidepressants showed a significant decrease of [11C]-verapamil uptake in different brain areas (in particular frontal and temporal regions), compared to healthy controls. The decreased [11C]-verapamil-uptake may be related to an increased function of P-gp due to their chronic use of psychotropic drugs. This mechanism may explain how treatment- resistant depression can develop.

2.2.4 Regional increase in P-glycoprotein function in the blood-brain-barrier of patients with chronic schizophrenia. A PET study with [11C]verapamil

In cooperation with Dept.Psychiatry

P-glycoprotein (P-gp), an important efflux pump in the blood-brain barrier (BBB) has a profound effect on entry of drugs and toxic substances into the central nervous system (CNS). The permeability of the BBB can be increased by modulation of the transport function of P-gp. Inflammatory mediators play a role in schizophrenia, and may affect the integrity of the BBB by modulating P-gp.

We hypothesized that P-gp function in the BBB is changed in schizophrenia. Positron-emission tomography (PET) was used to measure the brain uptake of [11C]-verapamil, which is normally extruded from the brain by P-gp.

We found that patients with chronic schizophrenia showed a significant decrease of [11C]-verapamil uptake in prefrontal cortex, basal ganglia and the amygdalae. A trend towards a decrease was also seen in the entire brain, although this did not reach statistical significance. The decrease of [11C]-verapamil uptake may be related to an up-regulation of P-gp. Increased activity of P-gp may be a mechanism underlying persistence of the schizophrenic symptoms and a factor causing drug resistance in schizophrenia. Our study is the first reported observation of a relationship between changes of P-gp function and schizophrenia.

2.2.5 The Dissociative Brain: Feature or ruled by Fantasy?

In cooperation with Institute of Psychiatry (IoP), King's College London , London, United Kingdom, BCN-Neuroimaging Center (BCN-NiC), Groningen, Universitair Centrum Psychiatrie (UCP) Groningen, Mental Health Care Drenthe, Assen, and Thorax Center, Dept Cardiology, Groningen

Dissociative identity disorder (DID), better known as multiple personality disorder, is probably the most disputed of psychiatric diagnoses. Despite its inclusion in the DSM IV, its origin and biological foundations remain elusive and supporters of the diametrically opposed iatrogenic and traumagenic positions are engaged in a passionate debate (Reinders, Neurocase 14:44-53, 2008). The traumagenic view states that DID constitutes a severe form of post-traumatic stress disorder while the iatrogenic view asserts that DID originates from suggestion, or role-playing, which is facilitated by a high level of suggestibility or fantasy-proneness.

DID patients function as two or more identities or dissociative identity states (DIS), named the `neutral identity state' (NIS) and the `trauma-related identity state' (TIS). The NIS inhibits access to traumatic memories thereby enabling functioning in daily life. The TIS does have access and responses to these memories.

We have investigated whether previously identified differential processing of trauma-related information between DIS in DID patients (Reinders et al., NeuroImage 20:2119-2125, 2003, Biological Psychiatry 60:730-740, 2006) hold after correction for iatrogenic factors (Huntjens et al., Psychological Medicine 36:857-863,2006), by including two groups of DID-simulating healthy controls.

The creative experiences questionnaire (CEQ (Merckelbach et al., Personality and Individual Differences 31:987-995, 2001)) was used to measure fantasy-proneness (FP, range 0 to 25) resulting in a high (CH: CEQ 13.7 ± 3.2) and low (CL: CEQ 3.9 ± 1.6) FP control group using a cut-off of 10 (Merckelbach et al., pers.comm., 2008).

A brain imaging study was performed applying a symptom provocation paradigm in a three (Group: DID patients (n=11; age 41.0 ± SD 6.1), CH (n=10; age 38.2 ± 10.9) and CL (n=8; age 42.5 ± 10.1))-by-two (DIS: NIS and TIS)-by-two (autobiographical neutral (n)/trauma-related (t) memory script) factorial design. Three psycho-biological parameters were tested: subjective ratings, cardiovascular responses, and regional cerebral blood flow (rCBF) as measured with PET.

Subjective ratings and cardiovascular responses were analysed in SPSS, the rCBF data with SPM5. For the rCBF data two within group contrasts ((i) NISt-TISt, (ii) TISt-NISt) were compared between the DID patient group and both the CH and CL group. The traumagenic view hypothesises different responses between patients and controls, which were tested by subtraction of the within group results (i.e. (i) DID(NISt-TISt) -CH/L(NISt-TISt), (ii) DID(TISt-NISt) -CH/L(TISt-NISt)). The iatrogenic view hypothesises similar responses between patients and controls, which were tested by conjunction of the within group results (i.e. (i) DID(NISt-TISt) and CH/L(NISt-TISt), (ii) DID(TISt-NISt) and CH/L(TISt-NISt)).

The subjective measures of the healthy controls showed a significant difference between NIS and TIS, which confirmed that the controls did simulate the DIS as requested (Figures 1 & 2).

When comparing DID patients to the high or low FP DID-simulating controls genuine and simulated identity states showed significant differences in subjective ratings, cardiovascular responses and rCBF patterns while processing the autobiographical trauma-related text (traumagenic test: Figure 3). In contrast, the conjunction analysis did not show any overlap in brain activation between DID patients and the CH or CL group (iatrogenic test: Figure 3).

In conclusion, in a direct comparison with patients, neither high nor low FP DID-simulating controls were able to (fully) mimic dissociative identity states observed in DID patients. Thus, our results do not support an iatrogenic origin of DID.
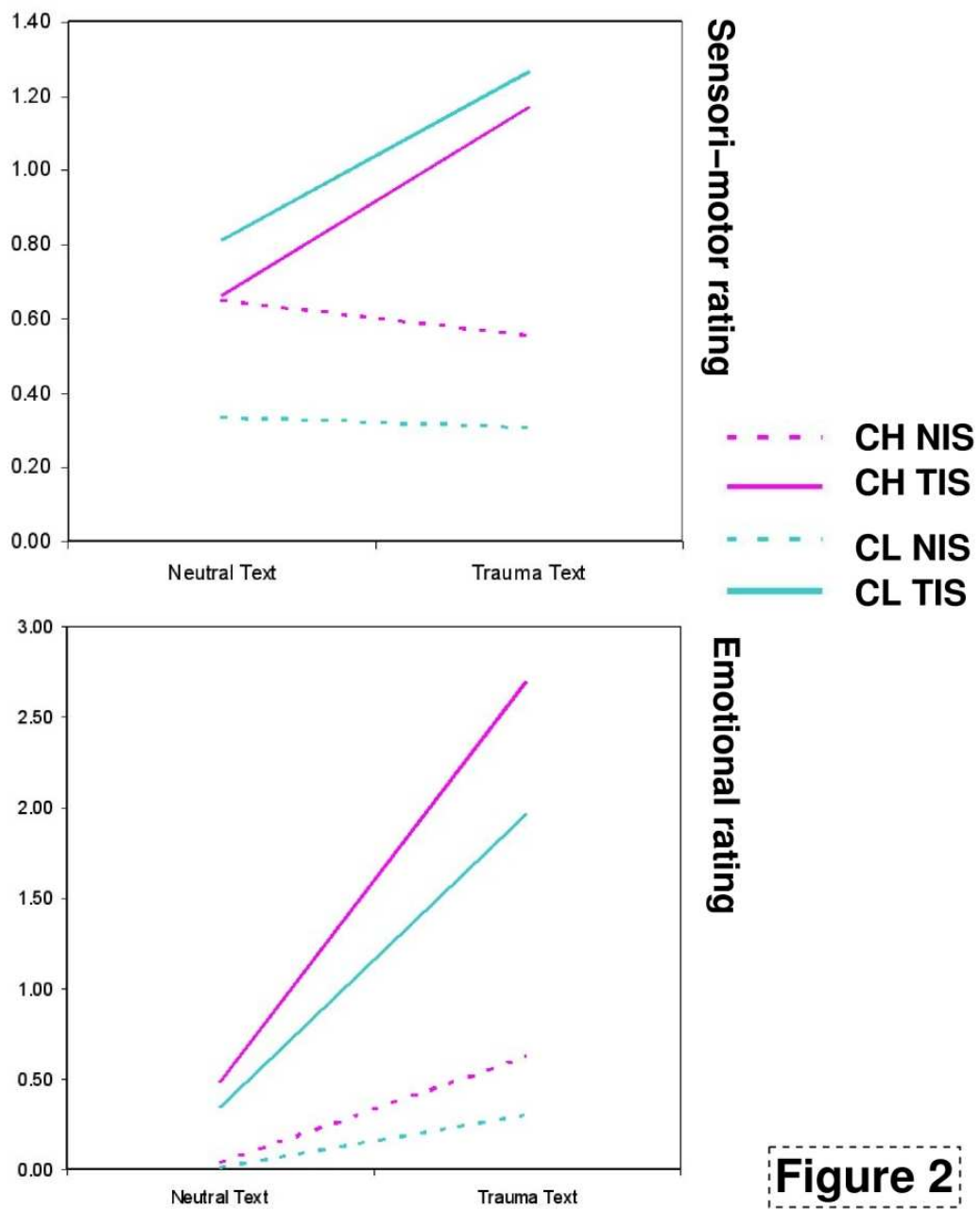
Figure 1

High fantasy–prone controls (CH)

	DIS	MS	DIS * MS
Subjective ratings			
sensory rating	0.003	n.s.	0.065
emotional rating	0.024	0.007	0.023
Autonomic reactions			
heart rate frequency	n.s.	n.s.	n.s.
systolic blood pressure	n.s.	n.s.	n.s.
diastolic blood pressure	n.s.	n.s.	0.030
HRV			
AVGNN	n.s.	n.s.	n.s.
HF	n.s.	n.s.	n.s.
LF	n.s.	n.s.	n.s.
HF_nu	n.s.	n.s.	n.s.
LF_nu	n.s.	n.s.	n.s.

Low fantasy–prone controls (CL)

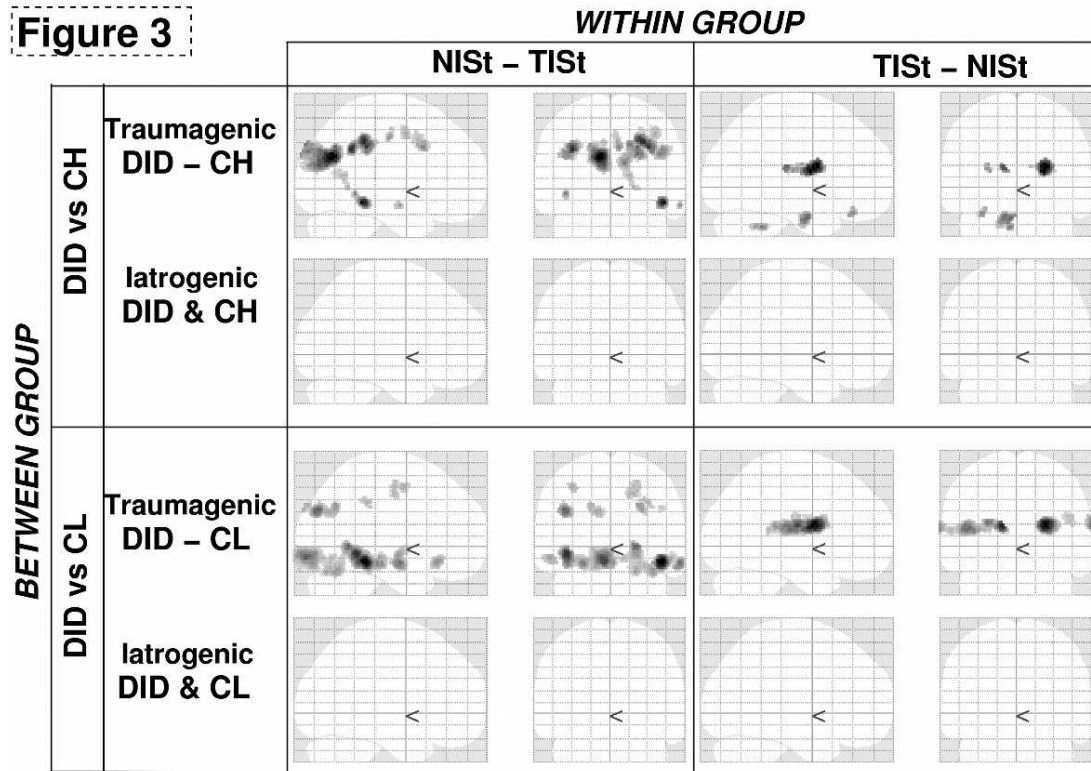|	DIS	MS	DIS * MS
Subjective ratings			
sensory rating	0.013	0.063	0.017
emotional rating	0.003	0.014	0.005
Autonomic reactions			
heart rate frequency	n.s.	n.s.	n.s.
systolic blood pressure	n.s.	n.s.	n.s.
diastolic blood pressure	n.s.	n.s.	n.s.
HRV			
AVGNN	n.s.	n.s.	n.s.
HF	n.s.	n.s.	n.s.
LF	n.s.	n.s.	0.036
HF_nu	n.s.	n.s.	n.s.
LF_nu	n.s.	n.s.	n.s.

DIS = dissociative identity state
MS = memory script
DIS * MS = interaction effect
HRV = heart rate variability
AVGNN = average of normal-to-normal time intervals
HF = high frequency domain
HF_nu = high frequency domain in normalized units
LF = low frequency domain
LF_nu = low frequency domain variable in normalized units

Figure 2

Figure 3

2.3   Oncology

2.3.1   ^{11}C-Choline PET has low accuracy for the detection of the site of recurrence in patients with PSA rise after radical prostatectomy

In cooperation with Dept.Urology

An elevated serum PSA level alone cannot distinguish between local, regional recurrences and the presence of distant metastases after curative treatment for prostate cancer. For long, it has been difficult to localize the site of recurrence (local or distant). Salvage radiotherapy is advised at low PSA levels, but does not result in high cure rates. In this study the potential of ^{11}C-choline positron emission tomography (PET) to identify site of recurrence was studied in a cohort of patients with rising PSA after radical prostatectomy.

64 patients (mean age 66 yrs) with histologically proven prostate cancer treated with radical prostatectomy showing biochemical recurrence (3 consecutive rises after nadir PSA $\leq$ 0.2 ng/ml) were included. Also, 7 patients (mean age 61 yrs) without recurrence underwent a PET scan to serve as controls. After receiving 400 MBq ^{11}C-choline intravenously, a PET scan was made using an ECAT HR+ camera. Attenuation-corrected images were made using an iterative reconstruction algorithm (ordered subset expectation maximisation). As reference we used biopsy-proven histology from the site of suspicion, positive findings with other imaging modalities (CT), clinical follow-up and/or a response to salvage therapy (radiotherapy) as reflected by a PSA decline.

No false positive PET scans were noted (specificity 100%). 23 out of 64 patients with biochemical recurrence (median PSA 2.2 ng/ mL; mean PSA 7.4) showed an abnormal uptake in PET (sensitivity 35%). 41 patients had a false negative PET scan (median PSA 1.4 ng/ mL; mean PSA 3.1 at recurrence). The site of recurrence was local in 11 out of 22 patients (mean PSA 6.4 ng/ mL; median 1.1), locoregional in 12 out of 22 patients (mean PSA 6.8 ng/ml; median 4.6) of which 3 out of 22 had distant metastases (mean PSA 4.1 ng/mL; median 4.3). 28 of patients with a false negative PET were treated with radiotherapy or hormones for progressive prostate cancer. The overall positive predictive and negative predictive values for ^{11}C-choline PET scan were 1.0 and 0.14, respectively. The accuracy was 32%.

In conclusion, ^{11}C-Choline PET has a low accuracy in the detection of the site of recurrence after radical prostatectomy on PSA rise and is therefore not useful for the guidance of salvage treatment.

2.3.2 Detection of local, regional and distant recurrence in patients with PSA relapse after radiotherapy using ^{11}C-choline PET

In cooperation with Dept. Urology

An elevated serum PSA level alone cannot distinguish between local or regional recurrences and the presence of distant metastases after curative treatment for prostate cancer. With the advent of salvage treatment such as cryotherapy, it has become important to localize the site of recurrence (local or distant). In this study, the potential of ^{11}C-choline positron emission tomography (PET) to identify the site of recurrence was investigated in patients with a rising PSA after external beam radiotherapy (EBRT).

70 patients with histologically proven prostate cancer treated with external beam radiotherapy with curative intent and showing biochemical recurrence as defined by the American society for Therapeutic Radiology and Oncology (ASTRO) consensus statement were included. Additionally, 10 patients without recurrence underwent a PET scan. After receiving 400 MBq ^{11}C-choline intravenously, a scan was made using an ECAT HR+ camera. Attenuation-corrected images were made using an iterative reconstruction algorithm (ordered subset expectation maximization). As reference, we used biopsy-proven histology from the site of suspicion, positive findings with other imaging modalities, clinical follow-up and/ or response to adjuvant therapy expressed through PSA decline.

None of the patients without biochemical recurrence had a positive PET scan (no false positives). 57 out of 70 patients with biochemical recurrence (median PSA 9.1 ng/ ml; mean PSA 12.3 ng/ ml) showed an abnormal uptake with PET (sensitivity 81%). Site of recurrence was only local in 41 out of 57 patients (mean PSA 12 ng/ml at scan), locoregional and/ or distant in 16 out of 57 patients (mean PSA 17.7 ng/ml. The overall positive predictive and negative predictive values for an ^{11}C-choline PET scan were 1.0 and 0.44 respectively. The accuracy was 84%. The table outlines PSA profiles of patients in the study with a PSA relapse.

In conclusion, ^{11}C-choline PET scan is a sensitive and accurate method to identify the site of recurrence in patients with PSA relapse after EBRT for prostate cancer. It can be a valuable tool in selecting candidates for local salvage treatment.

Table 6. Sensitivity of ^{11}C-choline-PET for the detection of recurrence

	No of patients	Negative scan	Local recurrence	Regional/ distant metastases	Sensitivity
0-4	n=15	3	10	2	80 %
4-10	n=22	6	12	4	73 %
>10	n=33	4	21	8	87 %

2.3.3 Early prediction of response to Sorafenib treatment in patients with hepatocellular carcinoma (HCC) with ^{18}F-FDG-PET

In cooperation with Dept. Medical Oncology

Recently, systemic therapy has for the first time shown a survival advantage for patients with inoperable HCC. Although toxicity in the pivotal study seemed mild, our initial experience in 6 out of 6 patients (Child Pugh A, mean age(yrs) 56,3 (42-78)) was less favorable: only *half* of the projected dose could be given due to grade 3 / 4 problems; diarrhea, abdominal pain, skin reaction on the hand or foot indicating a need for dose reduction 48 (13-113) days after the onset of treatment.

These findings highlight the importance of early determination of response during treatment in order to limit unnecessary toxicity. Many patients with HCC do not have easily measurable disease on CT scan or MRI due to infiltrative growth of the tumor and a background pattern of cirrhosis. Alfa-fetoprotein(AFP) elevation can also be related to hepatitis of cirrhosis activity and is therefore not a reliable marker. Moreover, true remissions were rare in the initial studies on sorafenib. Therefore we studied changes in ^{18}F-FDG uptake in patients with HCC during treatment with sorafenib.

In six patients with inoperable HCC who were treated with sorafenib, ^{18}F-FDG-PET (at baseline and after three weeks) was added to conventional imaging (a CT scan in week 12), in order to evaluate treatment response.

Two patients showed a decreased uptake of ^{18}F-FDG after 3 weeks, in accordance with a partial response as indicated by the CT scan in week 12. One patient showed also a decreased uptake of ^{18}F-FDG but sorafenib treatment was discontinued due to toxicity. One patient showed no change in ^{18}F-FDG uptake, in accordance with stable disease on the CT scan. One patient showed negligible ^{18}F-FDG uptake both at baseline and after 3 weeks. The CT scan indicated stable disease. One clinically progressive patient showed multiple new lesions on ^{18}F-FDG-PET, in accordance with progressive lesions on a lung X-ray/bone scan. This person died within 12 weeks.

In conclusion, early changes in ^{18}F-FDG uptake in HCC patients seem predictive of response (or an absence of response) to treatment with sorafenib. ^{18}F-FDG-PET can be useful to differentiate in an early phase between responders and non-responders.

2.3.4 Zirconium-89 trastuzumab for clinical HER2 immunoPET imaging

There is a need for non-invasive diagnostic tools to optimize and evaluate HER2 directed therapy in patients with HER2 positive breast cancer. SPECT imaging with ^{111}In-DTPA-trastuzumab identified new tumor lesions, undetected with conventional staging, in 13/15 patients with HER2 positive breast cancer (Perik *et al.*, J Clin Oncol 2006). In an attempt to further optimize HER2 imaging, we decided to use Positron Emission Tomography instead of conventional nuclear medicine, because of its higher spatial resolution and better signal-to-noise ratio. Zirconium-89 ([89]Zr) radiolabeled trastuzumab, suitable for patient use, was therefore developed and tested *in vivo*. In a clinical feasibility study we intended to evaluate visualization of HER2 positive lesions and to determine the minimal required trastuzumab dose for optimal imaging.

Trastuzumab has essentially been radiolabeled as described by Verel *et al.* (J Nucl Med 2003). Radiochemical purity and stability were determined by SE-HPLC, immunoreactivity with a Lindmo assay. The immunoreactive fraction of [89]Zr-trastuzumab was 0.96, labeling efficiency > 90% and rcp > 95%. [89]Zr-trastuzumab was stable for 7 days in buffer at 4 °C and in human serum at 37°C.

In an ongoing feasibility study, HER2 positive metastatic breast cancer patients are included. They are injected with [89]Zr-trastuzumab (10, 50 or 200 mg trastuzumab) and undergo PET-scanning at an early and a later timepoint. PET scans are compared with conventional imaging.

Until now, 12 patients with HER2 positive metastatic breast cancer have been included. [89]Zr-trastuzumab detected lesions corresponded to known tumor lesions in the brain, lung, liver and bone. The minimally required trastuzumab dose for optimal imaging seems to be greater than 10 mg.

In conclusion, [89]Zr-trastuzumab is a stable PET tracer which can detect HER2 positive breast cancer metastases. Preliminary clinical data indicate an excellent tumor uptake and a high image resolution.

.

2.3.5 ^{11}C-MET PET(/CT) vs ^{18}F-FDG PET(/CT) in the follow-up of differentiated thyroid cancer

In cooperation with Dept.Medical Oncology

Although FDG PET(/CT), under TSH stimulation, is now considered as a valuable, established diagnostic imaging tool in the follow-up of ^{131}I-negative patients for the detection of recurrences or metastases, the interest for new tracers and improved diagnostic tools in thyroid cancer is growing. Another target for tumor imaging is the increased protein metabolism and transport in cancer cells, which can be visualized with radiolabeled amino acids. Amino acid transport is generally increased in malignant tissue, which could be associated with specific cell surface changes in transformed cells. The process of malignant transformation is associated with an increased use of nutrients for energy metabolism, protein synthesis and cell division. It is conceivable that thyroid cancer would significantly accumulate amino acids because of its protein synthesis (e.g. thyroglobulin) and slow progression of the well-differentiated tumors (e.g. Hurthlecell carcinoma).

The feasibility of ^{11}C-methionine (MET) PET for visualisation of differentiated thyroid cancer (DTC) has been proven (Phan et al, NMC 2008). An interesting finding in our previous study was a complementary uptake of MET and FDG in 25% of the patients. It has been hypothesized that this finding might be related to the degree of tissue dedifferentiation. Hürthlecell carcinoma is known to be less radioiodine-avid than the well-differentiated papillary and follicular carcinoma and can even noet accumulate iodine or FDG at all. For this group of patients, MET PET could be of complementary value.

An in vitro study in rat thyroid cells has suggested that the TSH level does not influence amino acid uptake. However, no clinical intra-individually comparative studies between ^{18}F-FDG PET and ^{11}C-MET PET during (rh)TSH stimulation in DTC are available. It would be of interest to evaluate the diagnostic performance of MET PET under (recombinant human, rh)TSH stimulation and to compare these data with TSH stimulated FDG-PET.

Therefore, we have initiated a pilot study with the following objectives:

1. To evaluate the clinical performance of MET PET during rhTSH stimulation and to compare the results of the rhTSH stimulated MET PET with the standard rhTSH stimulated FDG PET in patients with negative post-treatment ^{131}I scans and elevated serum thyroglobulin (Tg).

2. To evaluate the (complementary) value of MET PET in patients with persistent or recurrent Hürthlecell carcinoma in the post-ablation phase and during follow-up.

Study population:

Obj 1. 25 DTC patients with patients negative post-therapeutic 131I-WBS and elevated Tg_{on} (>5 ng/ml), age >18 years
Obj 2. 15 patients with Hürthlecell carcinoma, post-ablation, age >18 years

Intervention (if applicable):

Obj 1. Patients will undergo 2 whole body PET scans: 1 MET PET and 1 clinical FDG PET under rhTSH stimulation. Both PET scans will be performed on the same day.

Obj 2. Patients will undergo 2 whole body PET scans: 1 MET PET and 1 clinical FDG PET under (rh)TSH stimulation. Both PET scans will be performed on the same day.

Main study parameters/endpoints: A qualitative and semi-quantitative (standardized uptake values (SUVs)) reading of all the PET studies will be performed. Comparisons with data derived from clinical CT, and where feasible histological or cytological confirmation, will be made.

Obj 1: the results of MET PET will be compared with the standard clinical FDG PET

Obj 2: the results of MET PET will be compared with the standard clinical FDG PET

2.3.6   Visualization of recurrent laryngeal cancer with positron emission tomography (PET): Comparison of ^{11}C-methionine and 18F-FDG - Addendum about the RELAPS study

This multicenter study is still in progress; patients are included both in Amsterdam (Free University Medical Center) and in Groningen (UMCG). By the end of 2008, 20 patients had been scanned (7 from Amsterdam and 13 from Groningen). The study will be finished when 48 patients have been examined. We hope to reach this goal in the summer of 2010.

2.4 Miscellaneous

2.4.1 Somatostatin receptor scintigraphy might be useful for detecting skeletal abnormalities in patients with multiple myeloma and plasmacytoma

In cooperation with Depts Pathology, Internal Medicine, Div Hematology, Groningen and Dept Nuclear Medicine, McMaster University, Hamilton, Canada

In vitro studies with plasma cell lines have shown that the somatostatin receptor is highly expressed on malignant plasma cells and that octreotide can inhibit the proliferation of plasma cell lines. It is therefore conceivable that somatostatin receptor scintigraphy (SRS) using ^{111}In-pentetrotide may be an alternative to study the presence of the malignant plasma cells. So far, SRS has been used for the detection of neuro-endocrine tumors and aggressive malignant lymphoma especially to define the extent of the disease. In the present study, we investigated the value of SRS in patients with multiple myeloma (MM) upfront treatment.

29 patients were prospectively included in this study including newly diagnosed (n=9) or relapsing (n=18) MM patients or patients with localized plasmacytoma (n=2). In all patients, total whole body radiography was performed in conjunction with SRS. A positive SRS was demonstrated in 44% of the newly diagnosed patients, in 82% of the relapsed patients and in both patients with plasmacytoma. The SRS findings corresponded with radiographic abnormalities in 52% of the patients. However, in relapsed patients 60% demonstrated increased SRS uptake in areas without new radiographic abnormalities. It was demonstrated that a positive SRS corresponded with histologically proven disease activity. Moreover, immuno-histochemical staining of MM material demonstrated concordant somatostatin receptor-sstr3 staining in 5 out of 6 patients. To study the effect of treatment, follow-up scans were made after 3-4 months of treatment. A complete (n=3) or partial (n=2) disappearance of lesions was observed that corresponded with a decline of disease related parameters.

These results demonstrate that SRS is a valuable tool for the detection of disease activity, especially in relapsing MM patients.

BASIC RESEARCH

3.1 Animal studies

3.1.1 Functional PET imaging of developmental neurotoxicity: Methyl mercury

In cooperation with TNO Quality of Life Zeist, the Netherlands.

Methyl mercury is one of the most hazardous industrial pollutants. Emitted methyl mercury is deposited in soil and water, enters the marine food chain and accumulates in high concentrations in predatory fish. The developing brain is particularly vulnerable to methyl mercury due to the ability of the compound to cross the placenta and the blood-brain barrier, which is not fully developed in the first year. Consequently, fish consumption by pregnant women is a high risk factor for neurotoxicity. Pollution incidents in Japan (Minamata) and Iraq and epidemiological studies on populations with high fish consumption have shown that in utero exposure has serious detrimental effects on brain development. Neurotoxic effects in the offspring include decreased IQ, language skills, memory function and attention. However, there is still considerable controversy about the levels of methyl mercury in diet that can induce these toxic effects.

Existing international guidelines for toxicity testing mainly focus on exposure of adult animals and on physical malformations of the newborn after exposure during pregnancy, not on functional defects. To fill in the omission in the regulatory requirements, regulatory agencies like the US EPA and the European OECD have issued guidelines for developmental neurotoxicity studies. The study design proposed by these guidelines, however, is very complex and time-consuming. Logistics are complicated, expenses are high and hundreds of laboratory animals (mainly rats) are required. Another complicating factor is that primarily morphological and behavioral end points are used that are not well validated, are not very sensitive and lack specificity. For example, a conventional developmental (neuro)toxicity study could not demonstrate any adverse effects for methyl mercury (up to 1.5 mg/kg) according to the guideline end points (data TNO).

We explored whether functional brain imaging with FDG PET would be a more sensitive marker for developmental neurotoxicity than the end points proposed in the guidelines. Female rats were subcutaneously injected with 1.5 mg/kg methyl mercury daily from day 8 of gestation until day 10 of lactation. In female offspring from differently exposed mother animals (n=4) and controls (n=4), brain activity was measured using FDG PET. On postnatal day 18, 22, 37 and 61, the pups were intraperitoneally injected with 20 MBq FDG and placed in a black wooden box (1x1x1 meter) in a dark room for 45 minutes to allow tracer distribution in conscious, active animals. Then, the animals were anesthetized with isoflurane and positioned in the camera with the brain in the center of the field-of-view. An emission scan was made for 20 minutes, followed by a transmission scan. After the scans the animals were placed back into their cages to recover. PET data were reconstructed and co-

registered to an age-matched FDG template scan. FDG uptake in various brain regions was determined by ROI analysis and expressed as SUV-values.

In control animals, the average FDG brain uptake *decreased* by 9% between day 18 and 22, then *increased* by 30% between day 22 and 37 and was further *increased* by 32% between day 37 and 61 (Figure 5a). In contrast, FDG brain uptake in the methyl mercury group *increased* by 38% between day 18 and 22, *decreased* by 12% between day 22 and 37 and *increased* again by 43% between day 37 and 61 (Figure 5a). On day 18, the average brain uptake of FDG was 27% *lower* in methyl mercury-treated animals than in the control group, but this difference was not statistically significant in any specific brain region. On day 22, on the other hand, average FDG uptake was 11% *higher* in the methyl mercury group, but the difference in FDG uptake was only significant for the cerebellum / brain stem (SUV 1.70 vs. 1.48, p=0.02). On day 37, FDG uptake was again significantly lower in in all brain regions of the methyl mercury group as compared to the control group (average difference 25%; Figures 4 and 5a). On day 61, the average FDG brain uptake was still 19% *higher* in the treatment group, but this difference was not significant anymore in any of the individual brain areas.

A characteristic feature of brain development in healthy rats is a dip in FDG uptake around day 22. A similar dip was also observed in a comparable study in male animals. Interestingly, this dip in FDG brain uptake was only observed at day 37 in the methyl mercury-treated group (Figure 5a). When the curve describing FDG uptake as a function of time for the methyl mercury-treated group was translated 15 days to the left, it nicely overlapped with the curve of the control group (Figure 5b). From these results can therefore be concluded that exposure to methyl mercury during pregnancy and lactation results in a substantial delay in the development of functional activity of the brain, as measured by FDG PET.
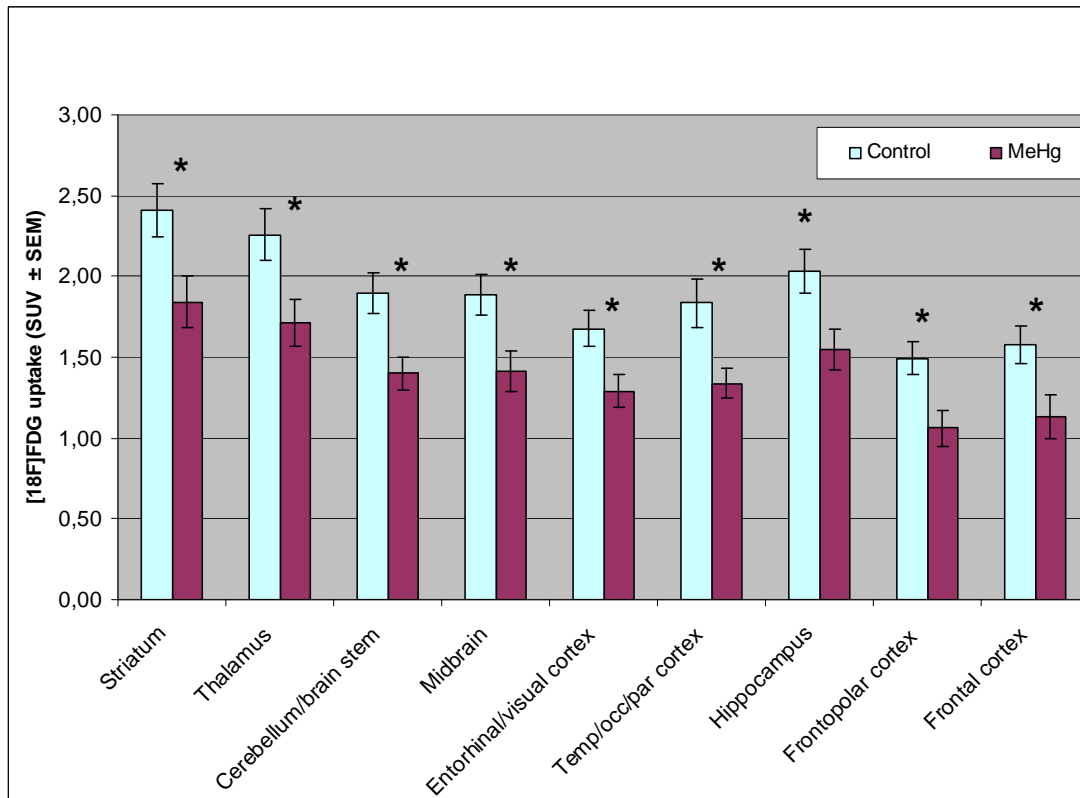
Figure 4: FDG brain uptake on day 37 in the offspring of rats that were exposed to methyl mercury between day 8 of gestation and day of lactation and in control animals. * indicates a significant difference between groups (Student's T-test, p<0.05).
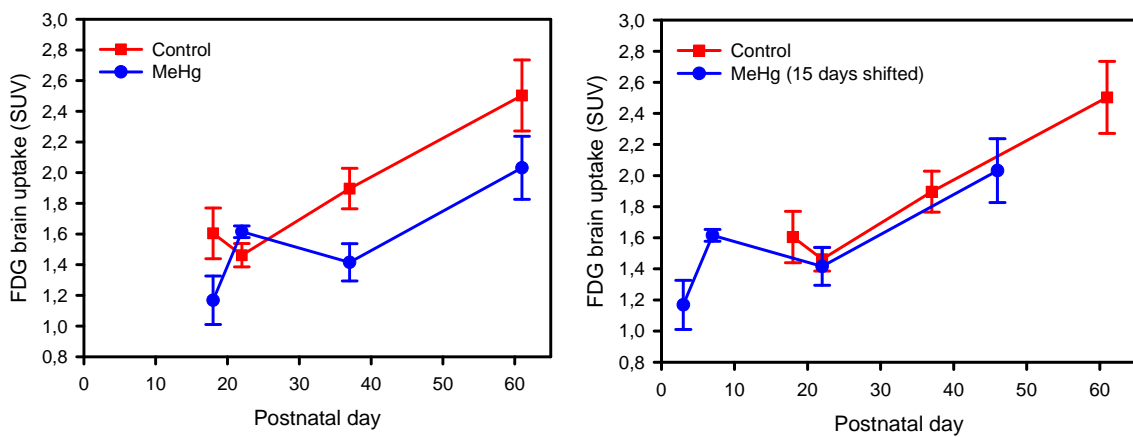
Figure 5: FDG brain uptake as a function of time in the offspring of rats that were exposed to methyl mercury between day 8 of gestation and day of lactation and in control animals (Left panel). Graphs of both groups overlap when the curve of the treatment group is shifted 15 days to the left (Right panel).

3.1.2 Radiation-induced cardiac damage assessed by FDG-PET

In cooperation with Dept. Radiotherapy

For many thoracic tumors treated with radiotherapy, escalation of the radiation dose is expected to result in increased local control. However, the dose that can be administered safely is limited by early radiation-induced pneumonitis which will occur if a certain lung dose is exceeded. The risk of radiation-induced pneumonitis was found to be increased when the heart was co-irradiated with a dose greater than 18 Gy (van Luijk et al., Cancer Res 65:6509,2005; van Luijk et al., Int J Radiat Oncol Biol Phys 69:552,2007). With the conventional methods of analysis, the heart is considered to be a late-responding tissue. The aim of the present study was therefore to investigate whether functional changes in the myocardium can be detected as early as 6-12 weeks after irradiation, using PET.

Three groups of six animals were included. Group 1 received 25 Gy, both to the heart and to 25% of the total lung volume located anterior and posterior of the heart. A second group was irradiated to 16 Gy. Group 3 consisted of non-irradiated controls. All animals were scanned at intervals of 2 weeks, using ^{18}F-FDG, from 2 to 12 weeks and at 16 weeks after irradiation. Depending on the injected dose of the tracer (30 or 60MBq in 1 ml), scans of 30 or 60 minutes duration were made. Gated acquisition was employed, using the animal's electrocardiogram; eight images were reconstructed at different time points in the cardiac cycle. In all images, the outline of the left ventricle was defined using contour detection (Biedenstein et al., Eur J Nucl Med 26:201,1999). The left ventricular ejection fraction (LVEF) was calculated from the images with minimal and maximal ventricular volumes. In addition, two orthogonal cross-sections were made through the axis running from apex to base. In these cross-sections, decreases in FDG uptake were quantified.

No decrease in LVEF was observed at any time up to 16 weeks after irradiation, but evident reductions in FDG uptake were noted in the apex of the heart. This effect was dose-dependent and occurred mainly in the high-dose group. The onset and recovery of these effects matched the time course of radiation-induced pneumonitis.

In conclusion, though the heart is generally regarded as a late-responding organ, we could observe functional changes as early as 6-12 weeks after irradiation, using FDG-PET. Further studies are required to determine whether these changes can explain the enhanced loss of pulmonary function after combined irradiation of the heart and lungs.

3.1.3 Evaluation of the usefulness of microPET in erythropoietin-treated rats with chronic heart failure

In cooperation with Dept. Experimental Cardiology

Erythropoietin (EPO) is a hematopoietic hormone with extensive non-hematopoietic effects. The discovery of an EPO-receptor outside the hematopoietic system has stimulated research on the beneficial effects of EPO in cardiovascular disease. Experimental evidence has been obtained for cytoprotective and angiogenic properties of EPO. The EPO–EPO receptor system seems a powerful target for treatment of the effects of acute and chronic myocardial ischemia.

Experimental research on the myocardium requires assessment of cardiac function in a repetitive and non-invasive way. PET is an established tool for the diagnosis, treatment and prognostic evaluation of cardiac disease in the clinical setting. Possibly microPET can be used in a similar way for assessing myocardial function in rodent models which are commonly employed in basic research.

Research questions addressed in this ongoing study are: (1) Is microPET scanning a suitable tool for the assessment of heart failure in experimental animals? (2) Are reliable measurements of the left ventricular ejection fraction (LVEF) possible? (3) Are there any differences in the measured LVEF between EPO- and placebo-treated rats with chronic heart failure?

Chronic heart failure was induced in rats by ligation of the coronary artery, resulting in myocardial infarction. We studied the effects of darbepoetin alpha treatment (EPO, 40 mg/kg, every 3 weeks, starting 3 weeks after MI) on longitudinal changes in left ventricular (LV) function, determined 9 weeks after MI. Prior to and 3 and 9 weeks after MI, a PET scan was made using 2-fluoro-2-deoxy-D-glucose (^{18}F-FDG), a commonly used tracer which can assess myocardial glucose consumption. ^{18}F-FDG was injected via a penile vein and the animals were scanned for 45 minutes, using ECG gating.

Data analysis is still in progress, values for LVEF have not yet been calculated for all intervals and all study groups. However, microPET scanning seems feasible in rats with experimental chronic heart failure. All animals survived the repeated isoflurane anesthesia (more than 1 h per scan).

3.1.4   Micro-PET imaging of the cardio-renal axis in healthy Wistar rats

In cooperation with Depts. Cardiology and Nephrology

Renal dysfunction is an important prognostic parameter in patients with chronic heart failure. The mechanisms behind this cardiorenal interaction are not fully understood. Therefore we intend to evaluate to what extent important mechanisms like blood flow, glucose metabolism and sympathetic innervation contribute to cardiorenal dysfunction.

Non-invasive imaging with positron emission tomography (PET) was used to study myocardial and renal blood flow and metabolism. Healthy Wistar rats were initially studied to evaluate the normal physiological tracer distribution. We also evaluated the feasibility of simultaneous scanning of the heart and the kidneys with micro-PET. Myocardial and renal blood flow were visualized using $[^{15}O]$-water and $[^{13}N]$-ammonia. $[^{18}F]$-FDG was used to visualize myocardial glucose consumption and $[^{11}C]$-mHED to examine sympathetic innervation.

Data analysis is still in progress. Dynamic scans are being made and time-activity curves are analyzed using pharmacokinetic modeling and input function data from arterial blood samples. ECG-gated scans are used to calculate left ventricular ejection fraction (LVEF).

Based on the preliminary results of this study it can be concluded that heart and kidneys of an adult rat can be visualized simultaneously with micro-PET, rendering good quality micro-PET images. Both $[^{15}O]$-water and $[^{13}N]$-ammonia appear to be suitable for imaging of myocardial and renal blood flow. Quantitative measurements of blood flow with micro-PET will be validated against flow data obtained by injection of microspheres. Measured uptake of $[^{18}F]$-FDG and $[^{11}C]$-mHED in the healthy rat heart was comparable with results reported in the literature. In future studies, $[^{18}F]$-FDG and $[^{11}C]$-mHED data will be used for analysis of glucose metabolism and sympathetic innervation of the heart in animals with cardio-renal dysfunction. These studies will hopefully give insight in the role of these processes during the pathophysiology of the cardiorenal syndrome.

3.1.5 MicroPET and microSPECT imaging of radiolabeled stem cells in living animals

In cooperation with Dept. Membrane Cell Biology

The neural stem cell line C17.2 is known for its migratory potential towards gliomas (brain tumors) *in vivo*. The mechanism responsible for this migration has not been fully elucidated. We investigated if C17.2 cells migrate specifically towards gliomas or also towards (other) sites of inflammation.

We used a tumor-inflammation model, i.e. rats subcutaneously inoculated with C6 glioma cells in the right shoulder, and injected with turpentine in a muscle of the left hindleg to induce a sterile inflammation. Radiolabeled C17.2 cells were i.v. injected, and scans of the animals were made using either positron emission tomography (PET) or single photon emission-computed tomography (SPECT). For PET imaging, the C17.2 cells were labeled with ^{18}F-FDG (fluorodeoxyglucose, an analog of glucose), while for SPECT imaging, labeling with ^{99m}TcHMPAO was employed.

Substantial leakage of the PET tracer ^{18}F-FDG from the cells was observed. This leakage could be blocked by phloretin (an inhibitor of glucose GLUT2 transporter) *in vitro*, but not *in vivo*. Immediately after injection, the stem cells were shown to migrate to the site of inflammation as well as the tumor site. However, the majority of the cells were trapped in the capillary network of lungs, spleen and liver. In both the phloretin- and DMSO (solvent)-treated groups, decreased uptake of radioactivity was noted in lungs, spleen and liver, possibly as a result of the vasodilating effect of DMSO.

Rats injected with free ^{99m}TcHMPAO showed substantial uptake of radioactivity in the brain, but in rats treated with ^{99m}TcHMPAO-labeled stem cells, brain uptake of radioactivity was negligible. Since there was no inflammatory stimulus in the brain in our animal model, the absence of radioactivity from the brain indicates that stem cells do not migrate to the healthy organ.

In conclusion, the migration of neural stem cells in living animals can be visualized with PET and SPECT tracers. However, a considerable fraction of the PET tracer ^{18}F-FDG is released from labeled cells, which complicates interpretation of the scan data. The SPECT tracer ^{99m}TcHMPAO (half-life 6 hours) is suitable for the tracking of labeled cells during a period of 17 to 18 hours. Tracking of cells during a more prolonged period will require the use of radionuclides with longer half-lives, such as ^{111}In-oxine ($t_{1/2}$ 2.8 days).

3.1.6 The effect of methotrexate on neuroinflammation and brain energy supply: Comparison between PET and immunohistochemistry

In cooperation with Dept. Behavioral Physiology, University of Groningen and Dept. Psychosocial Research and Epidemiology, Netherlands Cancer Institute, Amsterdam

Methotrexate (MTX) is a cytostatic drug mostly applied in adjuvant chemotherapy for breast cancer and is associated with cognitive impairment. This deficit is a long-term side effect of chemotherapy in a sub-group of cancer patients, and the mechanism causing cognitive impairment is not known. We examined two potential mechanisms: neuroinflammation and brain energy supply, with two different techniques in rats. Animals were treated with a high dose of MTX or saline by tail vein injection. PET scans were made one week and three weeks after treatment. Parallel groups of animals were sacrificed one week or three weeks after treatment and immunohistochemistry was performed on hippocampal slices.

[^{11}C]PK11195, a marker of activated microglia, was used as a PET tracer for neuroinflammation while IBA-1, a microglial marker, was employed for immunohistochemistry. No significant increase of tracer uptake was seen in the hippocampal region during the PET scans. Immunohistochemistry revealed that animals treated with MTX had more activated microglia both at one week and at three weeks after treatment, as compared to control animals.

The effect of MTX on cerebral glucose metabolism was assessed using [^{18}F]FDG PET. Animals treated with MTX showed a reduction of tracer uptake in the hippocampal region one week after treatment, suggesting a reduced glucose metabolism, compared to saline-treated controls. No effect of MTX was not observed at three weeks after treatment. Since a reduced glucose metabolism may be related to decreased vascularization, an endothelial barrier antigen (EBA) was applied to visualize blood vessels. The antigen study revealed that animals treated with MTX sacrificed at one or three weeks after treatment had fewer blood vessels than control animals sacrificed one week after treatment, which might explain the reduction of glucose uptake.

In conclusion, MTX treatment results in activation of microglia and a reduced blood vessel density in the hippocampus. These negative effects may contribute to the cognitive impairment seen after adjuvant chemotherapy in a subgroup of cancer patients. Reduced glucose consumption in the brain after MTX treatment was detected with microPET, but the activated microglia could not be detected by a ^{11}C-PK11195 PET scan.

3.1.7 Chronic stress and antidepressant treatment have opposite effects on P-glycoprotein at the blood-brain barrier: an experimental PET study in rats

*In cooperation with Depts. Psychiatry and Molecular Neurobiology*

The multidrug efflux transporter P-glycoprotein (P-gp) is highly expressed at the blood-brain barrier (BBB) and affects the brain uptake of many drugs. A recent PET-study has provided evidence for an increased function of P-gp at the BBB in medicated patients suffering from major depressive disorder. We were interested in answering the question whether this increase is due to the disorder or to the medication which the patients used. Therefore we have studied P-gp function at the BBB of rats, using microPET and ^{11}C-verapamil. The animals were either treated with the antidepressant venlafaxine, or subjected to chronic stress, a factor contributing to the development of depression.

In the first experiment, male Wistar rats were subjected to chronic stress (a 3–week foot shock procedure, a commonly used model of human depression). In a second experiment, animals were chronically treated with venlafaxine (25 mg/kg/d via an implanted osmotic minipump). Control animals were left undisturbed in their home cage. At the end of the 3-week treatment, a ^{11}C-verapamil PET scan was made in all experimental groups.
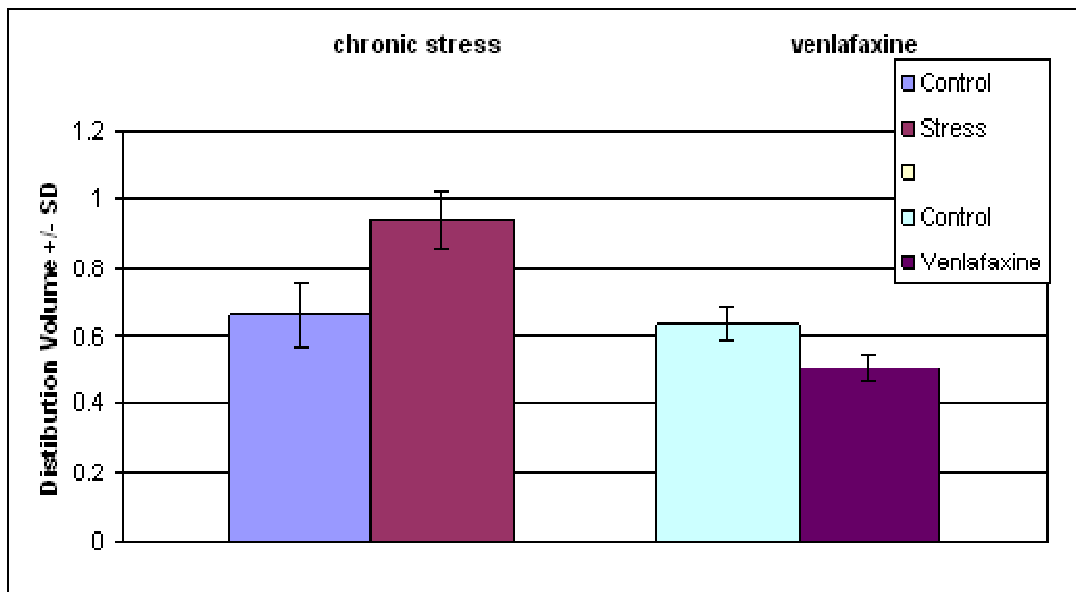
The cerebral distribution volume (VT) of ^{11}C-verapamil was significantly increased in the chronically stressed rats (from 0.66 ± 0.23 to 0.94 ± 0.36, $p < 0.05$). Treatment of animals with venlafaxine had the opposite effect, i.e. this caused a significant reduction in VT with respect to the control group (from 0.63 ± 0.05 to 0.50 ± 0.04, $p < 0.05$). The observed changes in VT could not be attributed to changes of the influx rate constant (K_1).

Our data suggest that P-gp function at the BBB is reduced after chronic stress and increased by chronic administration of venlafaxine The increased VT of ^{11}C-verapamil which we observed in patients with major depressive disorder may therefore be due to antidepressant medication.

Body weight gain
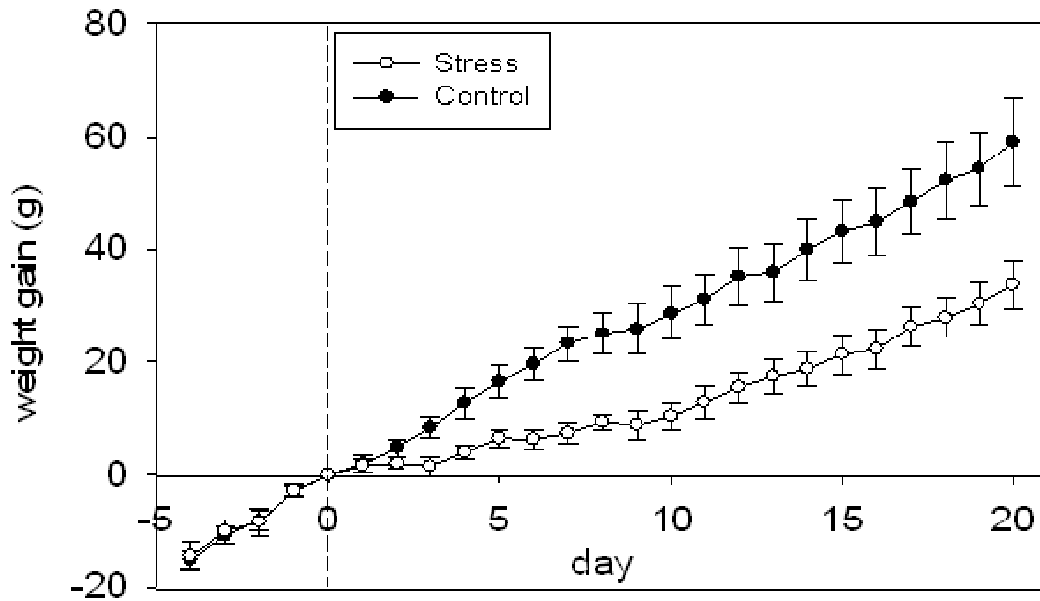
Figure 6. Effect of stress on rodent body weight. Chronically stressed rats (n=12) gained less weight than control rats (n=12). The animals were weighed every day starting 4 days before the first stress procedure (day 0, dotted line). Depicted are means ± SEM.

Figure 7. Cerebral distribution volumes of ^{11}C-verapamil (V_T) in the stress and venlafaxine experiments, showing increased V_T in chronically stressed rats and a significant decrease of V_T in rats receiving venlafaxine

3.1.8 Synthesis and evaluation of novel PET probes for P-gp expression and function

In cooperation with Dept. Pharmacochemistry, University of Bari, Italy

P-glycoprotein (P-gp) is an ATP-dependent efflux pump protecting the brain against toxic substances. We labeled a modulator (MC266) and inhibitor (MC18) of the pump with ^{11}C, resulting in potential tracers of P-gp function and expression (see Figure 8 for chemical structures).

MC18, MC266 and verapamil were labeled using ^{11}CH$_3$I. MicroPET scans (with arterial sampling) and biodistribution studies were performed in rats pretreated with saline, cyclosporin A (CsA), or cold MC18.

Cerebral distribution volumes (DV) of ^{11}C-MC18 (2.4 ± 0.2) and ^{11}C-MC266 (2.0 ± 0.2) in untreated rats were higher than of ^{11}C-verapamil (0.66 ± 0.11). DVs of ^{11}C-MC266 and ^{11}C-verapamil were significantly increased by 50 mg/kg CsA (to 5.2 ± 0.3 and 5.6 ± 0.3, respectively). The DV of ^{11}C-MC18 was reduced by cold MC18 (to 1.7 ± 0.1). Its SUV was also reduced (up to 67%) in several peripheral organs which express P-gp.

^{11}C-MC266 is a novel tracer of Pgp function with higher baseline uptake than ^{11}C-verapamil. Upregulation of P-gp function in response to treatment may be detectable using ^{11}C-MC266 and PET. Since ^{11}C-MC18 shows specific binding in target organs, this compound is a unique tracer of P-gp expression, although a derivative with higher affinity for the pump may be required for quantitative imaging. The use of a radiolabeled substrate and a radiolabeled inhibitor may allow independent assessment of the function and expression of the P-gp pump.
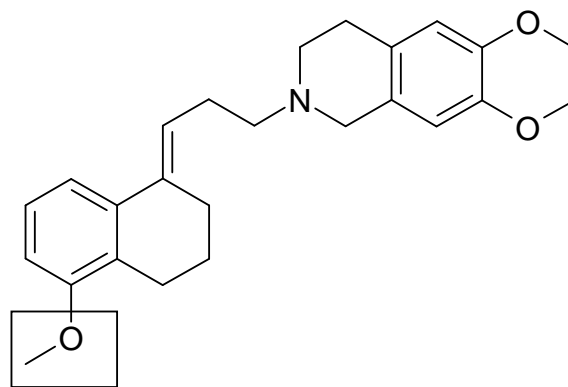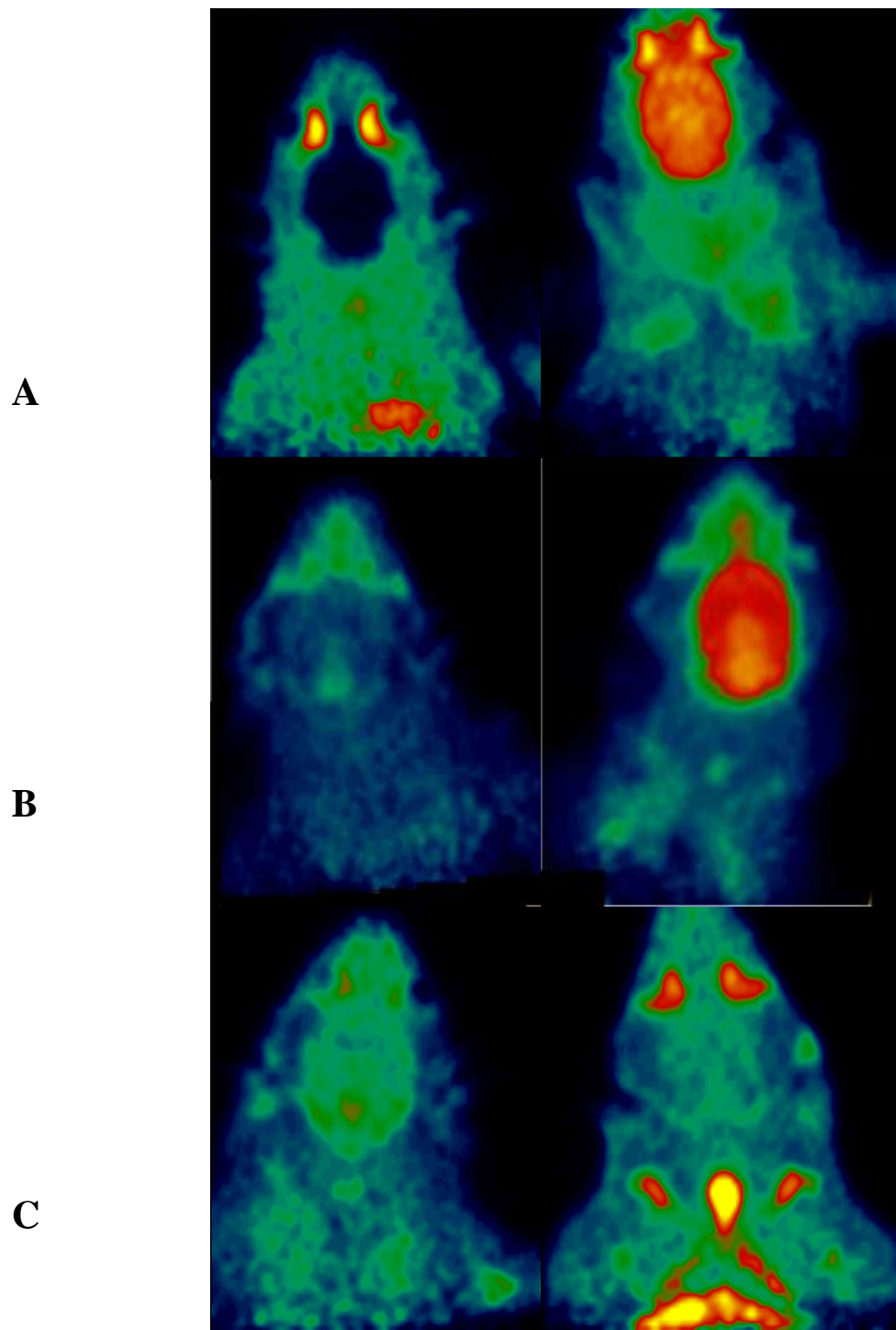
MC18
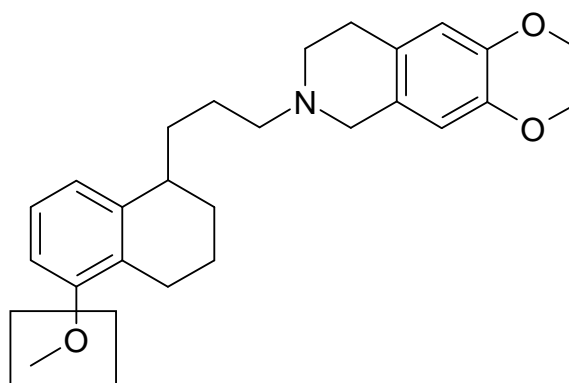
MC266

Figure 8. Chemical structures of ^{11}C-MC18 and ^{11}C-MC266. The positions of the ^{11}C-labels are indicated by the squares.

Figure 9. MicroPET images of rats (coronal views of the head and neck region) acquired with ^{11}C-verapamil (A), ^{11}C-MC266 (B) and ^{11}C-MC18 (C). The left animal of each pair was treated with saline, the right animal with cyclosporin A (50 mg/kg, rows A and B) or non-radioactive MC18 (15 mg/kg, row C) before tracer injection. Data from all frames were summed and smoothed with a Gaussian filter (1.35 mm). Images were normalized for body weight and injected dose. The nose of the animals is at the top.

3.1.9 Neuroinflammation is accompanied by a loss of the expression and function of P-gp

In cooperation with Depts. Molecular Cell Biology and Pathology, VU University Medical Center Amsterdam; Division of Pharmacology, Leiden Amsterdam Center for Drug Research, Leiden University, Leiden

The blood-brain barrier (BBB) between the central nervous system (CNS) and the systemic circulation is essential for maintenance and regulation of the neuro-parenchymal environment. Tight junctions (TJ) between brain endothelial cells (ECs) impede the entrance of hydrophilic molecules and immune cells from the circulation into the CNS and ensure that the BBB acts as a physical barrier. Transcellular traffic of essential nutrients to the brain is mediated by a variety of specific transporter systems, causing selectivity of BBB transport. In contrast, potentially harmful compounds are excluded from the CNS by the ATP-binding cassette (ABC) transporter family, causing multi-drug resistance (MDR) of the brain to xenobiotics. The best known and most widely studied representative of the ABC transporter family is P-gp (MDR1). P-gp is abundantly expressed in the BBB where it is located at the luminal membrane of brain capillary endothelial cells (ECs) and causes active efflux of a wide variety of chemical compounds.

An impaired function of the BBB has been described for a variety of brain disorders including multiple sclerosis (MS). Since efflux pumps at the BBB are of crucial importance for proper neuronal functioning, we suggest that impaired function of P-gp could lead to increased exposure of the highly vulnerable neuronal cells to toxic substances, which could contribute to neuronal dysfunction and the progression of lesions in MS. We observed a significant decrease of P-gp function in the EAE model of MS, using [11]C- verapamil and microPET, which corresponds to a decreased expression of P-gp in the brain endothelium measured by histochemical techniques, both in rodents with EAE and in tissue from patients with MS. *In vitro* analysis of P-gp function in brain endothelial cells (ECs) revealed that immune cells, like CD4+ T cells and monocyte-derived macrophages, can cause a striking downregulation of endothelial P-gp function. Interestingly, reactive astrocytes in MS lesions show a marked upregulation of P-gp expression. Moreover, astrocytes isolated from MS lesions display increased P-gp function compared to astrocytes derived from healthy brain, which corresponds with the increased P-gp expression.

Taken together, our results demonstrate marked changes of P-gp expression and function during EAE and MS, indicating an impaired BBB function in neuroinflammation. Loss of P-gp results in a reduced protection of the CNS, which could be a crucial hallmark of the pathogenesis of MS and the progression of lesions in this disease.

3.1.10 Detecting tumors using a platelet-derived growth factor-beta receptor specific carrier with radiolabeled techniques

In cooperation with Dept. Pharmacokinetics, Toxicology and Targeting

Platelet-derived growth factor-beta receptor (PDGFβR) is highly expressed in many human tumors. We have synthesized a carrier against PDGFβR by modifying human serum albumin (HSA) with a PDGFβR-recognizing cyclic peptide (pPB).

We found that radiolabeled (^{125}I)-pPB-HSA bound specifically to PDGFβR-expressing tumor cells and was rapidly internalized into the cells after incubating at 37°C. In addition, we examined the *in vivo* distribution of pPB-HSA and found that pPB-HSA was accumulated into the subcutaneous tumor of colon carcinoma C26 cells in mice as indicated by anti-HSA immunohistochemical staining. In addition, there was no significant accumulation of the construct in other organs. These results indicate that pPB-HSA could be used for tumor diagnosis in imaging studies.

Therefore, we examined the biodistribution of ^{123}I-pPB-HSA in C26 tumor-bearing mice at 2h, 6h and 24h after intravenous injection. We found that a large amount of radioactivity was detected in thyroid, stomach and urine within 2h after injection. From these data, we concluded that the ^{123}I-label was not stable *in vivo*. For successful imaging, a more stable label such as ^{111}In seemed to be required.

Thus, we performed stability studies of ^{111}In-pPB-HSA *in vitro* in serum and *in vivo* in normal mice. We found that a ^{111}In-radiolabel was indeed more stable than the ^{123}I-label. Then, we performed imaging studies with ^{111}In-pPB-HSA in C26 and B16 melanoma tumor-bearing mice using microSPECT at 2h and 24h after injection.

We observed uptake of the radiolabeled construct in B16 subcutaneous tumors whereas the uptake was less in C26 tumors. However, the low accumulation of ^{111}In-pPB-HSA into tumors and significant background radioactivity due to accumulation of free/bound ^{111}In-label in liver and intestines may complicate identification of unknown tumors in imaging studies.

We are now trying to optimize the binding efficiency of pPB-HSA to PDGFβR by modification of the linker between peptide and HSA.

3.1.11 *In vivo* VEGF imaging with a radiolabeled anti-VEGF Fab-fragment in a human ovarian tumor xenograft model using microPET and microCT

VEGF, released by tumor cells, is an important growth factor in tumor angiogenesis as it induces tumor neovascularization. $VEGF_{121}$ is freely soluble whereas splice variants like $VEGF_{165, 189, 206}$ are mainly located in the extracellular matrix resulting in high concentrations in the tumor micro-environment. Previously, we have shown that radiolabeled bevacizumab, an intact humanized IgG, is a novel tracer for VEGF imaging (*Nagengast et al, JNM, Aug 2007, 1313-9).* Ranibizumab (Lucentis®) is a humanized Fab-fragment (48 kDa) with high affinity for all VEGF-A isoforms. Ranibizumab is more rapidly cleared from the circulation than bevacizumab. We hypothesized that this characteristic could lead to more rapid imaging after tracer administration and a lower radiation dose for patients, as compared to radiolabeled bevacizumab.

For these reasons, we have labeled ranibizumab with positron emitters for non-invasive VEGF imaging and have compared the biodistributions of this anti-VEGF Fab-fragment and radiolabeled bevacizumab.

Labeling, stability and in-vitro immunoreactivity studies were performed. Subsequently, nude mice were inoculated with VEGF-producing human SKOV-3 ovarian tumor cells. After the tumors reached a size of 6-8 mm, a dose escalation study was performed using 3, 8 and 40 μg of ranibizumab per mouse. Radiolabeled Fab-IgG served as a control. MicroPET-, microCT and ex-vivo biodistribution studies were performed at 1, 3, 6 and 24 hr after injection.

The labeling efficiencies of ranibizumab with ^{18}F and ^{89}Zr were adequate. The tracers were stable for more than 24 hr at 37°C in serum, with preserved immunoreactivity. MicroPET images showed a rapid renal clearance with a high kidney uptake of the Fab-fragment (>100% ID/g). Kidney uptake could be lowered by co-injection of lysine with the tracer. Tumor uptake was already high at 6 hr post injection. The highest tumor uptake was observed at a low injected mass of ranibizumab (3 μg). Tumor uptake of radiolabeled ranibizumab was significantly (p=0.034) higher than that of Fab-IgG with tumor/blood (T/B) ratios of 5.72 ± 0.93 and 1.92 ± 0.23, respectively, at 24 hr post injection, and was also higher than that of radiolabeled bevacizumab (T/B ratio 2.85 ± 1.63 after 168 hr). Maximal tumor uptake (%ID/gram) of the novel radiopharmaceutical was not negatively affected by the rapid clearance, simce ^{89}Zr-ranibizumab (24 hr) and ^{89}Zr-bevacizumab (168 hr) showed comparable uptake values, 5.49 ± 1.42 vs 6.82 ± 1.80 %ID/g, respectively.

In conclusion, the radiolabeling of an anti-VEGF Fab-fragment with PET isotopes allows high resolution microPET imaging. Due to the rapid distribution of radiolabeled ranibizumab, images could be made at shorter intervals after injection as compared to radiolabeled bevacizumab. Ranibizumab (labeled with ^{18}F or ^{89}Zr) may be a new tracer to monitor VEGF-levels for the evaluation of anti-VEGF targeted therapy.

3.1.12 Characterization of ^{89}Zr-trastuzumab for clinical HER2 immunoPET imaging

There is a need for non-invasive diagnostic tools to optimize and evaluate HER2 directed therapy in patients with HER2 positive breast cancer. SPECT imaging with ^{111}In-DTPA-trastuzumab identified new tumor lesions, undetected with conventional staging, in 13/15 patients with HER2 positive breast cancer (Perik *et al.*, J Clin Oncol 2006). In an attempt to further optimize HER2 imaging, we decided to use Positron Emission Tomography (PET) instead of conventional nuclear medicine, because of its higher spatial resolution and better signal-to-noise ratio. Zirconium-89 (^{89}Zr)-labeled trastuzumab, suitable for patient use, was therefore developed and tested *in vivo*. In a clinical feasibility study, we intend to evaluate visualization of HER2 positive lesions and to determine the minimal required trastuzumab dose for optimal imaging.

Trastuzumab was radiolabeled as described by Verel *et al.* (J Nucl Med 2003). Radiochemical purity (rcp) and stability were determined by SE-HPLC, immunoreactivity with a Lindmo assay. Biodistribution studies were performed in nude mice bearing HER2 positive (SKOV3) or HER2 negative (GLC4) xenografts. Five animals per group were injected with ^{89}Zr-trastuzumab, imaged at days 1, 3 and 6 using a microPET camera (Focus 220), and sacrificed at day 6.

The immunoreactive fraction of ^{89}Zr-trastuzumab was 0.96, labeling efficiency > 90% and rcp > 95%. ^{89}Zr-trastuzumab was stable for 7 days in buffer at 4 °C and in human serum at 37°C. MicroPET imaging showed excellent tumor uptake. Metastases with a size approximating the spatial resolution of the microPET camra (1 mm) could easily be detected. In animals, ^{89}Zr-trastuzumab showed the highest uptake in the HER2 positive tumors at day 6 (33.4% injected dose ID/g tissue). Uptake in the HER2 negative control tumors was low (7.1% ID/g) and comparable to the liver uptake (7.7% ID/g).

In an ongoing feasibility study, HER2 positive metastatic breast cancer patients are included. These patients are injected with ^{89}Zr-trastuzumab (10, 50 or 200 mg trastuzumab) and undergo PET-scanning at an early and a later time point. PET scans are compared with conventional imaging.

Until now 12 patients with HER2 positive metastatic breast cancer have been included. ^{89}Zr-trastuzumab detected lesions correlated with known metastases in the brain, lung, liver and bone. The minimal required trastuzumab dose for optimal imaging seems to be greater than 10 mg.

^{89}Zr-trastuzumab is a stable PET tracer which can detect HER2 positive breast cancer metastases. Preliminary clinical data indicate excellent tumor uptake and a high resolution.

3.1.13 A new HYNIC-Bombesin analogue for targeting prostate tumors: ^{99m}Tc-labelling and preclinical evaluation

In cooperation with Molecular Imaging program at Stanford (MIPS), Department of Radiology and Bio-X Program, Stanford University School of Medicine, Stanford, USA and Medical Isotopes Research Center, Peking University, Peking, China

BN(Bombesin)-like peptides have a very high binding affinity for the gastrin-releasing peptide (GRP)receptor which is highly expressed in prostate cancer. In previous studies (Jia et al., Bioconjugate Chem 17,1069,2006; Shi et al., Bioconjugate Chem 19,1170,2008) we found that Tricine / TPPTS were outstanding coligands for ^{99m}Tc labelling of HYNIC-BN(7-14). In the present study, we have prepared a novel radiotracer, ^{99m}Tc(HYNIC-Aca-BN(7-14))(Tricine)(TPPTS), for the diagnosis of prostate cancer.

HYNIC-Aca-BN(7-14) and Aca-BN(7-14) were studied *in vitro* for their binding affinity to GRP-R using PC-3 cells. The full sequence of the bombesin peptide(1-14) was used as a standard. ^{99m}Tc(HYNIC-Aca-BN(7-14))(Tricine)(TPPTS) was synthesized as described previously (Shi et al., Bioconjugate Chem 19:1170,2008). After labeling, a sample of the resulting solution was analyzed by ITLC and radio-HPLC.

The internalization and efflux properties of the radioligands were tested *in vitro*. Their biodistribution profiles and imaging potential were determined in athymic mice bearing human PC-3 xenografts.

The radiochemical yield and purity of ^{99m}Tc-HYNIC-Aca-BN(7-14) after purification were 90% and > 95%, respectively. Aca-BN(7-14) and BN(1-14) displayed comparable binding affinities in PC-3 cells with IC_{50} values in the lower nanomolar range (3.27 ± 0.08 nM and 3.48 ± 0.08nM). The IC_{50} value of HYNIC-Aca-BN(7-14) was 12.8 ± 0.14 nM. The attachment of a HYNIC group seemed to reduce the affinity of Aca-BN(7-14) for binding to GRPR.

The internalization (left) and efflux (right) kinetics of ^{99m}Tc-HYNIC-Aca-BN(7-14) are presented in Figure 10. Internalization occurred during the initial 30 min after the onset of incubation, a maximum was reached with 79 ± 8 % of the radioactivity internalized at 15 min. ^{99m}Tc-HYNIC-Aca-BN(7-14) showed a long retention time in an efflux experiment using PC-3 cells. More than 50% of the internalized radioactivity was retained at 4 h after the onset of incubation.
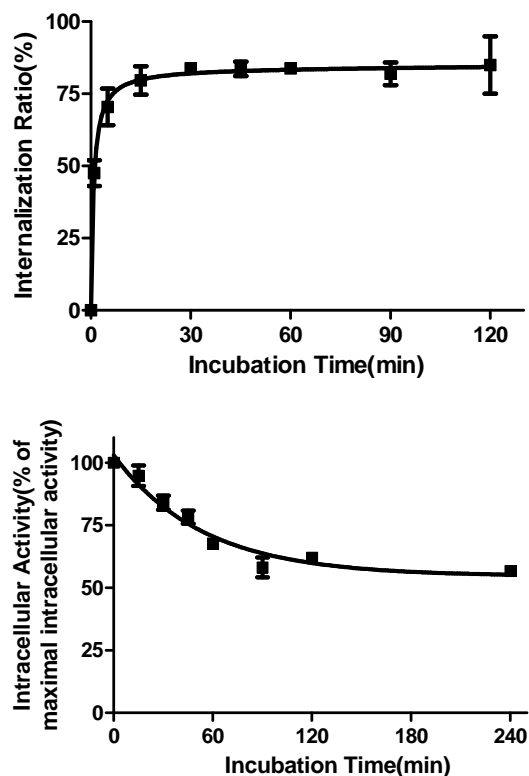
Figure 10. Internalization(left) and efflux(right) kinetics of ^{99m}Tc(HYNIC-Aca-BN(7-14))(Tricine) (TPPTS)

^{99m}Tc-HYNIC-Aca-BN(7-14) (Figure 11) showed a rapid clearance, predominantly through the renal route. In the biodistribution study, a relatively high uptake of ^{99m}Tc-HYNIC-Aca-BN(7-14)(2.24 ± 0.64 %ID/g) was observed in human PC-3 xenografts at 0.5 h post injection with a steady decrease over the 4 h study period. Tumour-to-normal tissue ratio increased over time because of the long retention time of the radiotracer in tumour.

In vivo blocking experiments (Figure 11, bottom) with HYNIC-Aca-BN(7-14) showed a significant reduction in tumour uptake of radiotracer and in several other organs including pancreas and intestine, indicating that tracer uptake was GRPR-mediated.
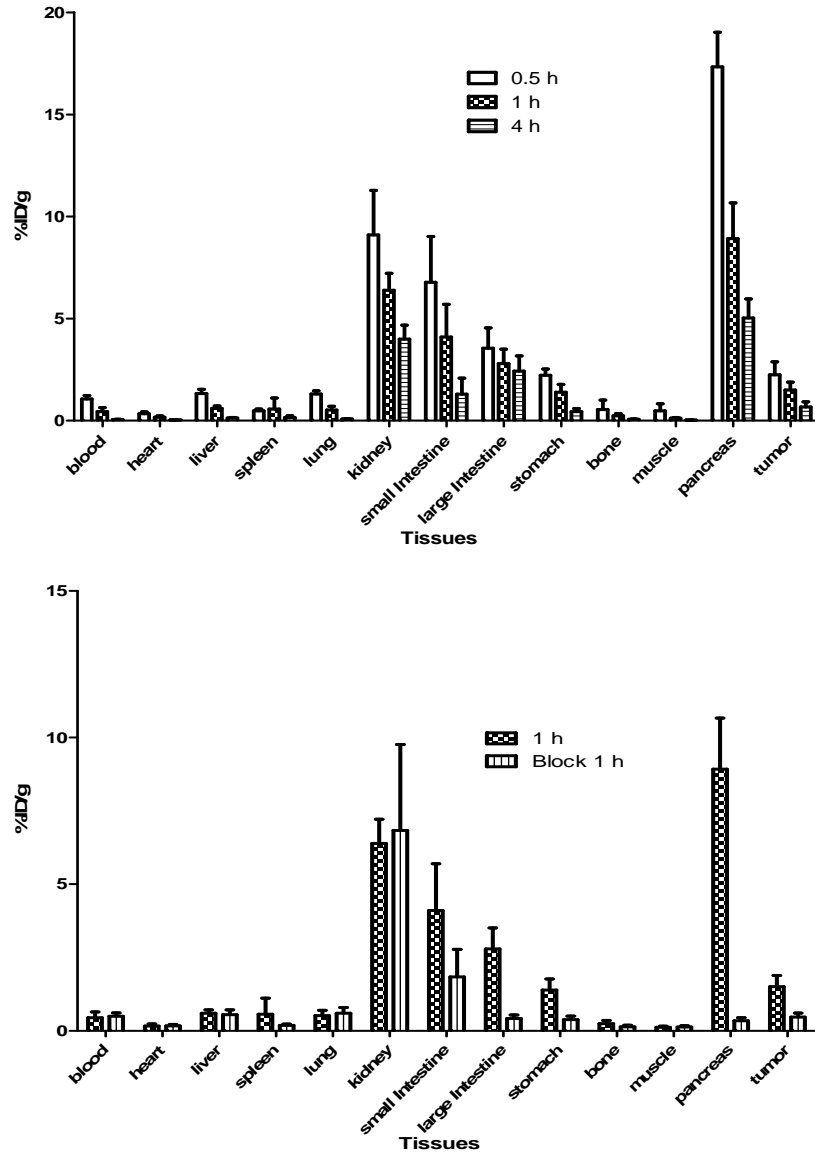
Figure 11. Organ uptake of ^{99m}Tc(HYNIC-Aca-BN(7-14))(Tricine)(TPPTS) in athymic mice bearing PC-3 human prostate cancer xenografts.

In conclusion, the present study indicated that ^{99m}Tc(HYNIC-Aca-BN(7-14))(Tricine)(TPPTS) is a suitable tracer for *in vivo* tumour targeting. Work is in progress to implement this radiotracer for clinical studies.

3.2 In vitro studies

3.2.1 Cancer cell killing by sigma ligands and sTRAIL: monitoring synergy with PET

In cooperation with Dept. Medical Biology

We examined whether sub-toxic amounts of haloperidol (HAL) or rimcazole (RIM), sigma ligands which potentiate the anti-tumor actions of cytostatics, and sTRAIL (a tumor-selective pro-apoptotic protein) can synergistically kill human cancer cells. We assessed early metabolic responses in tumor and healthy cells and we determined if the uptake of metabolic PET tracers reflects synergistic cell killing.

A375M (human melanoma) and HUVEC (human umbilical cord endothelial) cells were incubated (24h) with sTRAIL, RIM, RIM + sTRAIL, HAL or HAL+ sTRAIL, respectively. Cytotoxicity was assessed by cell counting. Cellular metabolism was quantified using ^{18}F-FDG, ^{18}F-FLT and ^{11}C-choline. Cellular ATP levels were measured and cell cycle analysis was performed. A cooperativity index (CI) smaller than 0.9 indicates synergy.

Sigma ligands and sTRAIL synergized in A375M ($CI_{HAL} = 0.51$; $CI_{RIM} = 0.71$) but not in HUVEC (100% survival). Sigma ligand-treated A375M cells synchronized at G1/G0 in a dose-dependent manner. Addition of sTRAIL did not significantly change the G1/G0 population. Cellular ATP decreased significantly, by 37%, 45-54% and 88-92% after sTRAIL, σ-ligand and co-treatment, respectively. FDG uptake reflected synergistic cell killing ($CI_{HAL} = 0.54$; $CI_{RIM} = 0.55$), in contrast to the cellular uptake of FLT or choline.

In conclusion, combination therapy with sigma ligands and sTRAIL resulted in synergistic decreases of cell number and in corresponding increases of cellular glucose transport. However, uptake of the PET tracers FLT or choline did not reflect cooperativity.
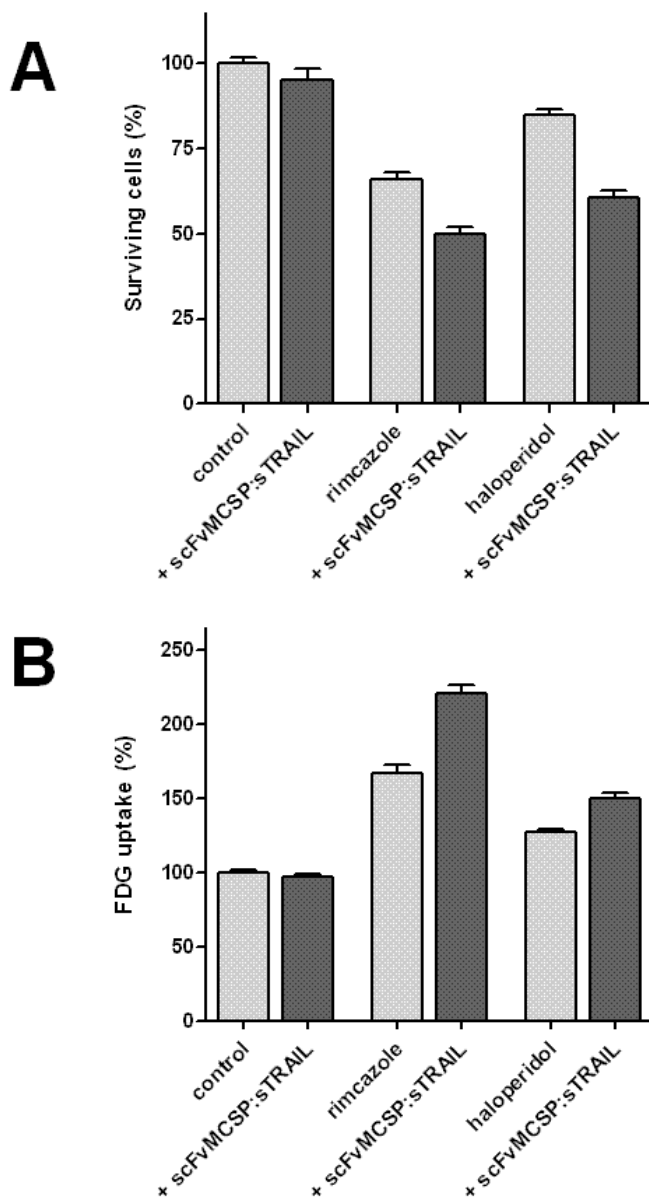
Co-treatment of A375M with scFvMCSP:sTRAIL (0.1 ng/ml) and sigma ligands (38 µM haloperidol or 15 µM rimcazole) results in synergistic decreases of cell number (A) and increases of FDG uptake/cell (B)

Figure 12.

3.3 Radiochemistry

3.3.1 [^{18}F]FEAnGA: a PET tracer for extracellular β-glucuronidase (GUS)

In cooperation with Dept. Therapeutic Gene Modulation, University Center of Pharmacy, Groningen

High levels of extracellular β-glucuronidase (GUS) are observed in tumors, infections and diseases with an inflammatory component such as arthritis. The enzyme breaks down the extracellular matrix, kills bacteria and produces tissue damage. Beta-glucuronidase has been exploited to convert nontoxic prodrugs to cytostatic drugs at the target site. HMR1826 is an example of such a prodrug, in which the cytostatic drug doxorubicin is linked to a glucuronic acid moiety (Florent *et al*. J Med Chem 1998; **41**:3572). PET imaging could be a useful tool to optimize GUS-based prodrug therapies. Here, we describe the first PET tracer for extracellular GUS, [^{18}F]FEAnGA **3**, in which the doxorubicin moiety in HMR1826 is replaced by a 2-[^{18}F]fluoroethylamine ([^{18}F]FEA **2**) group (see Figure 13). GUS is expected to cleave the glucuronic acid moiety from the tracer and to release [^{18}F]FEA, which will be trapped in tissue by non-specific binding.

[^{18}F]FEA was labeled by fluorination of *N*-[2-(toluene-4-sulfonyloxy)-ethyl]-phtalimide, followed by deprotection of the amine with hydrazine (Tewson, Nucl Med Biol 1997; **26**:1891). [^{18}F]FEAnGA **3** was obtained by alkylation of precursor **1** (Duimstra *et al*. J Am Chem Soc 2005; **127**:12847) with [^{18}F]FEA, followed by deprotection of the sugar moiety with NaOMe / NaOH. The product was purified by HPLC. The stability of the tracer in PBS and rat plasma was determined by radio-TLC. The cleavage of tracer **3** by either *Escherichia coli* or bovine liver GUS was measured with UV spectrophotometry and radio-TLC, in order to determine V_{max} and K_m. Unlabeled *p*-nitrophenyl β-glucuronide (PNPG) was used as a reference compound in the enzymatic studies.

Radiolabeling of the β-glucuronidase tracer was achieved by synthesis of [^{18}F]FEA in 25-40 % decay-corrected yield, followed by conversion of this intermediate into [^{18}F]FEAnGA. After HPLC purification, [^{18}F]FEAnGA was obtained in 10-20% overall radiochemical yield (corrected for decay, based on [^{18}F]fluoride) with a total synthesis time of 150 min. The lipophilicity of [^{18}F]FEAnGA was shown to be about 10-fold lower than the cleavage product [^{18}F]FEA (log P values -1.61 ± 0.01 and -0.69 ± 0.02 respectively). Because of its low lipophilicity, the tracer is expected not to penetrate the cell membrane and thus to be selective of *extracellular* β-glucuronidase.

[^{18}F]FEAnGA was stable in PBS and in rat plasma for at least 3 h. FEAnGA is a substantially better substrate for both *E.coli* and bovine liver GUS than the reference compound PNPG (Table 7). Radiolabeled [^{18}F]FEAnGA was also rapidly cleaved by either *E.coli* or bovine liver GUS, resulting in complete cleavage of the tracer to [^{18}F]FEA within 10 to15 min of incubation.

In conclusion, [^{18}F]FEAnGA was labeled with fluorine-18 in good yield. The novel radiopharmaceutical was stable and proved to be a good substrate of both *E.coli* and

bovine liver GUS. These results warrant further evaluation of [¹⁸F]FEAnGA in animal studies.
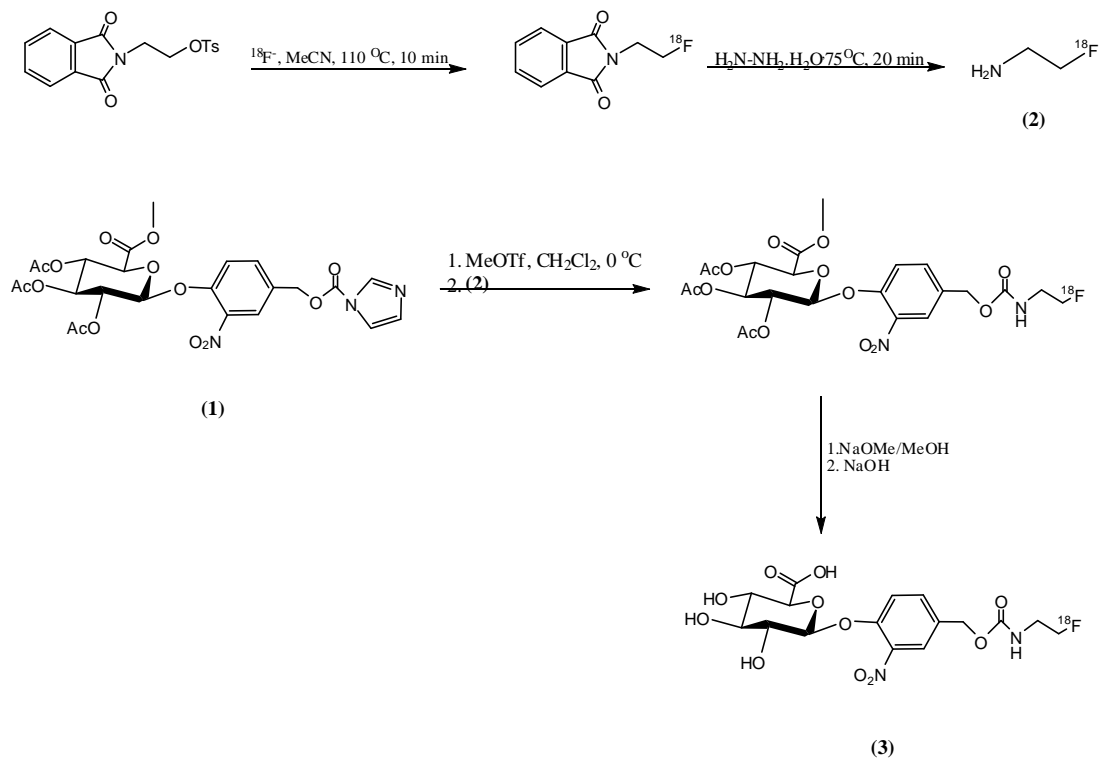
Figure 13.

Table 7. Kinetics of the cleavage of [¹⁸F]FEAnGA by various enzymes

Enzyme	Substrate	K_M (μM)	V_{max} (μmolmin^{-1}mg^{-1})	kcat (s^{-1})	k_{cat}/K_M (10^6 M^{-1}s^{-1})
Escherichia coli GUS	PNPG	322	670	3,236	10.0
	FEAnGA	206	7,538	36,415	176.5
Bovine liver GUS	PNPG	114	5	24	0.2
	FEAnGA	15	28	136	8.8

TECHNOLOGY

4.1   Cyclotron

Statistics regarding radionuclide production of the cyclotron (Scanditronix MC-17) are presented in Fig.14 and Table 8. The figure gives an overview of cyclotron use in 2008. Average values for the whole period of use since 1992 are presented in the Table. In 2008 all repairs could be performed within the scheduled time for maintenance. Maintenance work was done every Monday morning before 8:30 a.m.
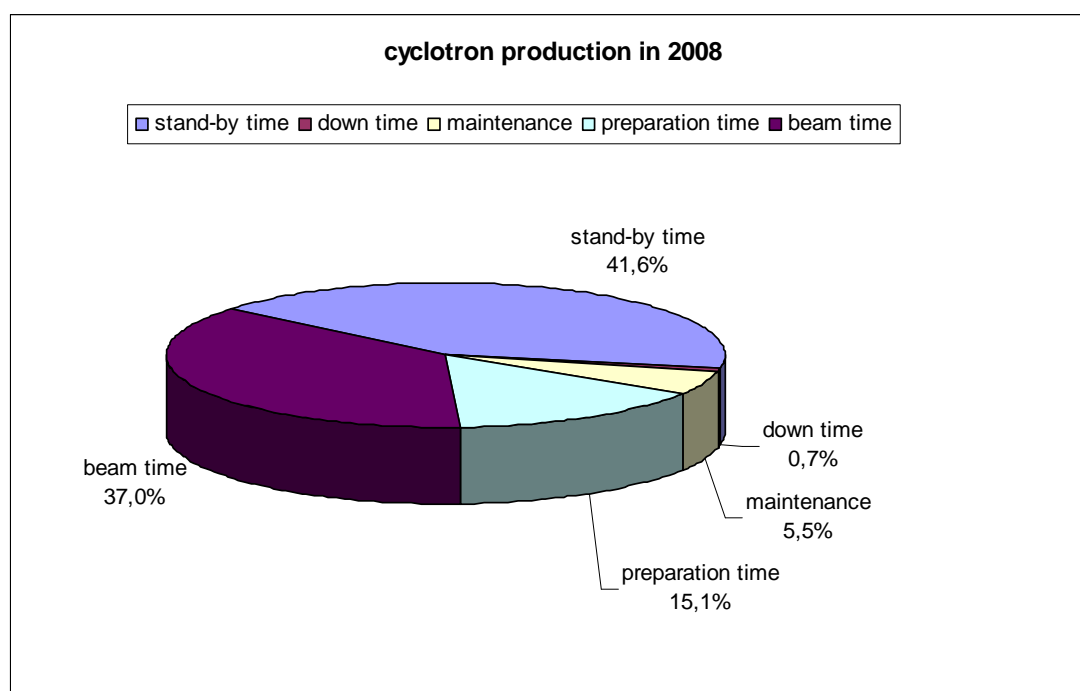
Figure 14: Cyclotron use in 2008

Table 8: Average values for cyclotron use (2008 and previous period)

	Average value (1992-2007)	2008
Number of beams	1876	1507
Beam time (hours)	574	847
Preparation time (hours)	242	347
Maintenance (hours)	202	126
Unscheduled down time (hours)	88	17
Stand-by time (%)	50	42

Down time of the cyclotron in 2008 was 0.7 % (or 17 h), significantly lower than the average value since 1992 (3.8 ± 2.2 %, or 84 ± 50 h) and the lowest number in the entire 17-year period (Figure 15). Causes underlying the 17 hours of down time in 2008 are listed in Table 9.
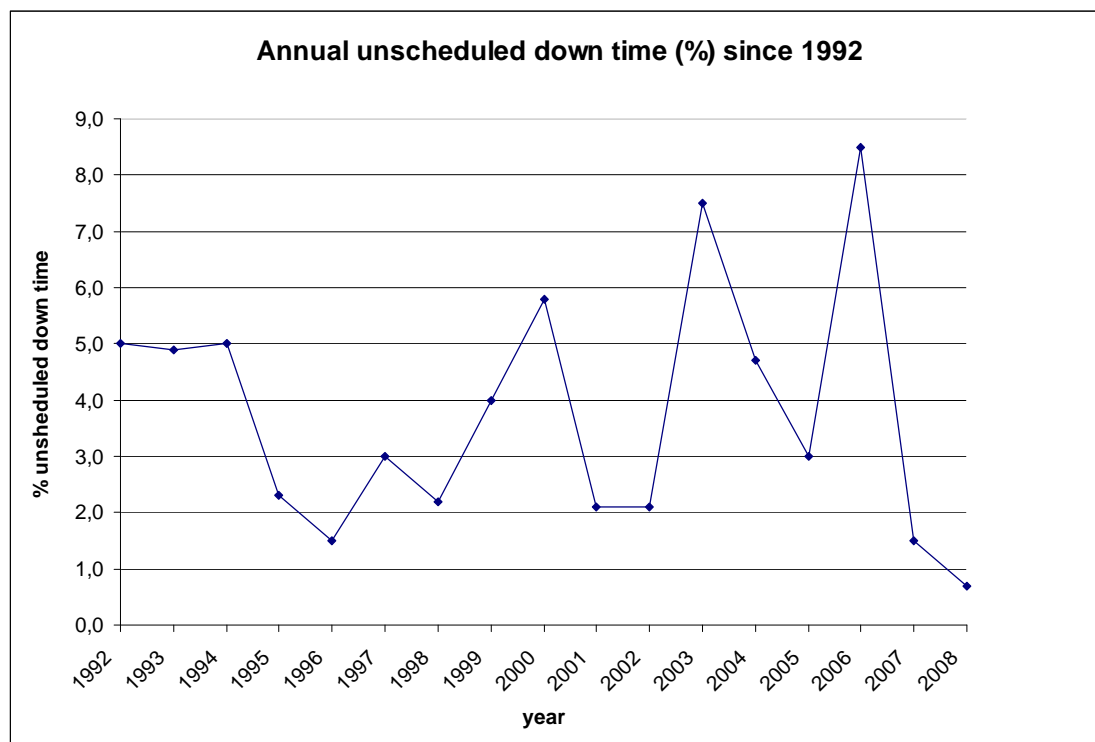
Figure 15. Yearly unscheduled down time (%) since the installation of the cyclotron

Table 9. Cyclotron failures in 2008

Subsystem	Hours
General (general supply hospital)	-
Magnet (gradient coils)	-
RF-system (APS)	-
Ion-source	-
Extraction	11
Diagnostic	-
Vacuum	-
Control	-
Target	6
Process system	-
Water cooling of cyclotron	-

One hundred and twenty-six hours were required for maintenance, which included replacement or modification of the following parts:

- Upgrading of PLC software (step-5 program)
- Festo air pressure valves
- Replacement of the tubing of the ^{13}N target
- Replacement of 2 valves of the filling system for the fluorine targets
- Replacement of the isolators of the deflector (3x)
- Installation of a new spark plate of the deflector
- Installation of new valves for the gas of the ion source
- Replacement of all teflon/PEEK tubing from target to hot cells
- Replacement of the high voltage throughput system of the deflector (Figure 16)
- Foils of the ^{18}F$_2$ target (5x)
- Installation of a new pump for helium cooling of the targets
- Replacement of the membranes of the pump for helium cooling (1x)
- O-ring of the target-chamber (3x)
- Bellow of the Faraday cup (2x)
- Installation of a ceramic pump for filling of the fluoride target.
- Replacement of the basement of the Faraday cup
- Replacement of the cathodes of the ion source (4x)
- Replacement of the 5 Volt Power Supply
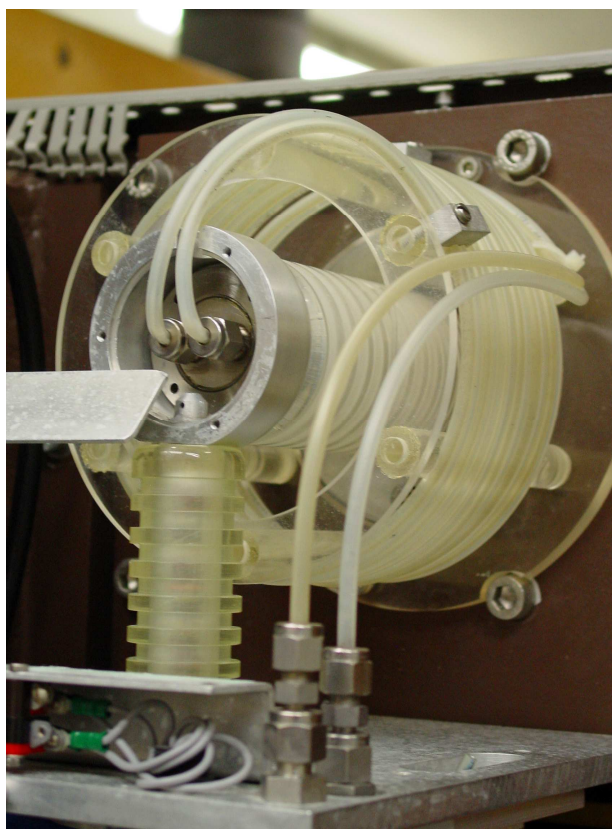
Figure 16. Photograph of the high voltage throughput system of the deflector

Figure 17. An inside view of the cyclotron during maintenance

4.2 Gamma cameras and clinical PET scanners

At present, there are four gamma cameras in our Department: an Orbiter, a Diacam, a MultiSpect2 and an Ecam, so two single and two dual head systems. The Ecam is the most recent camera showing the fewest problems but the other three systems need regular care to keep them up and running.

Of the two PET scanners which are present (both ECAT HR+), the oldest one needs more attention than the regular service.

During 2008, a European Tender for four new gamma cameras and one new PET/CT with the complementary computer platform was evaluated and the Board of Directors was advised to replace all cameras and computers by a Siemens platform. This advice was acted upon and the following configuration will be installed in 2009:

2 gamma cameras, type SymbiaS (dual head gamma camera systems)
1 SPECT/CT, type SymbiaT2 (dual head gamma camera with a dual slice CT)
1 SPECT/CT, type SymbiaT16 (dual head gamma camera with 16 slice CT)
1 Biograph mCT (PET/CT system with a 64 slice CT)
1 computer platform for data analysis

All these will be installed in 2009, but with the necessary precautions since the daily clinical routine should continue. The SymbiaT16 allows the initiation of new developments in cardiology. With the SymbiaT2, a better specification of lesions can be provided combined with a diagnosis, which is especially important in oncology

and orthopedics. Installation of he Biograph mCT will significantly increase the capacity for whole body FDG scans.

After the installation of this novel equipment, the Department will - from a technical point of view - enter a new era.

4.3 Cameras for small animal imaging

In 2008, a U-SPECT II (microSPECT camera for small animal imaging) was installed at the department of NMMI. The system was installed in May. After this month several tests were performed. The resolution and sensitivity of the system with the standard mouse collimator (0.6 mm resolution) were within specifications. In June, the system was ready for the first experiments.

During the summer of 2009, several adaptations were made to the scanner room to prepare this for animal scanning. An isoflurane anesthesia system and a cabinet for storage of animal beds and collimators were installed. In December 2009, the U-SPECT II system was expanded by the purchase of an additional rat collimator (1 mm resolution) with funding of the Faculty of Medicine. When large areas of the body must be examined, the rat collimator has a higher sensitivity than the mouse collimator. Therefore the rat collimator may also be considered for whole-body imaging of mice. In 2008, several test scans were made in rodents, using commonly available SPECT radiopharmaceuticals. In 2009, the interest of researchers for the U-SPECT II system is expected to grow. Several research protocols approved by the Animal Ethics Committee (DEC) will then be initiated.

The MicroCAT II (micro CT camera for small animal imaging) did not show any down time in 2008. This system is less frequently used by investigators than the MicroPET Focus 220. Most uCT images are made in combination with a µPET scan. Total usage of the uCT facility amounted to 300 hours (average occupancy during working hours nearly 20%). Since there was much demand from researchers for co-registration of high-resolution CT images and µPET images, a program was written to convert reconstructed CT slices to volumes that can be read by Inveon Research Workplace (IRW).

The MicroPET Focus 220 showed very little down time during 2008. On occasion, the system locks up after which a reboot of the camera is required. There is no indication that the frequency of this phenomenon is increasing. Since a reboot of the camera often resulted in the blowing of a fuse, we have installed a surge-limiting mains filter. After installation of this filter, the fuse did not blow any more. Because image reconstructions are heavy load for the acquisition computer, it was decided to add a dedicated second computer for reconstruction of µPET data. This computer will be added to the system in 2009. The µPET camera was very frequently used in 2008. Total usage amounted to 1400 hours (average occupancy during working hours nearly 85%).

A µPET reconstruction artifact was discovered and solved. An analysis of scans which were simultaneously made of two different animals revealed that data reconstruction with zoom results in unpredictable behavior if there is a significant

amount of radioactivity outside the reconstructed area. In particular, large deviations were found if the injected amount of radioactivity in the two animals was very different. In such a case, the calculated radioactivity values in the image of the animal with the lowest injected activity were too high, and the error could be as large as 30%. A solution was found by reconstructing the image at a lower zoom factor, incorporating all areas with radioactivity in the image, and with a larger matrix. A program was written to finally split up the combined image in two separate images for the two individual animals.

## 4.4 Quantitative Monitoring of Leakage during Chemotherapeutic Limb Perfusion

Irresectable extremity limb malignancy can be treated by hyperthermic isolated limb perfusion (HILP) with chemotherapeutic agents, followed by additional surgery. During this procedure, the perfusion of the extremity is isolated from the systemic circulation and is regulated separately. Then, a very high concentration of chemotherapeutics is administered to the blood circulation of the extremity. In order to prevent exceeding the maximally tolerated systemic levels of the chemotherapeutics, continuous monitoring of the leakage of the chemotherapeutics into the systemic circulation is mandatory.

The present perfusion detector used for HILP procedures is strongly outdated. Moreover, hardware components cannot be replaced in case of malfunction, jeopardizing continuity for these procedures. Therefore, a new detection system was developed. Moreover, a new algorithm for the quantitative real-time monitoring of leakage, insensitive to detector displacement, is developed. The detector system is shown in Fig 18.

After surgical isolation of the extremity blood circuit has been accomplished a scintillation probe is placed over the blood pool of the patient's heart. Then, a low-level dose of ^{131}I-HSA [0.5 MBq] is administered to the systemic circulation ($A_{I,S}(0)$) in order to establish a baseline count level. Also, an amount of ^{99m}Tc pertechnetate [5.0 MBq] is injected into the systemic circulation ($A_{T,S}(0)$) which labels the erythrocytes in vivo. Once the systemic radioactivity is distributed throughout the vascular circulation, a relatively high-dose of ^{131}I-HSA [5.0 MBq] is administered to the isolated perfusion circuit ($A_{I,E}(0)$). As a result of the high activity concentration present in the extremity circulation, any leakage from the extremity to the systemic circuit will cause an increase in the activity concentration in the systemic circulation. A schematic presentation of the situation is shown in Fig 19.

Figure 18: Detector system.
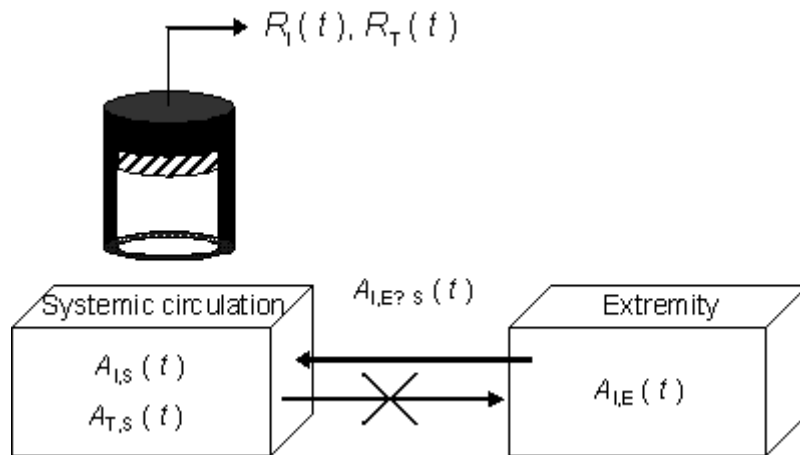
Figure 19. Schematic presentation of isolated limb perfusion

The classic method to quantify the leakage factor is given by

$$LF(t) = 1.5 \frac{A_{I,S}(0)}{A_{I,E}(0)} \left(\frac{R_I(t)}{R_I(0)} - 1 \right) \times 100\% \, ,$$

with $A_{I,S}(0)$ and $A_{I,E}(0)$ the ^{131}I-HSA activity injected into the main and extremity circulation respectively and $R_I(t)$ the ^{131}I count rate at time t. The factor 1.5 is a correction for the different blood volumes in the main and extremity circulations.

The new method to quantify the leakage factor is given by

$$LF(t) = 1.5 \frac{A_{I,S}(0)}{A_{I,E}(0)} \left(\frac{R_I(t)/R_T(t)}{R_I(0)/R_T(0)} - 1 \right) \times 100\% \, ,$$

with $R_I(t)$ the ^{99m}Tc count rate at time t. An advantage of the new method is that the determined leakage factor is not affected by detector movement. From experiments simulating detector movement it is shown in Fig 20 that detector movement during a perfusion measurement can strongly affect leakage value determined with the old method, but not the new method.
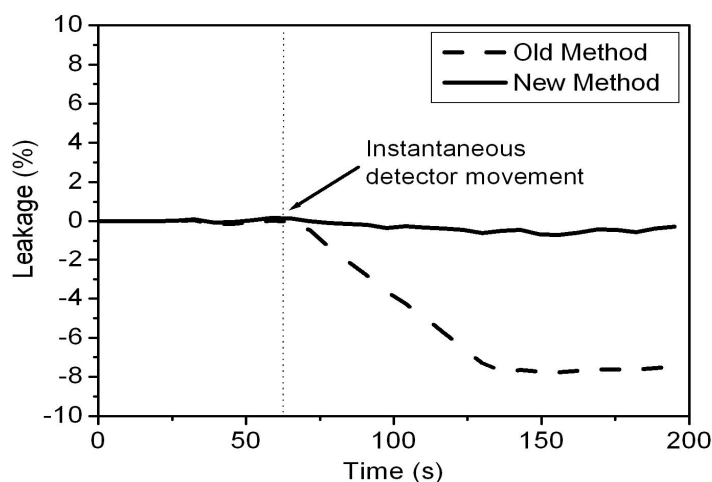
Figure 20. Comparison between the old and new method from measurements simulating detector movement.

However, a requirement for using the new method is that both tracers are stable and not excreted from the vascular circuit during perfusion. At the moment, the stability of the in vivo labeling of ^{99m}Tc to the erythrocytes is questionable and requires further investigation.

4.5   Click for PET: Development and Application of Accelerated 1,3-dipolar Cycloadditions of Azides and Alkynes to [^{18}F]-Positron Emission Tomography

In cooperation with Stratingh Institute for Chemistry, University of Groningen

The discovery by Sharpless in 2002 that copper (I) catalyzes the 1,3-dipolar cycloaddition of azides and alkynes to form 1,4- disubstituted triazoles (CuAAC) strongly contributed to the popularization of 'click' chemistry (V.V. Rostovtsev, L.G. Green, V.V. Fokin and K. B. Sharpless, *Angew. Chem. Int. Ed.,* 2002, 41, 2596; R. Huisgen in *1,3-Dipolar Cycloaddition Chemistry* (Ed.: A. Padwa), Wiley, New York, 1984, pp. 1-176).

Our interest in applying this reaction to time sensitive [^{18}F]-radiolabelling methodology for PET led us to consider recent advances in ligand accelerated CuAAC. The rate of the ligand free reactions can hinder the application of click chemistry to [^{18}F]-radiolabelling.

Phosphoramidites are used as monodentate ligands for copper in a number of transformations and have demonstrated ligand accelerating effects (D.J. Berrisford, C. Bolm, and K.B. Sharpless. *Angew. Chem. Int. Ed.,* 1995, **34**, 1059). They are inexpensive, stable and easily accessible (B.L. Feringa, *Acc. Chem. Res.*, 2000, **33**,

346). We report the first example of dramatic rate acceleration of the [3+2] cycloaddition of azides and alkynes using phosporamidite ligands and application of the methodology to PET-imaging analogues.

A thorough screening of phosphoramidites and related ligands revealed that MonoPhos, the simplest BINOL based phosphoramidite (Table 10, entry 2) decreases the reaction time of a standard click reaction from 24 h to 2 h. Similar rate accelerating effects were seen with other phosphoramidites. A selection of the results is delineated in Table 10.

Table 10. Effect of Ligand on the Copper (I)-Catalyzed [3+2]Cycloaddition of Phenylacetylene and Benzyl Azide
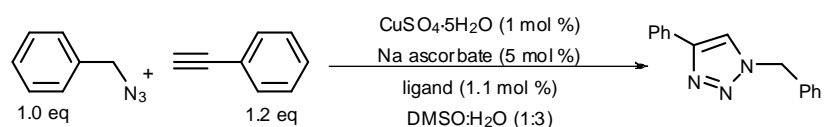
	Ligand	Time (h)	Yield (%)
1	-	30	88
2		2	98
3		2	90
4		2	93
6		7	86
8		4	85
9		10	75
10		15	58
12		10	93
13		4	78

We proceeded with MonoPhos to investigate other reaction parameters. Varying the concentration of the azide and the alkyne showed that a fourfold excess of either improves rates; after 10 min conversions were 47 and 80 %, respectively.

Experiments were also conducted to determine the effect of catalyst loading upon the rate, demonstrating, as expected that an increase in the copper loading translates into a decreased reaction time.

As a copper source for the CuAAC, $CuSO_4 \cdot 5H_2O$ in combination with the reducing agent sodium ascorbate is overwhelmingly favoured. Although Cu(I) salts can also be used, they require an equivalent of nitrogen containing base to promote the reaction (D.J. Berrisford, C. Bolm, and K.B. Sharpless. *Angew. Chem. Int. Ed.*, 1995, **34**, 1059). We anticipated that the phosphoramidite might stabilize the catalytically active Cu(I) oxidation state. Our experiments proved our hypothesis to be correct; we found similar rates and yields in our reaction using Cu (I) halide salts, and no evidence of the expected side products.

Substrate screening showed that various functional groups, including acids, halides, esters, and amines were tolerated in both substrates. Reactions remained fast and high yielding highlighting system versatility.

Testing our methodology for radiolabelling, we synthesized [^{18}F]-fluorinated 1-ethynyl-4-(fluoromethyl)benzene (Fig.21). After fluorination, it was ligated to benzyl azide. Full conversion was detected after 10 min (HPLC and radio-TLC). Under identical conditions but in the absence of ligand, only minor conversion to the triazole was detected (<20 %).
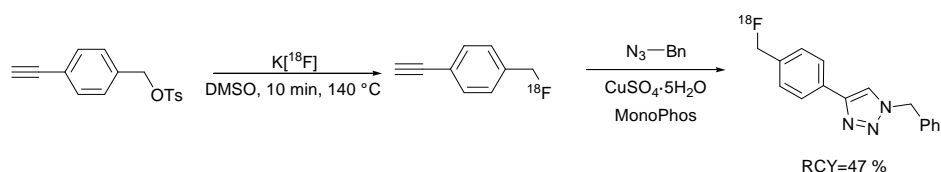
Figure 21. Synthesis of [^{18}F]-labelled triazole

We have applied phosphoramidite copper complexes to the azide alkyne cycloaddition and found that they enhance the rate of the reaction and stabilize the copper(I) oxidation state. The system is versatile and functional group independent. The methodology has been applied to the ligation of small [^{18}F]-labelled prosthetic groups to a model azide.

## 4.6 Exploration of reaction parameters in F-18 click chemistry

In cooperation with Stratingh Institute for Chemistry, University of Groningen, Groningen, The Netherlands.

The Huisgen 1,3-dipolar cycloaddition of azides and alkynes using copper-I as catalyst, has now been recognized as the most commonly applied 'click reaction'. This reaction has been widely applied to many bioorganic and medicinal research fields, because it proceeds under mild and tolerable conditions, in aqueous media, at neutral pH, and at room temperature, all within a reasonable reaction time. We report herein the first example of dramatic rate acceleration of the 1,3-dipolar cycloaddition using phosporamidite ligands and the application of the developed methodology to positron emission tomography imaging precursors. Phosphoramidites prove to be excellent, high yielding, easily recovered ligands.

Preliminary studies to find an optimal condition of 1,3-dipolar cycloaddition for the two-step F-18 labeling procedure were performed in which 1,3-dipolar cycloaddition of 4-methoxybenzyl azide and phenyl acetylene was employed as a model reaction. In a CuSO4/ Na-ascorbate system, aqueous DMSO was the best reaction media regardless of the water content.

In addition, monodentate phosphoramidite ligands are used to accelerate the Huisgen 1,3-dipolar cycloaddition rapidly yielding a wide variety of functionalized 1,4-disubstituted-1,2,3-triazoles. Phosphoramidites are used as monodentate ligands for copper in a number of stereoselective transformations and have demonstrated strong ligand accelerating effects. Cu(I) and Cu(II) salts both function as the copper source in aqueous solution to provide excellent yields.

To test our methodology on the required time scale of radiolabelling, we designed a small azido prosthetic group, [^{18}F]-fluorinated 1-azido-4-fluorobutane (Scheme 1) and [^{18}F]-fluorinated 1-ethynyl-4-(fluoromethyl)benzene (Scheme 2).
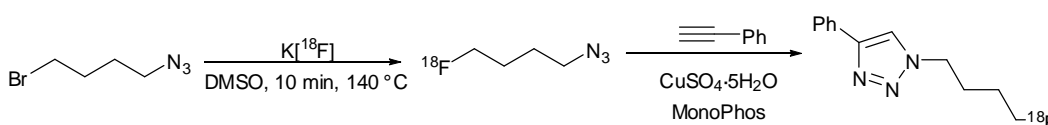
Scheme 1 Synthesis of [18F]-labelled triazole using [18F]alkyl azide
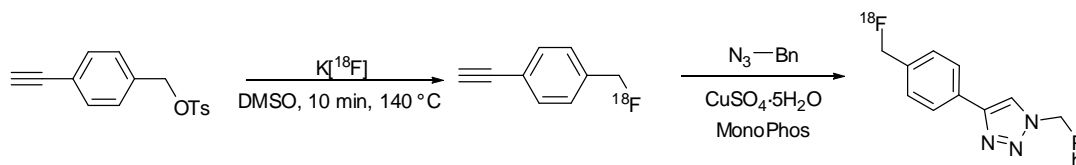
Scheme 2 Synthesis of [18F]-labelled triazole using [18F]acetylene

After fluorination, the tag was attached to its complementary cold acetylene or azide in the presence of CuSO4·5H2O and MonoPhos. Further optimization reaction was performed by varying the amount of acetylene from 0.01 mg to 0.5 mg (Fig. 23) or azide from 0.05 mg to 0.1 mg, to find the optimal yield of reaction in DMSO/H2O (1/3).

Full conversion to the labelled triazole was detected after 10 min (as determined by HPLC and radio-TLC). In the absence of MonoPhos under identical conditions, only minor conversion to the triazole product was detected (<20 %) (Figure 22).

With regard to F-18, 1mol % of CuSO4 showed a sufficient catalysis effect within a short time (Figure 23).
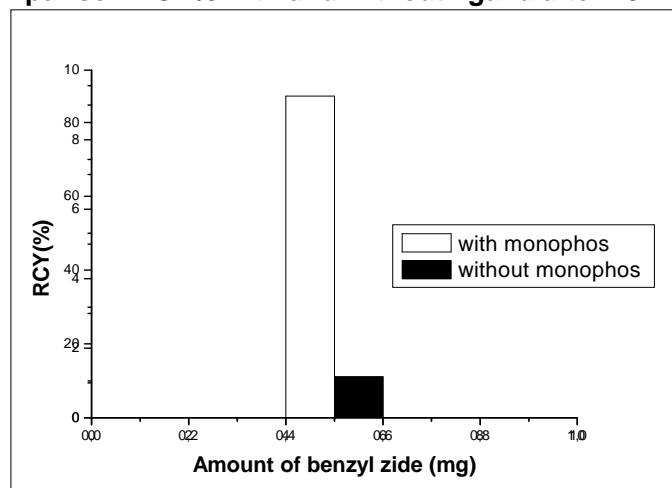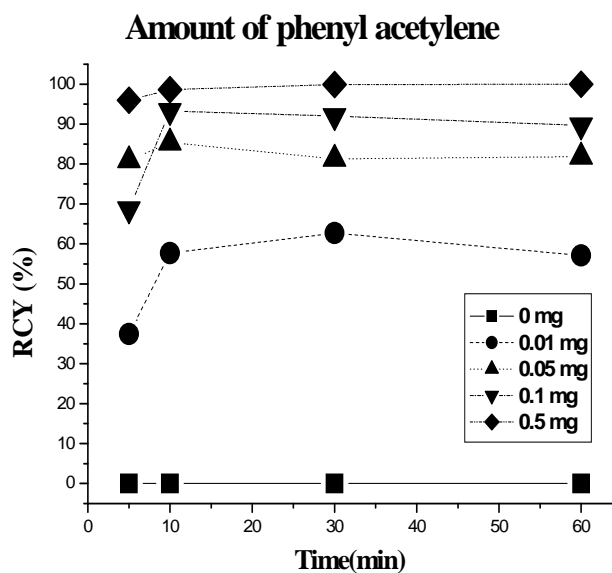
Figure 22

Figure 23

In conclusion: the Cu(I)-catalyzed, 1,3-dipolar cycloaddition 'click chemistry' reaction was applied successfully to the synthesis of small, F-18-labeled molecules, and an optimal condition was developed for one-pot, two-step reaction after purification by semipreparative HPLC. The [^{18}F]fluoroalkyne and azide were

prepared in yields ranging from 36% to 81%. Conjugation of [^{18}F]fluoroalkynes and azides to various amount (> 0.01 mg) of acetylenes or azide with via CuI mediated 1,3-dipolar cycloaddition yielded the desired ^{18}F-labeled products in 10 min with yields of 54–99% and excellent radiochemical purity 99%. The total synthesis time was 30 min from the end of bombardment.

4.7   Simplified   and   automated   preparation   method   for ^{18}F-fluoromethylcholine
using a new synthesis module

In cooperation with Universitaetsklinikum Zurich, Switzerland, and Veenstra Instruments, Joure, The Netherlands

Our aim was development of a fast, reproducible preparation method of ^{18}F-fluoromethylcholine with a new synthesis module developed by Veenstra Instruments. The method should be simplified as much as possible while maintaining reproducibility and high yields for clinical studies. Critical steps to be solved were radiochemical yield of ^{18}F-fluoromethylbromide and its conversion to the corresponding ^{18}F-fluoromethyltriflate. The reactivity of both ^{18}F-synthons with dimethylethanolamine to ^{18}F-Fluoromethylcholine was investigated (Figure 24).

(1) Fluoride
(2) Fluorobromomethane
(3) Fluoromethyltriflate
(4) Fluoromethylcholine
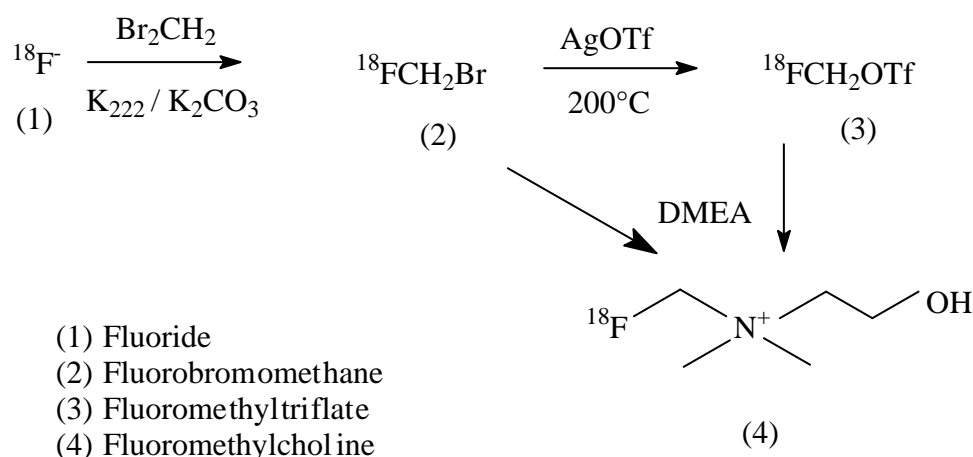
Figure 24

The production of ^{18}F-Fluoromethylcholine (Iwata et al., *Appl.Radiat.Isotopes* 57:347,2002; DeGrado et al., *Cancer Res* 61:110,2001) consists of 4 steps: 1) Work-up of ^{18}F-Fluoride; 2) Preparation of the intermediate ^{18}F-Fluorobromomethane; 3) Conversion to ^{18}F-Fluoromethyltriflate and 4) Reaction with the choline precursor dimethylethanolamine (DMEA) to ^{18}F-Fluoromethylcholine. These 4 steps were evaluated and optimised. The elution and drying of ^{18}F-fluoride was simplified to a single step resulting in a faster azeotropic evaporation. The reaction of ^{18}F-fluoride (1) with (50-60 µl) dibromomethane in 1 ml acetonitrile gave ^{18}F-Fluorobromomethane (2) which was purified by distillation through a series of 4 Silica SepPak plus cartridge with a 100ml/min flow. ^{18}F-Fluoromethyltriflate (3) was obtained by passing (2) through a silver triflate column with similar flow. The compound (2) or (3) was trapped on a C18 plus cartridge containing 50 µl DMEA. Reaction to ^{18}F-Fluoromethylcholine (4) was instantaneous and at RT. After washing

the C18 plus and CM accell light cartridge with 10 ml ethanol and 10 ml water, the product was eluted with 5 ml NaCl (0.9% solution) and passed through a 0.22-µm sterile filter (Millex LG; Millipore). Radiochemical purity was measured by analytical HPLC (Astec C18, 250 x 4.6 mm, 50mM Sodium borate / 100mM Sodium hydroxide (45/55) 1 ml/min, retention time = 4.4 min)

Production scheme for [^{18}F]-Fluoromethylcholine
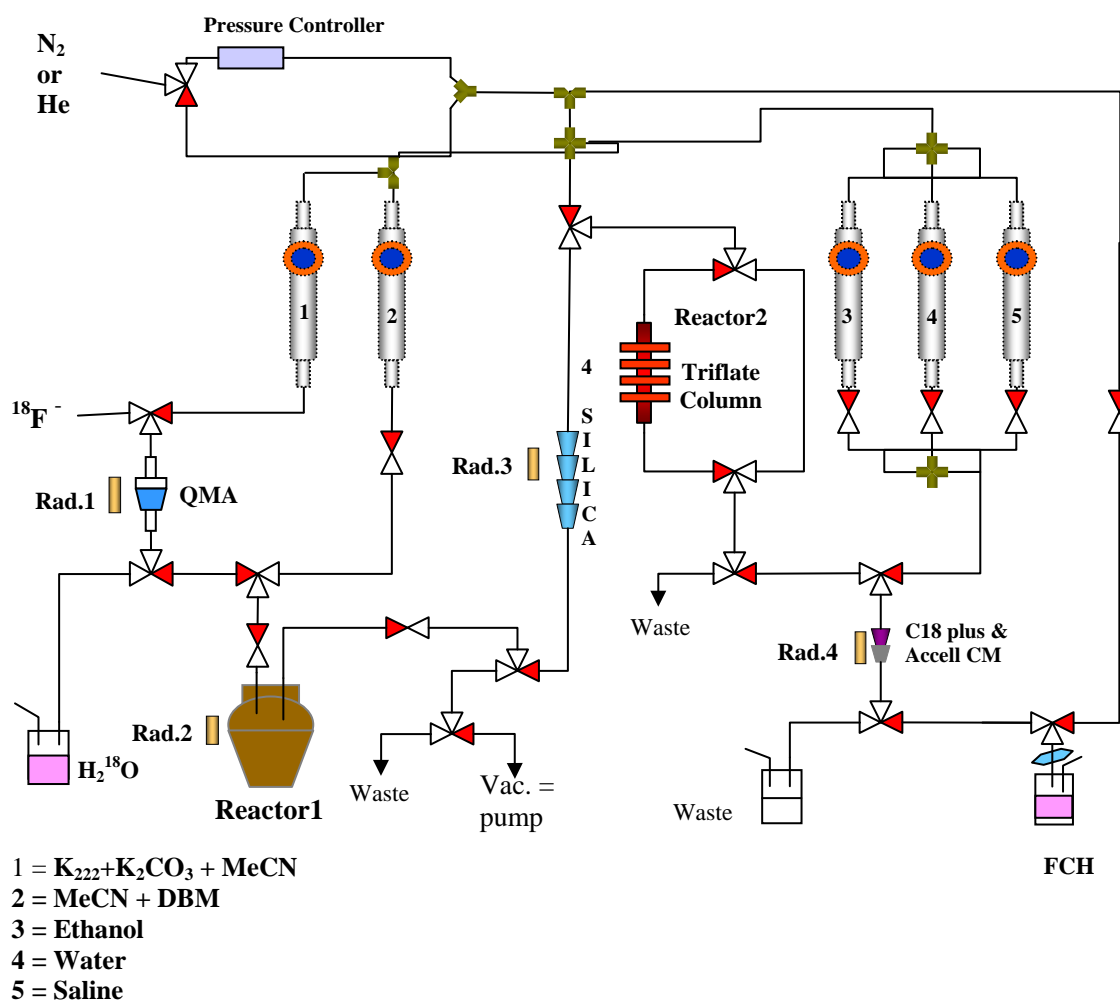
Figure 25

The elution and drying of (1) was simplified resulting in a 5 min. reduction of synthesis time. The yield of (2) was 40-55 %.The conversion of (2) to (3) was accomplished with an efficiency > 95%.The overall yield of (4) by reacting directly from (2) was 2-4%. The yield (4) formed from DMEA and (3) was 30–40 % overall. Total synthesis time was 29 – 32 min. Radiochemical purity > 95%. The concentration of DMEA was 50 mg/l and pH= 6.5 – 7.

In conclusion, the Veenstra ^{18}F-Fluoromethylcholine synthesis module produced ^{18}F-Fluoromethylcholine in a fast and simple manner according to Figure 26. The overall yields of the module are high. A single synthesis-run can produce a multi-dose vial product up to 10 GBq. The synthesis module can be used as a universal fluoromethylating unit.

Production of ^{18}F-Fluoromethionine and ^{18}F-Fluororaclopride is currently under investigation.

4.8 Radionuclide and radiopharmaceutical production

Production of the various radionuclides is summarized in Table 11. Fifteen PET radiopharmaceuticals were used for clinical and microPET studies in 2008. An overview of the tracer production since 1992 is given in table 12.

Table 11: Production of radionuclides in 2008

Nuclide	Irradiations	Irradiation time in h	Mean irradiation time (min)	Total activity (GBq)
^{15}O	30	1.5	3.0	239
^{13}N	158	18.2	6.9	1056
^{11}C	412	270.1	39.3	33671
^{18}F$^-$	465	201.0	25.9	12868
^{18}F$_2$	442	356.5	48.4	3784
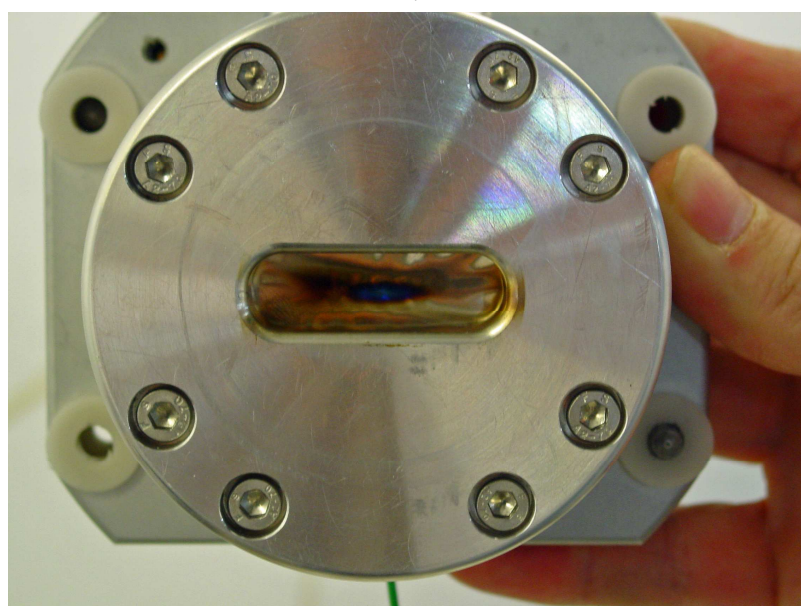
Figure 26, Front of an ^{18}F$^-$ target with the typical beam distribution of the MC-17

		2008	2007	2006	2005	2004	2003	2002	2001	2000	1999	1998	1997	1996	1995	1994	1993	1992
1.	^{18}F-FDG	256	262	225	272	251	239	219	222	200	210	191	147	101	95	105	110	82
2.	^{18}F-Dopa	144	128	134	99	104	66	50	59	42	50	41	-	-	-	-	-	-
3.	^{13}NH$_3$	120	144	73	50	210	160	200	222	461	381	432	566	536	313	273	204	225
4.	^{11}C-Raclopride	75	43	3	32	18	30	61	49	25	11	9	-	-	-	-	-	-
5.	^{11}C-Methionine	56	48	38	29	22	16	6	-	-	-	-	-	-	-	-	-	-
6.	^{11}C-Verapamil	44	4	30	40	-	2	24	14	15	10	-	2	-	-	-	-	-
7.	^{11}C-5-HTP	38	37	60	7	-	-	-	-	-	-	-	-	-	-	-	-	-
8.	^{11}C-Choline	38	21	28	30	26	22	13	22	57	35	31	-	-	-	-	-	-
9.	^{11}C-mHED	24	10	-	-	-	-	-	-	-	-	-	-	-	-	-	-	-
10.	^{11}C-PK11195	23	38	-	-	-	-	-	-	-	-	-	-	-	-	-	-	-
11.	H$_2$^{15}O	20	30	126	538	393	507	245	491	557	448	216	234	724	581	629	290	154
12.	^{18}F-FLT	17	19	8	12	31	46	56	11	-	-	-	-	-	-	-	-	-
13.	^{11}C-PIB	6	-	-	-	-	-	-	-	-	-	-	-	-	-	-	-	-
14.	^{18}F-NaF	3	2	3	16	19	-	-	-	-	-	-	-	-	-	-	-	-
15.	^{18}F-FES	3	-	-	-	-	-	-	-	-	-	-	-	-	-	-	-	-
16.	^{11}C-SA4503	-	1	21	3	-	-	-	-	-	-	-	-	-	-	-	-	-
17.	^{15}O-CO	-	-	-	4	-	-	-	-	1	5	4	4	11	17	-	-	-
18.	^{18}F-FMISO	-	-	-	2	2	2	2	2	-	-	-	-	-	-	-	-	-
19.	^{18}F-FHBG	-	-	4	1	-	-	-	-	-	-	-	-	-	-	-	-	-
20.	^{11}C-CGP12388	-	-	-	-	4	3	13	9	12	6	2	-	-	-	-	-	-
21.	^{11}C-Carvedilol	-	-	-	-	1	2	-	-	-	-	-	-	-	-	-	-	-
22.	^{11}C-Tyrosine	-	-	-	-	-	-	11	42	35	32	57	83	148	158	147	39	9
23.	^{18}F-MPPF	-	-	-	-	-	-	9	9	8	10	2	-	-	-	-	-	-
24.	^{11}C-Acetate	-	-	-	-	-	-	-	2	8	2	8	27	19	29	-	-	-
25.	^{11}C-VC002	-	-	-	-	-	-	-	-	-	-	2	4	2	-	-	-	-
26.	^{18}F-Carazolol	-	-	-	-	-	-	-	-	-	-	-	-	-	5	14	3	-
27.	^{11}C-Thymidine	-	-	-	-	-	-	-	-	-	-	-	-	-	7	13	13	-
28.	^{18}F-FESP	-	-	-	-	-	-	-	-	-	-	-	-	-	-	9	-	-
29.	^{11}C-CGP12177	-	-	-	-	-	-	-	-	-	-	-	-	-	-	16	6	-
30.	^{11}C-HCO$_3$$^-$	-	-	-	-	-	-	11	34	12	-	-	-	-	-	-	-	-

Table 12. Overview of radiochemical syntheses for clinical use since 1992

PUBLICATIONS 2008

5.1   Ph.D. theses and books

1. **Been LB.** Imaging Proliferation with [^{18}F]FLT-PET: Therapy Evaluation Studies. Ph.D. Thesis, University of Groningen, May 28, 2008. 141 pages. [Promotores: Hoekstra HJ, **Elsinga PH**]

2. Gielkens PF. Guided Bone Regeneration: The Influence of Barrier Membranes on Bone Grafts and Bone Defects. Ph.D. Thesis, University of Groningen, June 11, 2008. *[this Ph.D. student performed microCT scans in our institution, the results are reported in chapters 4, 5.1 and 6.1 of his thesis]*

3. **Koopmans KP.** Metabolic PET Tracers for Neuroendocrine Tumors. Ph.D. Thesis, University of Groningen, January 22, 2008. 143 pages. [Promotores: de Vries, EGE, **Jager PL,** co-promotores: Kema IP, **Elsinga PH**].

4. **Neels OC.** Tracer Development for Detection and Characterization of Neuroendocrine Tumors with PET. Ph.D. Thesis, University of Groningen, January 21, 2008. 129 pages. [Promotores: de Vries EGE, **Jager PL, Dierckx RA**]

5. **Popkov A.** Development of New Precursors for Asymmetric Preparation of Alpha-[^{11}C]methylamino Acids for PET. Ph.D. Thesis, University of Groningen, June 18, 2008. 200 pages. [Promotores: **Dierckx RA, Elsinga PH,** Lycka A]

6. Tan ES. Advanced Clinical Approaches in Complex Cardiovascular Disease. Invasive Options at the Crossroad of Ischemia, Heart Failure, and Arrhythmias. Ph.D. Thesis, University of Groningen, December 3, 2009. 144 pages. *[in this thesis, PET was employed as an imaging modality]*

5.2   Papers in international journals

1. Ananias HJ, De Jong IJ, **Dierckx RA, Van de Wiele C,** Helfrich W, **Elsinga PH**. Nuclear imaging of prostate cancer with gastrin-releasing-peptide-receptor targeted radiopharmaceuticals. Curr Pharm Des. 2008;14(28):3033-3047.

2. **Antunes IF,** Haisma HJ, **de Vries EF.** Tumor-specific activation of prodrugs: is there a role for nuclear medicine? Nucl Med Commun. 2008;29(10):845-846.

3. Bakker NA, van Dijk JM, **Slart RH,** Coppes MH, van Imhoff GW, Verschuuren EA. Extradural thoracic spinal cord compression: unusual initial presentation of post-transplant lymphoproliferative disorder. J Heart Lung Transplant. 2008;27(10):1165-1168.

4. Bartels AL, **Willemsen AT,** Kortekaas R, de Jong BM, de Vries R, de Klerk OL, van Oostrom JC, Portman A, Leenders KL. Decreased blood-brain barrier P-glycoprotein function in the progression of Parkinson's disease, PSP and MSA. J Neural Transm. 2008;115(7):1001-1009.

5. Beerens AM, Rots MG, Bermudez B, **de Vries EF,** Haisma HJ. Secretion of thymidine kinase to increase the effectivity of suicide gene therapy results in the loss of enzymatic activity. J Drug Target. 2008;16(1):26-35.

6. Belonje AM, Voors AA, van Gilst WH, Anker SD, **Slart RH,** Tio RA, Zijlstra F, van Veldhuisen DJ. Effects of erythropoietin after an acute myocardial infarction: rationale and study design of a prospective, randomized, clinical trial (HEBE III). Am Heart J. 2008;155(5):817-822.

7. Boellaard R, Oyen WJ, Hoekstra CJ, Hoekstra OS, Visser EP, **Willemsen AT**, Arends B, Verzijlbergen FJ, Zijlstra JM, **Paans AM,** Comans EF, **Pruim J.** The Netherlands protocol for standardisation and quantification of FDG whole body PET studies in multi-centre trials. Eur J Nucl Med Mol Imaging. 2008;35(12):2320-2333.

8. **Brouwers AH**, Mulders PF, Oyen WJ. Carbonic anhydrase IX expression in clear cell renal cell carcinoma and normal tissues: experiences from (radio) immunotherapy. J Clin Oncol. 2008;26(22):3808-3809.

9. Campbell-Verduyn L, **Elsinga PH, Mirfeizi L, Dierckx RA,** Feringa BL. Copper-free 'click': 1,3-dipolar cycloaddition of azides and arynes. Org Biomol Chem. 2008;6(19):3461-3463.

10. Casneuf VF, Fonteyne P, Van Damme N, Demetter P, Pauwels P, de Hemptinne B, de Vos M, **van de Wiele C,** Peeters M. Expression of SGLT1, Bcl-2 and p53 in primary pancreatic cancer related to survival. Cancer Invest. 2008;26(8):852-859.

11. **Chianelli M,** Mather SJ, Grossman A, Sobnak R, Fritzberg A, Britton KE, **Signore A.** ^{99m}Tc-interleukin-2 scintigraphy in normal subjects and in patients with autoimmune thyroid diseases: a feasibility study. Eur J Nucl Med Mol Imaging. 2008;35(12):2286-2293.

12. **Chianelli M,** Parisella MG, Visalli N, Mather SJ, D'Alessandria C, Pozzilli P, **Signore A.** Pancreatic scintigraphy with ^{99m}Tc-interleukin-2 at diagnosis of type 1 diabetes and after 1 year of nicotinamide therapy. Diabetes Metab Res Rev. 2008;24(2):115-122.

13. **Chianelli M,** Boerman OC, Malviya G, Galli F, Oyen WJ, **Signore A.** Receptor-binding ligands to image infection. Curr Pharm Des. 2008;14(31):3316-3325.

14. Cicone F, **Signore A**, Scopinaro F. Studying the metabolic activity of red bone marrow by means of FDG-PET: the need for a standardization. Mol Imaging Biol. 2008;10(3):129-130.

15. Cicone F, Loose D, Deron P, Vermeersch H, **Signore A**, Van de Vyvere F, Scopinaro F, **van de Wiele C.** Prognostic value of FDG uptake by the bone marrow in squamous cell carcinoma of the head and neck. Nucl Med Commun. 2008;29(5):431-435.

16. De Bruin D, de Jong IJ, van der Laan JG, **Slart RH.** A patient with renal cell carcinoma: Tumour thrombus was suggested on FDG-PET imaging. Eur J Radiol 2008;66(2):e51-e53.

17. De Decker M, Bacher K, Thierens H, Slegers G, **Dierckx RA,** De Vos F. In vitro and in vivo evaluation of direct rhenium-188-labeled anti-CD52 monoclonal antibody alemtuzumab for radioimmunotherapy of B-cell chronic lymphocytic leukemia. Nucl Med Biol. 2008;35(5):599-604.

18. De Jong BM, van de Hoeven JH, **Pruim J,** Meertens JH, van der Naalt J. Cortico-thalamic activation in generalized status epilepticus, a PET study. Clin Neurol Neurosurg. 2008;110(2):182-185.

19. **De Vries EF, Doorduin J, Vellinga NA, van Waarde A, Dierckx RA, Klein HC**. Can celecoxib affect P-glycoprotein-mediated drug efflux? A microPET study. Nucl Med Biol. 2008;35(4):459-466.

20. **De Vries EF, Doorduin J, Dierckx RA, van Waarde A.** Evaluation of [^{11}C]rofecoxib as PET tracer for cyclooxygenase 2 overexpression in rat models of inflammation. Nucl Med Biol. 2008;35(1):35-42.

21. **De Vries EF.** Imaging of tumor characteristics for tailored therapy. Curr Pharm Des. 2008;14(28):2912-2913.

22. De Vries MM, Persoon AC, **Jager PL,** Gravendeel J, Plukker JT, Sluiter WJ, Links TP. Embolization Therapy of Bone Metastases from Epithelial Thyroid Carcinoma: Effect on Symptoms and Serum Thyroglobulin. Thyroid. 2008;18(12):1277-1284.

23. De Winter O, Van De Veire N, De Bondt P, **van de Wiele C,** de Buyzere M, de Backer G, Gillebert TC, **Dierckx RA,** de Sutter J. Poststress left ventricular ejection fraction is an independent predictor of major cardiac events in patients with coronary artery disease and impaired left ventricular function. Q J Nucl Med Mol Imaging. 2008;52(3):296-304.

24. Decristoforo C, **Elsinga P**, Faivre-Chauvet A. Farstad B, Meyer G, Mikolajczak R, Penuelas J, Unak P, Westera GL. The specific case of radiopharmaceuticals and GMP--activities of the Radiopharmacy Committee. Eur J Nucl Med Mol Imaging. 2008;35(7):1400-1401.

25. **Dierckx RA, Van de Wiele C**. FDG uptake, a surrogate of tumour hypoxia? Eur J Nucl Med Mol Imaging. 2008;35(8):1544-1549.

26. Dijkers EC, de Vries EG, Kosterink JG, **Brouwers AH, Lub-de Hooge MN.** Immunoscintigraphy as potential tool in the clinical evaluation of HER2/neu targeted therapy. Curr Pharm Des. 2008;14(31):3348-3362.

27. **Doorduin J, de Vries EF, Dierckx RA, Klein HC.** PET imaging of the peripheral benzodiazepine receptor: Monitoring disease progression and therapy response in neurodegenerative disorders. Curr Pharm Des. 2008;14(31):3297-3315.

28. Fiebrich HB, **Brouwers AH,** Links TP, de Vries EG. Images in cardiovascular medicine: myocardial metastases of carcinoid visualized by ^{18}F-dihydroxy-phenyl-alanine positron emission tomography. Circulation. 2008;118(15):1602-1604.

29. Gielkens PF, Schortinghuis J, **de Jong JR, Paans AM,** Ruben JL, Raghoebar GM, Stegenga B, Bos RR. The influence of barrier membranes on autologous bone grafts. J Dent Res. 2008;87(11):1048-1052.

30. Gielkens PF, Schortinghuis J, **de Jong JR,** Raghoebar GM, Stegenga B, Bos RR. Vivosorb, Bio-Gide, and Gore-Tex as barrier membranes in rat mandibular defects: an evaluation by microradiography and micro-CT. Clin Oral Implants Res. 2008;19(5):516-521.

31. Gielkens PF, Schortinghuis J, **de Jong JR,** Huysmans MC, van Leeuwen MB, Raghoebar GM, Bos RR, Stegenga B. A comparison of micro-CT, microradiography and histomorphometry in bone research. Arch Oral Biol. 2008;53(6):558-566.

32. Hospers GA, Helmond FA, de Vries EG, **Dierckx RA, de Vries EF.** PET imaging of steroid receptor expression in breast and prostate cancer. Curr Pharm Des. 2008;14(28):3020-3032.

33. **Jager PL**, Chirakal R, Marriott CJ, **Brouwers AH, Koopmans KP,** Gulenchyn KY. 6-L-^{18}F-fluorodihydroxyphenylalanine PET in neuroendocrine tumors: basic aspects and emerging clinical applications. J Nucl Med. 2008;49(4):573-586.

34. Jirasko R, Holcapek M, Kolarova L, Nadvornik M, **Popkov A.** Characterization of Ni(II) complexes of Schiff bases of amino acids and (S)-N-(2-benzoylphenyl)-1-benzylpyrrolidine-2-carboxamide using ion trap and QqTOF electrospray ionization tandem mass spectrometry. J Mass Spectrom. 2008;43(9):1274-1284.

35. Jorna FH, **Jager PL, Lemstra C,** Wiggers T, Stegeman CA, Plukker JT. Utility of an intraoperative gamma probe in the surgical management of secondary or tertiary hyperparathyroidism. Am J Surg. 2008;196(1):13-18.

36. Kema IP, **Koopmans KP, Elsinga PH, Brouwers AH, Jager PL,** de Vries EG. Reply to: Premedication with carbidopa masks positive finding of insulinoma and beta-cell hyperplasia in ^{18}F-dihydroxy-phenyl-alanine positron emission tomography (Kauhanen S, Seppänen M, Nuutila P). J Clin Oncol 2008;26(32):5308-5309.

37. **Koopmans KP, Neels OC,** Kema IP, **Elsinga PH,** Sluiter WJ, Vanghillewe K, **Brouwers AH, Jager PL,** de Vries EG. Improved staging of patients with carcinoid and islet cell tumors with ^{18}F-dihydroxy-phenyl-alanine and ^{11}C-5-hydroxy-tryptophan positron emission tomography. J Clin Oncol. 2008;26(9):1489-1495.

38. **Koopmans KP, Jager PL,** Kema IP, Kerstens MN, Albers F, Dullaart RP. ^{111}In-octreotide is superior to ^{123}I-metaiodobenzylguanidine for scintigraphic detection of head and neck paragangliomas. J Nucl Med. 2008;49(8):1232-1237.

39. **Koopmans KP**, de Groot JW, Plukker JT, de Vries EG, Kema IP, Sluiter WJ, **Jager PL,** Links TP. ^{18}F-dihydroxyphenylalanine PET in patients with biochemical evidence of medullary thyroid cancer: relation to tumor differentiation. J Nucl Med. 2008;49(4):524-531.

40. Koot RW, Habraken JB, Hulshof MC, **Paans AM,** Bosch DA, **Pruim J.** What is the value of emission tomography studies in patients with a primary glioblastoma multiforme treated by ^{192}Ir brachytherapy? Acta Neurochir (Wien). 2008;150(4):345-349.

41. Kortekaas R, Maguire RP, **van Waarde A,** Leenders KL, **Elsinga PH.** Despite irreversible binding, PET tracer [^{11}C]-SA5845 is suitable for imaging of drug competition at sigma receptors-the cases of ketamine and haloperidol. Neurochem Int. 2008;53(1-2):45-50.

42. Krabbe CA, Dijkstra PU, **Pruim J,** van der Laan BF, van der Wal JE, Gravendeel JP, Roodenburg JL. FDG PET in oral and oropharyngeal cancer. Value for confirmation of N0 neck and detection of occult metastases. Oral Oncol. 2008;44(1):31-36.

43. Krug B, **Van Zanten A,** Pirson AS, Crott R, Vander Borght T. Activity-based costing evaluation of [^{18}F]-fluorodeoxyglucose production. Eur J Nucl Med Mol Imaging. 2008;35(1):80-88.

44. Loose D, **Signore A,** Bonanno E, Vermeersch H, **Dierckx RA,** Deron P, **van de Wiele C.** Prognostic value of CD25 expression on lymphocytes and tumor cells in squamous-cell carcinoma of the head and neck. Cancer Biother Radiopharm. 2008;23(1):25-33.

45. Loose D, **Signore A,** Staelens L, vanden Bulcke K, Vermeersch H, **Dierckx RA,** Bonanno E, **van de Wiele C.** ^{123}I-Interleukin-2 uptake in squamous cell carcinoma of the head and neck carcinoma. Eur J Nucl Med Mol Imaging. 2008;35(2):281-286.

46. Loose D, Vermeersch H, De Vos F, Deron P, Slegers G, **Van de Wiele C.** Prognostic value of ^{99m}Tc-HYNIC Annexin-V imaging in squamous cell carcinoma of the head and neck. Eur J Nucl Med Mol Imaging. 2008;35(1):47-52.

47. Malviya G, **Signore A,** Lagana B, **Dierckx RA.** Radiolabelled peptides and monoclonal antibodies for therapy decision making in inflammatory diseases. Curr Pharm Des. 2008;14(24):2401-2414.

48. Mansour K, Blanksma LJ, Vrakking H, **Jager PL.** Scintigraphic evaluation for tear drainage, after dacryocystorhinostomy, in relation to patient satisfaction. Eye. 2008;22(3):414-419.

49. Migliore A, **Signore A,** Capuano A, Bizzi E, Massafra U, Vacca E, Todino V, **Chianelli M.** Relevance of ^{99m}Tc-HYNIC-tir-octreotide scintigraphy in a patient affected by sarcoidosis with lung and joints involvement and secondary Sjögren's syndrome treated with infliximab: case report. Eur Rev Med Pharmacol Sci. 2008;12(2):127-130.

50. Nadvornik M, Langer V, Jirasko R, Holcapek M, Weidlich T, Lycka A, **Popkov A.** Syntheses, X-ray, MSn, NMR and CD structure determination of nickel(II) complexes of Schiff bases of (S)-N-(2-benzoylphenyl)-1-benzylpyrrolidine-2-carboxamide and aromatic α-amino acids. Polyhedron. 2008;27:3477-3483.

51. **Neels OC, Koopmans KP, Jager PL,** Vercauteren L, **van Waarde A, Doorduin J,** Timmer-Bosscha H, **Brouwers AH,** de Vries EG, **Dierckx RA,** Kema IP, **Elsinga PH.** Manipulation of [^{11}C]-5-hydroxytryptophan and 6-[^{18}F]fluoro-3,4-dihydroxy-L-phenylalanine accumulation in neuroendocrine tumor cells. Cancer Res. 2008;68(17):7183-7190.

52. Omloo JM, Sloof GW, Boellaard R, Hoekstra OS, **Jager PL,** van Dullemen HM, Fockens P, Plukker JT, van Lanschot JJ. Importance of fluorodeoxyglucose-positron emission tomography (FDG-PET) and endoscopic ultrasonography parameters in predicting survival following surgery for esophageal cancer. Endoscopy. 2008;40(6):464-471.

53. **Phan HT, Jager PL,** Plukker JT, Wolffenbuttel BH, **Dierckx RA,** Links TP. Comparison of ^{11}C-methionine PET and ^{18}F-fluorodeoxyglucose PET in differentiated thyroid cancer. Nucl Med Commun. 2008;29(8):711-716.

54. **Phan HT, Jager PL, Paans AM,** Plukker JT, Sturkenboom MG, Sluiter WJ, Wolffenbuttel BH, **Dierckx RA,** Links TP. The diagnostic value of ^{124}I-PET in patients with differentiated thyroid cancer. Eur J Nucl Med Mol Imaging. 2008;35(5):958-965.

55. **Phan HT, Jager PL,** van der Wal JE, Sluiter WJ, Plukker JT, **Dierckx RA,** Wolffenbuttel BH, Links TP. The follow-up of patients with differentiated thyroid cancer and undetectable thyroglobulin (Tg) and Tg antibodies during ablation. Eur J Endocrinol. 2008;158(1):77-83.

56. **Popkov A,** Nadvornik M, Kozisek J. { 2-[(S)-({2-[S}-1-Benzylpyrrolidine-2-carboxamido]-phenyl} (phenyl)methyl-ene)amino]-4-hydroxybutanoato-kappa-4,N,N',N'',O}nickel(II). Acta Crystallographica. 2008;E64:m364-m365.

57. **Rybczynska AA, Dierckx RA,** Ishiwata K, **Elsinga PH, van Waarde A.** Cytotoxicity of sigma-receptor ligands is associated with major changes of cellular metabolism and complete occupancy of the sigma-2 subpopulation. J Nucl Med. 2008;49:2049-2056.

58. Saleem BR, Berger P, Zeebregts CJ, **Slart RH,** Verhoeven EL, van den Dungen JJ. Periaortic endograft infection due to *Listeria monocytogenes* treated with graft preservation. J Vasc Surg. 2008;47(3):635-637.

59. Schreurs LM, Pultrum BB, **Koopmans KP,** Verhoef CC, **Jager PL,** van Dam GM, Groen H, van der Jagt EJ, Plukker JT. Better assessment of nodal metastases by PET/CT fusion compared to side-by-side PET/CT in oesophageal cancer. Anticancer Res. 2008;28(3B):1867-1873.

60. Senft A, de Bree R, Hoekstra OS, Kuik DJ, Golding RP, Oyen WJ, **Pruim J,** van den Hoogen FJ, Roodenburg JL, Leemans CR. Screening for distant metastases in head and neck cancer patients by chest CT or whole body FDG-PET: a prospective multicenter trial. Radiother Oncol. 2008;87(2):221-229.

61. Siemerink EJ, Mulder NH, **Brouwers AH,** Hospers GA. ^{18}F-Fluorodeoxyglucose positron emission tomography for monitoring response to sorafenib treatment in patients with hepatocellular carcinoma. Oncologist. 2008;13(6):734-735.

62. **Signore A,** D'Alessandria C, Lazzeri E, **Dierckx RA.** Can we produce an image of bacteria with radiopharmaceuticals? Eur J Nucl Med Mol Imaging. 2008;35(6):1051-1055.

63. **Slart RH,** Tio RA, Zeebregts CJ, **Willemsen AT, Dierckx RA,** De Sutter J. Attenuation corrected gated SPECT for the assessment of left ventricular ejection fraction and volumes. Ann Nucl Med. 2008;22(3):171-176.

64. **Slart RH,** Zeebregts CJ, Tio RA. Can nuclear medicine shed light on the dark side of angiogenesis in cardiovascular disease? Nucl Med Commun. 2008;29(7):585-587.

65. van Beilen M, Portman AT, Kiers HA, Maguire RP, Kaasinen V, Koning M, **Pruim J,** Leenders KL. Striatal FDOPA uptake and cognition in advanced non-demented Parkinson's disease: a clinical and FDOPA-PET study. Parkinsonism Relat Disord. 2008;14(3):224-228.

66. **Van de Wiele C,** Phonteyne P, Pauwels P, Goethals I, van den Broecke R, Cocquyt V, **Dierckx RA.** Gastrin-releasing peptide receptor imaging in human breast carcinoma versus immunohistochemistry. J Nucl Med. 2008;49(2):260-264.

67. **Van de Wiele C,** VandeVyver F, Debruyne C, Philippe J, van Meerbeeck JP. FDG uptake by the bone marrow in NSCLC patients is related to TGF-beta but not to VEGF or G-CSF serum levels. Eur J Nucl Med Mol Imaging. 2008;35(3):519-522.

68. **Van de Wiele C,** Boersma H, **Dierckx RA,** De Spiegeleer B, **van Waarde A, Elsinga PH.** Growth factor/peptide receptor imaging for the development of targeted therapy in oncology. Curr Pharm Des. 2008;14(31):3340-3347.

69. van der Vaart MG, Meerwaldt R, **Slart RH,** Van Dam GM, Tio RA, Zeebregts CJ. Application of PET/SPECT imaging in vascular disease. Eur J Vasc Endovasc Surg. 2008;35(5):507-513.

70. van der Vleuten PA, Rasoul S, Huurnink W, van der Horst WC, **Slart RH,** Reiffers S, **Dierckx RA,** Tio RA, Ottervanger JP, de Boer MJ, Zijlstra F. The importance of left ventricular function for long-term outcome after primary percutaneous coronary intervention. BMC Cardiovasc Disord. 2008;8:4.

71. van Heijl M, Omloo JM, Berge Henegouwen MI, Busch OR, Tilanus HW, Bossuyt PM, Hoekstra OS, Stoker J, Hulshof MC, van der Gaast A, Nieuwenhuijzen GA, Bonenkamp HJ, Plukker JT, Spillenaar Bilgen EJ, ten Kate FJ, Boellaard R, **Pruim J,** Sloof GW, van Lanschot JJ. NEOadjuvant therapy monitoring with PET and CT in Esophageal Cancer (NEOPEC-trial). BMC Med Phys. 2008;8:3.

72. **van Waarde A, Doorduin J, de Jong JR, Dierckx RA, Elsinga PH.** Synthesis and preliminary evaluation of (S)-[^{11}C]-exaprolol, a novel beta-adrenoceptor ligand for PET. Neurochem Int. 2008;52(4-5):729-733.

73. **van Waarde A.** PET and SPECT in drug evaluation and drug design: imaging inflammatory processes, tumors, and the endocannabinoid system. Curr Pharm Des. 2008;14(31):3295-3296.

74. **van Waarde A, Elsinga PH.** Proliferation markers for the differential diagnosis of tumor and inflammation. Curr Pharm Des. 2008;14(31):3326-3339.

75. Visser FW, Muntinga JH, **Dierckx RA,** Navis G. Feasibility and impact of the measurement of extracellular fluid volume simultaneous with GFR by ^{125}I-iothalamate. Clin J Am Soc Nephrol. 2008;3(5):1308-1315.

76. Wallis de Vries BM, van Dam GM, Tio RA, Hillebrands JL, **Slart RH,** Zeebregts CJ. Current imaging modalities to visualize vulnerability within the atherosclerotic carotid plaque. J Vasc Surg. 2008;48:1620-1629.

77. **Wierts R,** Janssen MJA, Kingma H. Measuring saccade peak velocity using a low-frequency sampling rate of 50 Hz. IEEE Trans Biomed Eng. 2008; 55(12),2840-2842.

5.3   Papers in international journals (by users of the NMMI facilities)

1. Bartels AL, Leenders KL. Brain imaging in patients with freezing of gait. Mov Disord. 2008;23 Suppl 2:S461-S467.

2. Bartels AL, van Berckel BN, Lubberink M, Luurtsema G, Lammertsma AA, Leenders KL. Blood-brain barrier P-glycoprotein function is not impaired in early Parkinson's disease. Parkinsonism Relat Disord. 2008;14(6):505-508.

5.4   Papers in Dutch journals

1. **de Vries EF, Elsinga PH.** 14th European Symposium on Radiopharmacy and Radiopharmaceuticals. Tijdschr Nucl Geneeskd 2008;30(4):151-152.

2. Koolhaas W, Prak A, Stiekema HM, Kreeftenberg HG, Wolffenbuttel BH, **Jager PL.** Efficient and improved diagnosis of osteoporosis by simultaneous bone density measurement and spinal morphometry. Ned Tijdschr Geneeskd. 2008;152(16):938-943.

3. **Koopmans KP.** Metabolic PET tracers for neuroendocrine tumors. Tijdschr Nucl Geneeskd 2008:30(2):83-85.

4. **Lub-de Hooge MN, Sturkenboom MG,** Boersma HH, Kosterink JG. Nucleaire beeldvorming in de oncologie: Radiofarmaca op maat van het individu. Pharmaceutisch Weekblad 2008;1 februari;48-53.

5. **Lub-de Hooge MN.** ImmunoSPECT and PET imaging: towards patient tailored targeted therapy. Tijdschr Nucl Geneesk. 2008; 30:111-116.

6. Mulders PF, **Brouwers AH**, Hulsbergen-van der Kaa CA, van Lin EN, Osanto S, de Mulder PH. Guideline 'Renal cell carcinoma'. Ned Tijdschr Geneeskd. 2008;152(7):376-380.

7. **Neels OC.** Tracer development for detection and characterization of neuroendocrine tumors with PET. Tijdschr Nucl Geneeskd 2008;30(2):80-82.

8. **Phan TT.** Imaging strategy in differentiated thyroid cancer. Tijdschr Nucl Geneeskd 2008;30(1):31-33.

9. Rij CM van, **Sturkenboom MG,** Luurtsema G, Franssen EJ. Productie en klinische toepassingen van [^{15}O]-gelabelde gassen. Pharmaceutisch Weekblad 2008(43):69-71.

10. **Sturkenboom MG,** Kosterink JGW, **Lub-de Hooge MN.** Ontwikkeling van een nieuw radiofarmacon in een academische, niet-commerciële setting. Tijdschr Nucl Geneesk. 2008; 30:125-132.

11. Van der Horst-Schrivers AN, **Brouwers AH,** Links TP. Functional imaging of neuroendocrine tumours. Tijdschr Nucl Geneeskd 2008;30(2):61-63.

5.5   Abstracts in international journals

1. Boellaard R, Oyen WJ, Hoekstra CJ, Comans E, Visser E, **Willemsen AT**, Arends B, Verzijlbergen F, Zijlstra F, **Pruim J**. The Netherlands protocol for standardization of FDG whole body PET studies in multi-center trials (NEDPAS). J Nucl Med 2008;49(Suppl 1):106P.

2. Chianelli M, Todino V, Graziano F, Panunzi C, Guglielmi R, **Signore A**, Papini E. Low dose (2.0 GBq) radioiodine postsurgical treatment ablation in thyroid cancer: comparison between hormone withdrawal and use of rhTSH in low risk patients. Eur J Nucl Med Mol Imaging 2008: 35(Suppl.2):S344.

3. de Groot DMG, Voet B, Wolterbeek A, **Dierckx RA, van Waarde A, Willemsen AT, de Vries EF.** [^{18}F]FDG micro PET in vivo imaging, an animal-saving alternative in developmental neurotoxicity testing. Reprod Toxicol 2008: 26(1):63.

4. de Groot DMG, Jetten N, Voet B, Wolterbeek A, Veltien A, Heerschap A, **Dierckx RA, van Waarde A, Willemsen AT, de Vries EF.** Testing developmental neurotoxicity: Saving animals by in vivo imaging with PET and MRI. Toxicol Lett 2008: 180S,47.

5. **De Vries EF, Van Waarde A, Willemsen AT, Dierckx RA,** Wolterbeek A, Wesselius A, De Groot DMG, Protection of the unborn child form harmful drugs: a role for PET? Eur.J.Nucl.Med.Mol.Imaging 2008; 35(Suppl. 2), S141.

6. **De Vries EF, Van Waarde A, Willemsen AT, Dierckx RA,** Wolterbeek A, Wesselius A, De Groot DMG, Functional PET imaging: a versatile tool for regulatory studies on developmental neurotoxicity. Q.J.Nucl.Med.Mol. Imaging 2008; 52(Suppl. 1), 50.

7. **Doorduin J, De Vries EF, Willemsen ATM, Dierckx RA, Klein HC,** Neuroinflammation in schizophrenic patients: a positron emission tomography study with [^{11}C]-(R)-PK11195. Eur.J.Nucl.Med.Mol.Imaging 2008; 35(Suppl. 2), S150.

8. **Douma JE,** Blaauw M, Mathlener MH, Schuurmans EP, **Dierckx RA, Jager PL, Slart RH**. Vertebral fracture assessment in supine position: comparison with semiquantitative and visual radiograph assessment. Eur J Nucl Med Mol Imaging 2008; 35(Suppl.2):S215.

9. Goethals I, Ham H, Dobbeleir A, **van de Wiele C**, Vermeersch H, D'Asseler Y. The effect of scan duration of F-18 FDG PET studies on lesion detection rate and quantitative measures of FDG uptake and volume in head and neck tumours. Eur J Nucl Med Mol Imaging 2008;35(Suppl.2):S284-S285

10. **Klerk OL de, Willemsen AT,** Bartels AL, Hendrikse NH, Bosker FJ, den Boer JA. Therapy resistant depression explained? Regional increase of P-glycoprotein function in the blood-brain barrier in patients with major depressive disorder. Neuroimage 2008;41:O22

11. **Lemstra C, van der Knaap Y,** de Vries J, **Dierckx RA, Brouwers AH**. Primary non-visualisation and the value of re-injection of radioactive tracer in sentinel lymph node mapping for breast cancer. J Nucl Med 2008;49(Suppl 1):419P.

12. Links TP, Verbeek HH, de Groot JW, Sluiter WJ**, Koopmans KP,** de Vries EG, Plukker JT, Wolffenbuttel BH, van der Horst-Schrivers AN, **Brouwers AH**. ^{18}F-FDG PET and ^{18}F-DOPA PET in distinguishing undifferentiated versus differentiated medullary thyroid cancer. Thyroid 2008; 18(Suppl.1):S59.

13. Malviya G, D'Alessandria C, Trotta C, Massari R, Soluri A, Scopinaro F, **Dierckx RA, Signore A.** Radiolabeled Visilizumab, a humanized anti-CD3 monoclonal antibody, for in vivo targeting of human CD3+ lymphocytes. Eur J Nucl Med Mol Imaging 2008; 35(Suppl.2):S142.

14. Malviya G, Lagana B, Milanetti F, Del Mastro C, Familiari D, **Dierckx RA**, Scopinaro F, D'Amelio R, **Signore A.** Use of 99m-technetium labelled rituximab for imaging of patients with chronic inflammatory diseases. Eur J Nucl Med Mol Imaging 2008; 35(Suppl.2):S142-S143.

15. Oyen WJ, Wiering B, van der Sijp JR, Roumen RM, de Jong KP, Comans EF, **Pruim J,** Dekker HM, Krabbe PF, Ruers TJ. Improved selection of patients for hepatic surgery of colorectal liver metastases with FDG-PET: A randomized study. J Nucl Med 2008;49(Suppl 1):41P.

16. **Paans AM,** Positron emission tomography: the conceptual idea using a multidisciplinary approach, Fundam Clin Pharmacol 2008;22(Suppl. 2), 26

17. Pacilio M, Betti M, Cicone F, Barone R, Del Mastro C, Di Santo G, **Signore A**, Chiacchierarelli L, Montani L, Rauco R, Monaco A, Santini E, Mango L, Scopinaro F. Improvement of ^{99}Y-Zevalin dosimetry by indirect Monte Carlo calculation of tumor biologically effective doses and their correlation with clinical outcomes. Preliminary results. Eur J Nucl Med Mol Imaging 2008;35(Suppl.2):S235.

18. **Rybczynska AA, Elsinga PH,** Ishiwata K, **Dierckx RA, van Waarde A**. High receptor occupancy is required for cytotoxicity of sigma ligands. J Nucl Med 2008;49(Suppl 1):101P.

19. **Rybczynska AA, Elsinga PH,** Ishiwata K, **Dierckx RA, van Waarde A.** Rapid cell killing by sigma receptor ligands is associated with striking metabolic changes and virtually complete occupancy of the sigma-2 subpopulation. Eur J Nucl Med Mol Imaging 2008; 35(Suppl.2):S153.

20. **Rybczynska AA, Elsinga PH, Sijbesma JW,** Ishiwata K, **de Jong JR, de Vries EF, Dierckx RA, van Waarde A.** Neurosteroid depletion and suppletion affects binding of the sigma ligand ^{11}C-SA4503 in tumor cells and tumor-bearing rats. J Nucl Med 2008;49(Suppl.1):131P.

21. **Signore A,** Familiari D, Vitale V, Prosperi D, Bagni O, Lenza A, Di Santo G, Fallucca S, Cavallini M, Scopinaro F. Imaging diabetic foot osteomyelitis by 3-phase FDG-PET/CT scan. Eur J Nucl Med Mol Imaging 2008; 35(Suppl.2):S136-S137.

22. **Signore A,** Malviya G, Ceccarelli F, Conti F, D'Alessandria C, Ragni P, Valessini G, Scopinaro F. ^{99m}Tc-Infliximab and ^{99m}Tc-Adalimumab for therapy decision making in patients with rheumatoid arthritis. Eur J Nucl Med Mol Imaging 2008; 35(Suppl.2):S137.

23. **Signore A**, Malviya G, Lazerri E, Prandini N, Viglietti AL, **Harms C, De Vries EF**, Devicienti A, Nano E, **Dierckx RA,** A new disposable sterile device (Leukokit) for labelling white blood cells (WBC) with radioisotopes. Eur.J.Nucl.Med.Mol.Imaging, 2008;35(Suppl. 2), S142.

24. **Signore A,** Parisella MG, D'Alessandria C, Del Prete F, Braesch-Andersen S, Massari R, Trotta C, Soluri A, Bartolazzi A, Scopinaro F. High-resolution immunoscintigraphy for in vivo imaging of thyroid cancer by using galectin-3 radio-immunotargeting. Eur J Nucl Med Mol Imaging 2008;35(Suppl.2):S318.

25. **Slart RH,** Tio R, **Dierckx RA,** Hillege H, de Sutter J, van Veldhuisen DJ, Siebelink H, Zeebregts C. Independent prognostic value of myocardial perfusion reserve in patients with coronary artery disease. J Nucl Med 2008:49(Suppl 1):193P.

26. **Slart RH,** Tio R, Franssen C, Dasselaar J, de Jong P, **Dierckx RA, Pruim J.** Myocardial perfusion falls during uncomplicated hemodialysis. J Nucl Med 2008:49(Suppl 1):127P.

27. Van Steenkiste M, Oltenfreiter R, Frankenne F, Murphy G, **van de Wiele C,** de Vos F. Evaluation of tissue inhibitors of matrix metalloproteinase as tumor imaging agents. J Nucl Med 2008;49(Suppl 1):293P.

28. **Van Waarde A.** Proliferation markers for the differential diagnosis of tumor and inflammation. Eur J Nucl Med Mol Imaging 2008; 35(Suppl.2):S154.

29. Wiering B, Krabbe PF, van der Sijp JR, Roumen RM, de Jong KP, Comans EF, **Pruim J,** Dekker HM, Ruers TJ, Oyen WJ. Improved selection of patients for hepatic surgery of colorectal liver metastases with FDG-PET: a randomized study. Eur J Nucl Med Mol Imaging 2008;35(Suppl.2):S191.

30. **Wierts R, de Jong JR, Lazarenko SV, Willemsen AT, Paans AM**, A new algorithm for the continuous quantitative monitoring of leakage during chemotherapeutic limb perfusion, IEEE Nuclear Science Symposium Conference Record 2008, p.4835-4837.

5.6 Invited lectures, conference proceedings, etc

1. Bastiaannet E, Wobbes T, Hoekstra OS, **Brouwers AH**, Oyen WJ, Meijer S, Hoekstra HJ. Diagnostic performance of FDG-PET and CT in the upstaging of melanoma patients with lymph node metastases and the clinical consequences. International Melanoma Research Congress, Sapporo, Japan, May 5-13, 2008.

2. Bastiaannet E, Wobbes T, Hoekstra OS, **Brouwers AH,** Oyen WJ, Meijer S, Hoekstra HJ. Change in treatment as result of FDG-PET and CT in clinically stage III melanoma patients: a prospective study in 221 patients. American Society for Clinical Oncology (ASCO), Chicago, USA, 2008

3. Breeuwsma AJ, **Pruim J,** van den Bergh AC, **Dierckx RA,** Nijman JM, de Jong IJ. Klinische waarde van ^{11}C-choline PET voor het opsporen van recidief prostaat-carcinoom na uitwendige radiotherapie bij biochemisch recidief. Wetenschappelijke vergadering NVNG, Groningen, May 23, 2008

4. **Brouwers AH.** Nieuwe PET tracers in de (neuro-endocriene) oncologie: ^{18}F-DOPA, ^{11}C-HTP en choline. Invited lecture, Lustrumsymposium Nederlandse Vereniging voor Nucleaire Geneeskunde, Amsterdam, November 21, 2008

5. **Brouwers AH.** Verschillende (nieuwe) aspecten van tumordiagnostiek mbv PET/(CT). Invited lecture, Afdeling Interne Geneeskunde, Universitair Medisch Centrum Groningen, August 29, 2008.

6. **Dierckx RA.** Modellen in de gezondheidszorg in Nederland. Invited Lecture, University of Ghent, Belgium, September 9, 2008

7. Dijkers EC, **Lub-de Hooge MN,** Kosterink JG, **Jager PL, Brouwers AH,** Oude Munnink TH, **Huisstede KW,** Perk LR, van Dongen GA, de Vries EG. Characterization of Zr-89 trastuzumab for clinical HER2 immunopet imaging. Towards patient tailored targeted therapy. Oral presentation, Dutch Society for Clinical Pharmacology & Biopharmacy (NVKF&B) during FIGON days (October 7th 2008).

8. Dijkers EC, **Lub-de Hooge MN,** Kosterink JG, **Jager PL, Brouwers AH,** Oude Munnink TH, **Huisstede KW,** Perk LW, van Dongen GA, de Vries EG. Characterization of zirconium-89 trastuzumab for clinical HER2 immunoPET imaging. Wetenschappelijke vergadering NVNG, Groningen, May 23, 2008

9. **Doorduin J, de Vries EF, Willemsen AT, Dierckx RA, Klein HC.** Neuroinflammation in schizophrenic patients: a PET study with [^{11}C]-(R)-PK11195. Wetenschappelijke vergadering NVNG, Groningen, May 23, 2008

10. **Eshuis SA, Jager PL,** Maguire RP, **Jonkman S, Dierckx RA, Leenders KL.** Vergelijking van FP-CIT SPECT en F-DOPA PET in patiënten met de ziekte van Parkinson en gezonde vrijwilligers. Wetenschappelijke vergadering NVNG, Groningen, May 23, 2008.

11. Fiebrich HB, Links TP, Pijl ME, Kerstens MN, **Koopmans KP, Dierckx RA, Elsinga PH,** Kema IP, Sluiter WJ, **Jager PL,** de Vries EG, **Brouwers AH.** Diagnostische waarde van ^{18}F-fluorodihydroxyphenylalanine (^{18}F-DOPA) PET in patiënten met een feochromocytoom. Wetenschappelijke vergadering NVNG, Groningen, May 23, 2008

12. Franssen CF, Dasselaar JJ, **Slart RH,** Knip M, **Pruim J,** Tio RA, de Jong PE. Cardio-renal interaction: the effect of hemodialysis on myocardial perfusion. Wetenschappelijke vergadering NVNG, Groningen, May 23, 2008

13. Harlaar NJ, van Dam GM, van Riezen M, Hillebrands JL, Tio RA, **Slart RH,** Zeebregts CJ. Feasibility of near-infrared fluorescence imaging to identify and quantify vulnerable plaque formation in human carotid specimen. 15th International Student Congress of Medical Sciences, Groningen (The Netherlands) June 2008.

14. **Klerk OL de, Willemsen AT,** Bosker FJ, den Boer JA. P-glycoprotein contributes to therapy-resistant depression. ECNP conference, Barcelona, Spain 2008

15. **Lub-de Hooge MN.** ImmunoSPECT and PET imaging: Towards patient-tailored (targeted) therapy. European Society of Hospital Pharmacists (Maastricht, The Netherlands, March 2008).

16. **Lub-de Hooge MN.** ImmunoSPECT and PET imaging: Towards patient-tailored (targeted) therapy. 19th IRIST International Congress (Krakow, Poland 25-28th June 2008).

17. Nagengast WB, De Vries EG, Warnders FJ, Hospers GA, Mulder NH, **de Jong JR, Brouwers AH, Lub-de Hooge MN.** In vivo VEGF imaging with an anti-VEGF Fab-fragment in a human ovarian tumour xenograft model using MicroPET and MicroCT. AACR Annual Meeting 2008, San Diego, US, April 12-16.

18. Nagengast WB, **Lub-de Hooge MN**, Hospers GAP, **Brouwers AH, Elsinga PH**, Mulder NH, Warnders FJ, De Vries EG. Towards clinical VEGF imaging using the anti-VEGF antibody bevacizumab and Fab-fragment ranibizumab. Poster discussion, ASCO Annual Meeting 2008 May 30-June 3, Chigago, US.

19. **Neels OC, Koopmans KP, Jager PL,** Vercauteren L, **van Waarde A, Doorduin J,** Timmer-Bosscha H, **Brouwers AH,** de Vries EG, **Dierckx RA**, Kema IP, **Elsinga PH.** Manipulation of $[^{11}C]HTP$ and $[^{18}F]DOPA$ accumulation in neuroendocrine tumors. Wetenschappelijke vergadering NVNG, Groningen, May 23, 2008.

20. **Paans AM**, PET & CT, What is next in hybrid imaging? Invited Lecture at the VZI Studiedag Beeldvormende Technieken, Eindhoven, May 30, 2008.

21. **Paans AM**, Positron Emission Tomography: The conceptual idea using a multi-disciplinary approach, Invited lecture at the Symposium: Technology in drug research and development, at the EPHAR2008 (Federation of European Pharmacological Societies), Manchester (UK), July 13-17, 2008.

22. Siemerink E, Mulder NH, **Brouwers AH**, Hospers GA. Early prediction of response to Sorafenib treatment in patients with hepatocellular carcinoma (HCC) with ^{18}F-fluorodeoxyglucose-Positron-Emission Tomography (^{18}F-FDG-PET). American Society of Clinical Oncology (ASCO), Chicago, USA, 2008

23. **Slart RH.** Mulitimodality imaging in cardiology. Invited lecture, VieCuri Medisch Centrum voor Noord Limburg, Venlo, Netherlands, September 18, 2008.

24. Tio RA, Dabeshlim A, Siebelink HM, de Sutter J, Hillege HL, Zeebregts CJ, **Dierckx RA,** van Veldhuisen DJ, Zijlstra F, **Slart RH.** PET-myocardial perfusion reserve: an independent prognostic factor in patients with advanced coronary artery disease. Wetenschappelijke vergadering NVNG, Groningen, May 23, 2008.

25. **van Waarde A.** PET imaging: Assessment of in vivo biochemistry. Course on Physiological, Biochemical and Imaging techniques. BCN Research Masters, Graduate School BCN, Groningen, September 15, 2008 [2 invited lectures]

26. **van Waarde A.** Proliferation markers for the differential diagnosis of tumor and inflammation. Invited lecture, CME6, European Association of Nuclear Medicine, Munich, Germany, October 13, 2008.

27. **van Waarde A.** Small Animal PET: Principles, Background, Applications. Topmaster II MPD 2008 Course on Research Methods, Groningen, November 27, 2008 [2 invited lectures]

28. **van Waarde A**. Binding studies in tumor cells to evaluate radioligands for PET. Lecture, 8th workshop Radiochemistry.NL, Erasmus University, Rotterdam, January 18, 2008.

29. Wallis de Vries BM, van Dam GM, Hillebrands JL, Harlaar NJ, van Riezen M, Tio RA, **Slart RH**, Zeebregts CJ. Near-infrared fluorescentie (NIRF) beeldvorming ter identificatie en kwantificering van plaque instabiliteit in humane carotis specimen. Chirurgendagen 2008, Veldhoven (The Netherlands) May 2008.

30. **Wierts R, de Jong JR, Lazarenko SV, Willemsen AT, Paans AM.** A new method for the continuous quantitative monitoring of leakage during chemotherapeutic limb perfusion. IEEE Medical Imaging Conference (NSS-MIC) 2008, Oct 19-25, Dresden. Germany.

31. **Willemsen AT**, Positron Emissie Tomografie. Invited Lecture at the Stellingwerf College, Oosterwolde on behalf of the program "Wetenschappelijke verdieping voor docenten van Universum-scholen binnen het vakgebied bèta en techniek". Oosterwolde, Netherlands, April 15, 2008

32. **Wu C,** Vastenhouw B, van der Have F, **Dierckx RA,** Beekman FJ. High-resolution cardiac rat SPECT: effect of dose and acquisition time. IEEE Medical Imaging Conference (NSS-MIC) 2008, Oct 19-25, Dresden, Germany

5.7   Book Chapters

1. **Paans AM, Willemsen AT,** Positron Emissie Tomografie. In: Leerboek Nucleaire Geneeskunde, Hoofdstuk 4. Elsevier Gezondheidszorg, Maarssen, Netherlands, 2008, 133-152.

2. **Paans AM,** Patiëntendosimetrie. In: Leerboek Nucleaire Geneeskunde, Hoofdstuk 9, Elsevier Gezondheidszorg, Maarssen, Netherlands, 2008, 223-238.

3. **Slart RH,** Hart. In: Leerboek Nucleaire Geneeskunde, Hoofdstuk 3. Elsevier Gezondheidszorg, Maarssen, Netherlands, 2008, 325-354.

PERSONNEL

Listed by function in alphabetic order

6.1   Medical Staff

Ali Agool MD
Adrienne H Brouwers MD PhD
Prof. Rudi A.Dierckx MD PhD (Head of the Department)
Andor Glaudemans MD
Jan Pruim MD PhD
Riemer HJA Slart MD PhD

6.2   Residents-in-Training

Sylvia Eshuis MD
Klaas Pieter Koopmans MD
Olga V.Mirankova MD
Niels Veltman MD
Leo Weijs MD

6.3   Medical Physics

Johan R de Jong PhD (medical physicist-in-training)
Sergiy Lazarenko MSc (medical physicist-in-training)
Prof Anne MJ Paans PhD (medical physicist)
Marcel Segbers MSc (medical physicist-in-training)
Klaas Willem Sietsma (system administrator)
Roel Wierts MSc (medical physicist-in-training)
Antoon TM Willemsen PhD (medical physicist)

6.4   Radiochemistry

Joost Bruns (lab technician)
Hilde Dekens (lab technician)
Prof Philip H.Elsinga PhD (radiochemist)
Marissa Heijnen (assistant)
Chantal Kwizera (lab technician)
Vanathee Logendran (assistant)
Marjolijn Lub-de Hooge PhD (pharmacist)
Bram Maas (lab technician)
Jitze Medema (lab technician)
Hugo Nijnuis (lab technician)
Esther Olthoff (assistant)
Hans Pol (lab technician)
Marieke Sturkenboom MSc (pharmacist)
Bertha Tamming (lab technician)
Erik FJ de Vries PhD (radiochemist)
Michel de Vries (lab technician)
Aren van Waarde PhD (biologist)

6.5 Nuclear Medicine Technologists

Marijke Broersma
José Douma
Karin Groeneveld
Yvonne van der Knaap
Remko Koning
Clara Lemstra
Bregtsje Negenman
Yvonne Reitsma
Eelco Severs
Jurgen Sijbesma
Paul van Snick
Hans ter Veen
Hedy C Vrakking
Johan Wiegers
Aafke Zeilstra

6.6 Medical & Financial Administration

Annelies Boer
Arja RJ Hoekman
Ilse Sewnandan
Hanna van der Sloot
Rika C van der Werff
Erna R van der Wijk
Annie K van Zanten ML

6.7 PhD Students

Janine Doorduin MSc
Inês Farinha Antunes MSc
Valentina di Gialleonardo MSc
Reza Golestani MD
Onno L de Klerk MD
Silvana Kruizinga MSc
Nisha Kuzhuppilly Ramakrishnan MSc
Nathalie Matusiak MSc
Leila Mirfeizi MSc
Ania Rybczynska MSc
Chao Wu MSc
Zilin Yu MSc

6.8 Visiting Scientists

Alessio Annovazzi MD (Roma)
Marco Chianelli MD PhD (Roma)
Hans C Klein MD PhD (Winschoten)
Prof. Alberto Signore MD (Roma)
Prof. Johan De Sutter MD PhD (Belgie)

Habib Zaidi PhD (Switzerland)

6.9   Trainees

Silke Vedelaar
Sarah de Wit
Melanie Wolters

OTHER RESPONSIBILITIES

7.1   Teaching activities

On May 22 and 23, 2008, the Department organized an international symposium (2 days, about 150 participants) entitled: "Nuclear Medicine Methods for the Study of Inflammatory Processes and Infection". The symposium was organized in cooperation with the Department of Nuclear Medicine, University Medical Center St.Radboud, Nijmegen, The Netherlands, and was held under auspices of the Netherlands Society of Nuclear Medicine (NVNG) and the International Society of Radiolabelled Blood Elements (ISORBE). Sponsors were GI Pharma, Cisbio, and GE Healthcare. The local organizing committee consisted of R.A.Dierckx, A.M.J.Paans, J.Pruim, M.G.G.Sturkenboom, G.J.de Voogd, E.F.J.de Vries and A.van Waarde, with external support from S.J.Klont and J.Zomer.

An overview of our other teaching activities is provided in Tables 13, 14 and 15. The total number of teaching hours was 393.

7.2   Appointments, diploms, (inter) national cooperation

Both E.F.J.de Vries and A.van Waarde were invited to edit a special issue of the international journal *Current Pharmaceutical Design*. These invitations have resulted in the appearance of issue 28, "Imaging of Tumor Characteristics for Tailored Therapy", edited by E.F.J.de Vries, with contributions of van der Veldt (Amsterdam), Minn (Turku), Cai (Stanford), Blankenberg (Stanford), Mishani (Jerusalem), Tolmachev (Uppsala), Hospers (Groningen), Ananias (Groningen) and Fu (Baltimore), and issue 31, "Imaging Inflammatory Processes, Tumors and the Endocannabinoid System", edited by A.van Waarde, with contributions of Doorduin (Groningen), Chianelli (Rome), van Waarde (Groningen), van de Wiele (Ghent), Dijkers (Groningen), Horti (Baltimore) and van Laere (Leuven).

A.van Waarde and P.H.Elsinga were contacted by N.A.Colabufo (Department of Pharmacochemistry, Bari, Italy) regarding the labeling of novel P-gp modulating molecules with ^{11}C and the evaluation of these radiopharmaceuticals as tracers of P-gp function and expression in experimental animals. Two compounds (provided by N.A.Colabufo) were successfully labeled. MicroPET scans of healthy and drug-treated Wistar rats were made in Groningen with both tracers. A publication about this joined effort is in preparation.

7.3   Social responsibilities

Algemeen Stralings Deskundige, Universitair Medisch Centrum Groningen
        (A.M.J.Paans)
Chairman, Dutch Society of Radiopharmaceutical Chemistry (P.H.Elsinga)
European Editor, Nuclear Medicine Communications (R.A.Dierckx)
Executive Guest Editor, Current Pharmaceutical Design (A.van Waarde, E.F.J.de
        Vries)

Lid, Beoordelingscommissie (20 proefschriften, R.A.Dierckx)

Lid, Beoordelingscommissie (3 proefschriften, A.M.J.Paans)

Lid, CBO richtlijn ontwikkeling Hypopharynxcarcinoom (namens de Nederlandse Vereniging voor Nucleaire Geneeskunde (J.Pruim)

Lid, Commissie Kwaliteit Bevordering, Nederlandse Vereniging voor Nucleaire Geneeskunde (A.H.Brouwers)

Lid, Commissie Voorziening Kernenergiewet, Nederlandse Vereniging voor Nucleaire Geneeskunde (A.M.J.Paans)

Lid, Concilium, Nederlandse Vereniging voor Nucleaire Geneeskunde (R.A.Dierckx)

Lid, Disciplinegroep Medische Beeldvorming, Stichting Kinderoncologie Nederland (A.H.Brouwers)

Lid, CIM, Universitair Medisch Centrum Groningen (M.N.Lub-De Hooge)

Lid, Examencommissie Biomedische Technologie (A.M.J.Paans)

Lid, Medisch-Ethische Toetsings Commissie, Universitair Medisch Centrum Groningen (A.M.J.Paans)

Lid, Netwerk Nederlands Kenniscentrum voor Farmacotherapie bij Kinderen (M.N.Lub-De Hooge)

Lid, Onderwijscommissie, Nederlandse Vereniging voor Nucleaire Geneeskunde (J.Pruim)

Lid, Onderwijscommissie, Nederlandse Vereniging voor Nucleaire Geneeskunde (R.H.J.A.Slart)

Lid, Redactie Leerboek Nucleaire Geneeskunde (C.Lemstra)

Lid, Redactie Tijdschrift voor Nucleaire Geneeskunde (R.H.J.A.Slart)

Lid, SIG Kindergeneeskunde, Nederlandse Vereniging van Ziekenhuis Apothekers (M.N.Lub-de Hooge)

Lid, Stuurgroep Ontwikkeling Zorgtraject (Bij)Schildklier, Universitair Medisch Centrum Groningen (A.H.Brouwers)

Lid, Visitatiecommissie Nederlandse Vereniging voor Nucleaire Geneeskunde (R.A.Dierckx)

Lid, Werkgroep Atriumfibrilleren, Proeftuin Groningen t.b.v. Groninger Transmuraal Formularium (M.N.Lub-De Hooge)

Lid, Werkgroep Nederlandse Federatie van Universitaire Ziekenhuizen (R.A.Dierckx)

Lid, Werkgroep Nucleaire Cardiologie, cardiale MSCT en MRI voor de Nederlandse Vereniging voor Cardiologie (R.H.J.A.Slart)

Member, Board of Directors, International Society of Radiopharmaceutical Sciences (P.H.Elsinga)

Member, Board International Research Group in Immuno-Scintigraphy and Therapy (IRIST) (M.N.Lub-De Hooge)

Member, Committee on Radiopharmacy, European Association of Nuclear Medicine (P.H.Elsinga)

Member, Editorial Board, European Journal of Nuclear Medicine and Molecular Imaging (R.A.Dierckx)

Member, HOVON Imaging work group (J.Pruim, A.T.M.Willemsen)

Member, Dutch Medicines for Children Research Network (MCRN) (M.N. Lub-de Hooge).

Opleider Klinische Fysica (A.M.J.Paans, A.T.M.Willemsen)

Opleider Nucleaire Geneeskunde (R.A.J.O.Dierckx)

Opleider Nucleaire Geneeskunde (J.Pruim)

Secretaris, Nederlandse Vereniging voor Nucleaire Geneeskunde (A.M.J.Paans)

Teacher, Annual Course on PET/CT, European Association of Nuclear Medicine, Vienna (J.Pruim)

Tutor, Pharmacokinetic Course, IEEE Medical Imaging Conference, Dresden (A.T.M.Willemsen)

Voorzitter, SIG Nucleaire Geneeskunde en Radiofarmacie, Nederlandse Vereniging van Ziekenhuis Apothekers (M.N.Lub-De Hooge)

Table 13.   Trainingships/Internships

Recipient(s)	Duration	Frequency	Location	Teacher(s)	Subject(s)	h
NMP resid. Radiol. Departm.	3-6 mths	Approx 1/yr	RAD	Dierckx, Pruim	General radiology	0
Radiol. resid. NM&MI departm.	Ad hoc	Not running	NM&MI	Dierckx, Pruim	General nuclear medicine	0
Endocr. resid.	2 d	1/yr	NM&MI	Brouwers	Endocr. diagn & therapy	10
Cardiol. resid.	1 hr	2/wk	NM&MI	Slart	Nuclear cardiology	0
Hospital Pharmacist i.t. yr 1	2 wks	1/yr	NM&MI	de Hooge, Sturkenboom	Radiopharmacy	0
Hospital Pharmacist i.t. yr 3-4	4-8 wks	1/yr	NM&MI	de Hooge, Sturkenboom	Radiopharmacy	0
Technologist i.t. yr 1	3 d	1/yr	NM&MI	ter Veen	Nuclear medicine technique	0
Technologist i.t. yr 3	20 wks	1/yr	NM&MI	ter Veen	Nuclear medicine technique	0
Technologist i.t. yr 4	12 wks dual	1/yr	NM&MI	ter Veen	Nuclear medicine technique	0
Clin phys. i.t.	Ad hoc	Frequently	NM&MI	Willemsen, NM physician	Nuclear medicine technique	0
Pharm. Student yr 4-5	6 mths	1/yr	NM&MI	de Hooge, Sturkenboom	Radiopharmacy subsidiary subject	0
Pharm. Student yr 3	3 wks	1/yr	NM&MI	de Hooge, Sturkenboom	Radiopharmacy scientific internship	0
M3 medical student yr 6	3-6 mths	On request	NM&MI	Slart	On request	0
Medical student PPP yr 3	10 d	1/yr	NM&MI	Slart	Blok 2.3 PPP Syllabus	8
Mentorship medical yr 1	17 d	1/yr	NM&MI	Glaudemans	Gen medical training and teaching	100
Foreign student cardiol.	1/2 d	1/yr	NM&MI	Slart	Nuclear cardiology	2
Semi-medical resid. Yr 6	3 mths	On request	NM&MI	Slart, Dierckx	General nuclear medicine	0
Radiochemists (foreign) i.t.	3 mths	On request	NM&MI	de Vries	Radiochemistry	0

NB Zero hours in the last column indicates that no regular teaching was performed by our Department but an internship (stage period) was provided

Table 14   Continuous Education

Recipient(s)	Duration	Frequency	Location	Teacher(s)	Subject(s)	h
Medical student yr 2	1/2 d	1/yr	NM&MI	Slart	Angina pectoris	2
Medical student yr 2	1/2 d	1/yr	NM&MI	Brouwers	Thyroid	2
Medical internship M1	1 hr	8/yr	NM&MI	Slart	General nuclear medicine	8
Medical internship M1	2 hr	8/wk	NM&MI	Brouwers, Pruim	Interactive lecture neck swellings	16
NMP resid. & Hospital Pharm. i.t.	3d	1/yr	PUOZ Eindhoven	de Hooge, Slart	Radiopharmacy, nuclear cardiology	2
Orthopedic Resident	1 hr	1/yr	Dept. Orthopedics	Nuclear medicine physicians	Bone and joint scintigraphy	1
Pharmacy Student yr 1	2 hr	1/yr	NM&MI	Elsinga	Organic chemistry	2
Pharmacy Student yr 4-5	1/2 d	1/yr	NM&MI	de Hooge, Sturkenboom	Introduction radiopharmacy etc	2
Pharmacy Student yr 4-5	5 hr	1/yr	NM&MI	Elsinga	Radiochemistry	5
Pharmacy Student yr 4-5	2 hr	1/yr	NM&MI	Pruim	Introduction radiopharmacy etc	2
Pharmacy Student yr 6	1/2 d	1/yr	NM&MI	de Hooge, Sturkenboom	Introduction radiopharmacy etc	2
Morning session cardiology	30 min	3/yr	NM&MI	Slart	Nuclear cardiology	1,5
Lecture evenings NM&MI	2 hr	5/yr	Teaching center	Dierckx	Various nuclear medicine subjects	10
Morning meetings (Mondays)	1 hr	35/yr	Teaching center	Elsinga	Various PhD subjects	35
Afternoon meetings	30 min	200/yr	NM&MI	Supervisor SPECT&PET	Various clinical cases	0
Interactive lectures	1.5 hr	40/yr	NM&MI	Piers	Various clinical cases	40
Morning presentations (Wednesdays)	1 hr	30/yr	NM&MI	Pruim	Various subjects	30
BMT & FWN	4 hr	10/yr	NM&MI	Paans, Willemsen, Pruim	Nuclear medicine and techniques	40
Researchers GUIDE (course)	1/2 d	1/yr	Teaching center	van Waarde	PET transporter systems	4
Junior Scientific Masterclass	Continuous	yr	NM&MI	Dierckx, Slart, de Vries	Various subjects	0
Researchers BCN (course)	2 hr	1/yr	NIC	van Waarde	PET-brain	2
MBRT	2 hr	1/yr	MBRT	Pruim	General nuclear medicine	2
MBRT	2 hr	1/yr	MBRT	de Vries	Radiochemistry	2
MBRT	2 hr	1/yr	MBRT	Paans	PET & gamma camera	2
University Hospital Ghent	1d	1/yr	Ghent	Dierckx	General NM introduction	5
Life Sciences students	1hr	1/yr	Haren	Slart	Oncology symposium	1
WLF Grammar school	3 hr	1/yr	Groningen	Pruim	General nuclear medicne	3
Oncology nurses	2 hr	1-2/yr	Groningen	Pruim, Slart	PET oncology	2

NB Zero hours in the last column indicates that no regular teaching was performed by our Department but an internship (stage period) was provided

Table 15 Ad hoc Teaching and Training

Recipients	Duration	Frequency	Location	Teacher(s)	Subject(s)	h
Biotechnology students	2 hr	2008	Rome, Italy	de Vries	PET oncology lecture	2
Biotechnology students	2 hr	2008	Rome, Italy	de Vries	Antibody labeling lab & workshop	2
Faculty tutorship (student S.Burke)	3 mths	2008	NM&MI	de Vries	Inflammation imaging	0
TNO	2 wks	2008	NM&MI, VUMC	de Vries	Data analysis uPET	0
NVMBR	30 min	2008 (4x)	Netherlands	Lemstra, Koopmans	Sentinel node, PET & carcinoid	2
Morning session internal med..	30 min	1-2 yr	Dep. Intern. Med.	Brouwers	PET	1
Oral surgery	1 hr	2008	NM&MI	Brouwers	Osteomyelitis	1
BCN research masters (course)	1/2 d	2008	NM&MI	van Waarde	PET & biochemistry	2
CME EANM	1 hr	2008	Munich, Germany	van Waarde	Proliferation markers	1
Topmaster II MPDI 2008 (course)	1 hr	2008	Groningen	van Waarde	Research methods: animal PET	2
Univ Hospital Ghent	1d	1/yr	Ghent	Dierckx	Models in Dutch healthcare	3
Grammar school -In de diepte	4 hr	2008 (2x)	Groningen	Willemsen	Clinical physics	8
EANM	1 d	2008	Munich, Germany	Elsinga	Radiochemistry	8
EANM	2 d	2008	Vienna, Austria	Pruim	PET-CT general	18

NB Zero hours in the last column indicates that no regular teaching was performed by our Department but an internship (stage period) was provided

Total number of teaching hours in 2008 (Tables 13,14 and 15 summed):   393.5